universität wien

DISSERTATION / DOCTORAL THESIS

Title of the Doctoral Thesis

"Optimizing molecularly imprinted polymer thin films for sensing lysozyme and bovine serum albumin"

verfasst von / submitted by

Wim Cuypers BSc MSc

angestrebter akademischer Grad / in partial fulfilment of the requirements for the degree of

Doktor der Naturwissenschaften (Dr. rer. nat.)

Wien, 2019

Studienkennzahl lt. Studienblatt / degree programme code as it appears on the student record sheet:	A 796 605 419
Dissertationsgebiet lt. Studienblatt / field of study as it appears on the student record sheet:	Chemie/Chemistry
Betreut von / Supervisor:	Univ.-Prof. Dr. Peter A. Lieberzeit

Preface and acknowledgements

First, I would like to thank Prof. Dr. Peter A. Lieberzeit for his support and guidance during the whole journey of my PhD thesis. I have learnt a lot of him, both practical skills and theoretical knowledge. His passion in pursuing science, and his attitude toward career and life inspired me to experience science in a different way. Moreover, I am happy that I could complete my thesis in the same group where I also finalized my Master thesis.

I would also like to pay tribute to Prof. Dr. Patrick Wagner for once giving me the opportunity to come to Vienna for an Erasmus Master program. A program that lasted longer than expected, surprisingly.

My gratefulness also goes to both the Department of Analytical Chemistry where I started my PhD as well as the Department of Physical Chemistry where I will end my academic career.

I would also like to pay tribute to the many coworkers I have encountered in the lab over the years. They were always very friendly and willing to help me when they could. Special thanks to Mathias, Ine, Moni, Martin, Felix and Birgit for making lunch time great again.

My special appreciation is dedicated to my wife Raphaela. Without her help, support and comforting words, finalizing my thesis would not have been possible. They were also responsible for the fact that working on my thesis was a pleasure. I am very grateful towards Dr. Stephan Puchegger who helped me to analyze the Scanning Electron Microscopy samples. I also want to show courtesy to "De Nederlandse Organisatie voor toegepast-natuurwetenschappelijk onderzoek" (TNO) Eindhoven for allowing me to do an interesting practical course in their labs.

Last but not least, I would like to acknowledge my church community ICF Vienna, where I have met many good friends. Aside of that, they gave me a platform to expand my leadership capacities and social skills.

Table of content

1. Introduction

"Life is the mode of actions of proteins" (1). This quote of Friedrich Engels highlights the emphasis of these intriguing polypeptide chains. Protection, signalling, transport and support are only few of the many functions related to proteins (2). Figure 1 lists a short summary of their major actions.

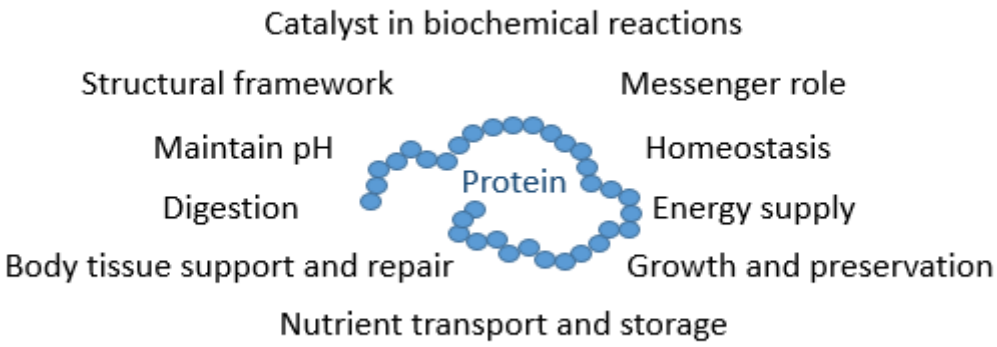

Figure 1: The role of proteins in human body.

Because their actions and manifold presence in our body, a healthy status and balance are of great importance (3). This is also what people thought in ancient Greek times. The word protein comes from the word "*proteios*" meaning "of first rank" (4). However, overexpression of proteins can be harmful to the cell and at larger scale to human (5). Overabundance can result in agglomeration, overburdening of biological pathways and embrangled regulation. It might be a relevant indicator for several infection-related diseases such as multiple myeloma (6), hepatitis B&C (7), HIV/AIDS and several cancers (8). On the other hand, insufficiency of certain proteins can be related to either a bad diet, malabsorption, renal and hepatic diseases (9) and even sepsis (10). Analysis of serum albumin or total blood protein is executed to determine if someone is suffering from hyperproteinaemia (11). Because of aforementioned reasons, there is a need for a technique to correctly determine the amount of specific proteins in blood (3) . If values lay out of the normal concentration spectrum, one needs to take actions.

Not only the amount of protein in blood is crucial, so is the "health status" of the relevant protein. This so-called conformation plays a vital role in the working mechanism of a protein (12). Mutations or folding failures may result in life-threatening diseases such as cystic fibrosis, Alzheimer´s disease, Huntington's disease and Sickle cell disease (13, 14). According to Helmfors, lysozyme plays a dual role in life, part hero, part villain. Her studies focused on amyloidosis indicated that both a right balance and conformation are crucial (15, 16).

This work highlights two proteins, namely lysozyme and bovine serum albumin (BSA). Lysozyme is chosen as a target protein because of the widespread interest it gets expanding from pharmaceutical towards food industry (17). It has established the status of being a model protein for research on both structure and functionality (15). The molecule is widely known and relatively low-priced (18). Of course, it is also of enormous clinical importance to investigate its presence in blood, saliva or other body liquids. Its presence in faeces is significantly related to inflammatory bowel disease (19). All of these reasons make it an interesting candidate for our experiments.

Due to the importance of lysozyme detection, a certain concentration framework has to be defined. Since lysozyme appears in different amounts in various bodily liquids (serum, urine, saliva and tears), it is crucial that detection limits are set for all fluids individually. In healthy situations, lysozyme occurs at a concentration of approximately 10, 0.5, 9 and 1267 mg/L for all previously named body liquids respectively (20).

Before starting with lysozyme experiments, BSA is selected as a starting model. A predecessor already did several experiments using this protein and I continued in his footsteps. Determination of serum albumin exhibits physiological relevance since it plays a role in the development of cardiovascular disease (21). After experiments concerning BSA, I took a sidewalk towards lysozyme imprinted sensors.

A distinction between various protein detection methods is made by Hisakazu Mihara and his co-workers, presented in Table 1 (22). Based on the table he published, the advantageous properties are marked by bright green whereas the drawbacks are dark red. Mediate functions have colours in between. The row displaying the QCM is highlighted in blue. This is done because the focus in this work is on this mass-sensitive approach. From the table, it can be seen that it the technique is highly valuable for low-throughput protein detection because of its prize and handling. Moreover, quantitative measurements can be done and this technique does not require labelling and its preparation is fairly simple.

Table 1: Detection methods applicable to the development of protein microarray technology. (22)

		Labeling/Preparation	Handling	Instrumentation Cost	Quantitative	High Throughput
Labeling	Fluorescent probe	Yes/Medium	Easy	Inexpensive	Yes/No	Yes
	Radioisotope	Yes/Difficult	Difficult	Medium	Yes	Yes/No
	Chemiluminescent probe	Yes/Medium	Easy	Inexpensive	Yes/No	Yes
	Electrochemical probe	Yes/Medium	Easy	Inexpensive	Yes	Yes/No
	Nanoparticles	Yes/Medium	Easy	Inexpensive	Yes	Yes
Non-Labeling	MS	No/Easy	Easy	Expensive	No	Yes/No
	Microcantilever	No/Difficult	Difficult	Expensive	Yes	No
	QCM	**No/Medium**	**Easy**	**Inexpensive**	**Yes**	**No**
	SPR	No/Medium	Easy	Expensive	Yes	Yes
	AR	No/Medium	Easy	Inexpensive	Yes	Yes

In the past, various techniques were developed for the detection of proteins (23, 24). Nonetheless, they were suffering from high cost, requiring trained personnel or taking long measurement times (25). This work describes the fabrication of low-cost sensors for rapid detection of biomolecules. Relying on molecularly imprinted polymer, detection of common proteins such as serum albumin and lysozyme is made possible at physiological concentrations. Sensor responses are monitored as well as their selectivity towards other similar molecules. Various polymer systems were tested and optimized to obtain better limits of detection as well as a low amount of unspecific interactions with other proteins. This thesis should open the door towards detection of many more proteins using the fairly cheap and fast QCMs.

1.1. Sensors

Sensors play an important role in human life to detect compounds in the environment (26, 27). They can be fabricated industrially but also appear in nature and human. An intriguing example of the latter kind is our nose. It accommodates receptors to discriminate the smell of coffee from potentially harmful substances. Technology also makes use of this principle for detection of a stimulus (28).

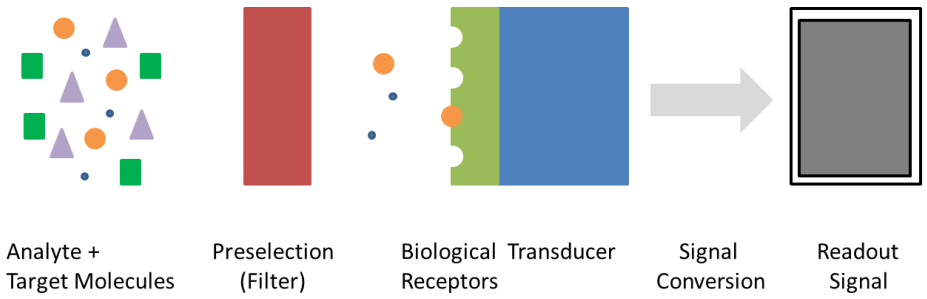

Figure 2: Schematic overview of a sensor.

Sensors can be subdivided into three major classes, namely physical, chemical and biosensors (29). In a quantitative and autonomous way, they all can measure and monitor various properties in their environment. Physical sensors can measure physical parameters such as distance, mass, temperature, pressure, depth, etcetera (30). By means of chemical sensors, it is possible to obtain information about its chemical environment. Typical for chemical sensors is the fact that the resulting signal is correlated to the concentration of target molecules in the analyte solution. Biosensors function similar to chemical sensors. Moreover, biosensors actually are a sub-set of chemical sensors but are frequently mentioned as a separate class (31). Distinction between the two classes is made based on the fact that biosensors typically incorporate a biological sensing element to a transducer. Examples of such biological recognition elements are antibodies, nucleic acids, enzymes, cells and even tissue (29). As a result, plenty of medical sensors (i.e. thermometers, blood pressure meters) are misjudged as biosensors since they do not contain any biological recognition element. An elaborate representation of the chemo-/biosensor working mechanism is given in Figure 2. Firstly, the target molecules bind to the biological detection element (32). This binding leads to a response that can be converted by the transducer into a signal that can be measured by a signal processor (33). The detection result is quantitative for target binding. Over the last decades, usage of biosensing devices expands and mainly focuses on diagnostics and patient monitoring (34). Think about glucose monitoring in diabetes patients (35), the beloved alcohol test (36) and the so-called pregnancy test (37). Other examples include detection of pathogens, drugs etcetera (38, 39) .

This work describes the complete process from scratch towards the accomplishment of a working sensor. The main interest lies in sensing biological analytes such as lysozyme and bovine serum albumin. Therefore, a biomimetic sensor based on polymers was fabricated for this purpose. Since these artificial chains mimic biological recognition, it is called a biomimetic rather than a chemical or biological sensor (40). Only analytes of a particular shape and functionality bind into preformed cavities. Due to an intrinsic property of quartz, piezoelectricity, it is possible to determine mass changes occurring at the sensor surface. These alterations are transduced to the computer where an in-house software program is used for analysis.

The aims of this thesis comprise the fabrication of a cheap sensor for fast and sensitive detection of BSA and lysozyme. The mechanism of this device relies on molecularly imprinted polymers binding to the protein. Several well-known polymers are synthesized and tested for both analytes. QCMs are tested on sensitivity to determine the limit of detection. For some quartzes, selectivity tests using different analytes are performed to determine the specificity of the sensor. AFM is employed to visualize the homogeneity/coverage of protein stamps.

1.2. Molecular Imprinting

1.2.1. Introduction

Molecular imprinting was primarily described by Wulff and Mosbach in the 1970s (41, 42) . Although there is no exact definition of a molecularly imprinted polymer (MIP), there exists a general consensus. According to this agreement, it comprises polymers possessing cavities in its matrix, which are imprinted by specific target molecules. By mimicking natural recognition entities, the matrix possesses molecular recognition properties of biological systems. Cavities synthesized in this way are complementary in size, shape and/or functionality to the template. So to say, the imprinted polymer exhibits a permanent memory from the target species (43-45). Therefore, binding of the target in these gaps can be very selective and can be seen as a "lock and key" model (44). Figure 3 explains the process of molecular imprinting in a simplified way.

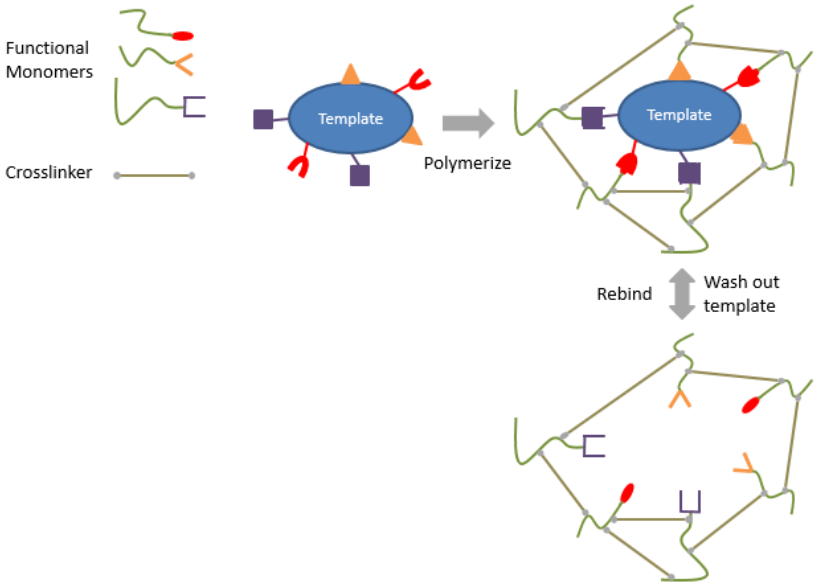

Figure 3: Schematic overview of molecular imprinting.

In fact it was Emil Fischer who postulated the "lock-and-key" principle in 1894 (46). However, his observations were based on interactions between enzymes with single substrates. This hypothesis can also be transferred to binding of target molecules in geometrically complementary pockets, namely molecular imprinted sites. This way, it is possible to distinguish the target from a plethora of closely related compounds. In 1958, Koshland came up with the idea of an induced fit model which states that the substrate plays a role in the regulation of the final shape of the enzyme (47). In other words, it defines the enzyme as a somehow flexible component which can help to make the substrate fit. However, molecules that are too small are not capable to react.

As mentioned before, in molecular imprinting, cavities towards a certain template of interest are formed. Molecular recognition makes a subdivision between covalent bonds and non-covalent interactions. The covalent approach benefits from its formation of well-defined recognition sites. However, challenging template removal and fairly restricted template selection make it less favorable. Non-covalent interactions such as van der Waals interactions, π-π stacking effects, hydrogen bonds, electrostatic interactions and hydrophobic effects play a major role in the usage and the success of MIPs (43, 48). Formation of these non-covalent intermolecular forces is characterized by the release of energy ranging from 4-20 kJ/mol depending on the type of interaction. In order to obtain an idea about unselective binding of a certain target towards the polymer strands, a reference made under the same conditions is developed. This reference polymer lacking the template molecule is called non-imprinted polymer. The difference between signals for MIP and NIP gives a good indication about the sensitivity of the sensor: Does the analyte really bind into the cavities or is it just attracted by the functional groups of the polymer surface? In order to perform polymerization experiments, some different chemicals are required. First of all, functional monomers are responsible for the chemical recognition of templates. There exists a wide range of possible candidates for molecular imprinting: acrylamide, methacrylic acid, vinyl-pyrrolidone to name but a few. A second component, named crosslinker, determines the hardness of the polymer. Ethylene glycol dimethacrylate is one of the most known examples. Furthermore, a catalyst can be used to speed up the reaction. Also a porogen may be beneficial to make the material more porous and thus more accessible for analytes. Also removal can be improved this way. Last but not least, a proper solvent has to be selected. Can all components above dissolve in the solvent? Does the solvent harm the template in case of bulk imprinting? Many questions have to be answered to come up with a proper solvent. All these parts contribute to the end-result of the MIP and therefore should be considered wisely.

1.2.2. Imprinting Techniques

Some distinctions can be made between different types of imprinting depending on time and mechanism of analyte-polymer interaction (49). To begin with, there exists surface imprinting. It can be subdivided into soft lithography/stamping, emulsion polymerization, grafting and template immobilization. Figure 4 describes the three different imprinting strategies performed in this work.

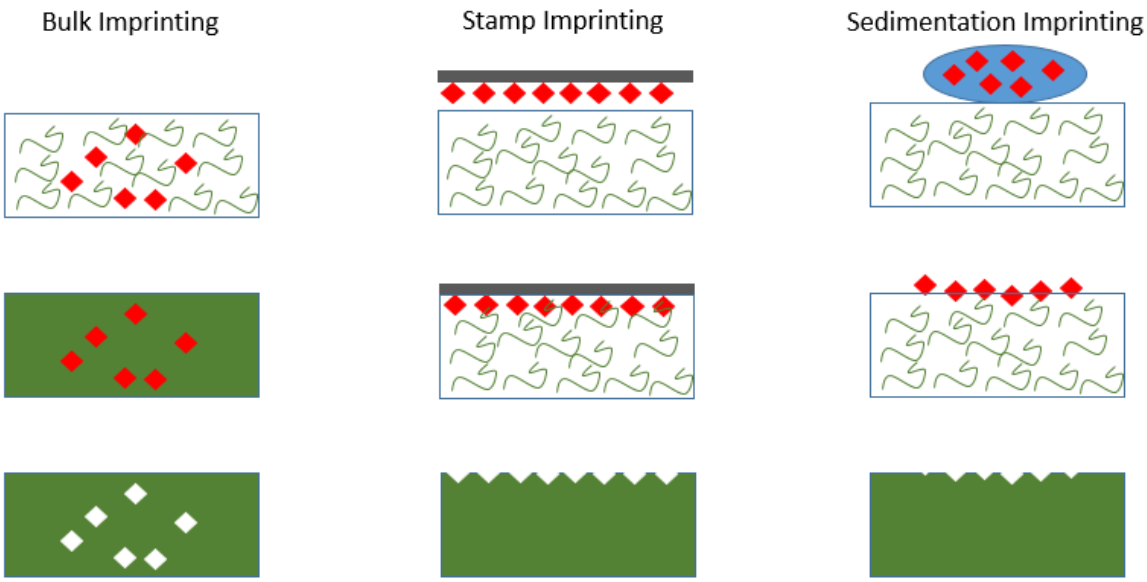

Figure 4: Visual representation of the most common imprinting strategies: bulk, stamp and sedimentation imprinting.

This thesis only focuses on the soft lithography approach. In this technique pre-polymer is prepared. Aside of that, a stamp containing the analyte of interest is prepared. The analyte might be linked to the stamp, but this is not a requisite. After pressing the stamp onto the pre-polymer, the whole is exposed to further polymerization for a certain amount of time. It can occur through elevated temperatures or UV radiation. After hardening, the sample has to be removed out of the polymer. In this approach, cavities typically only arise at the surface of the polymer, as the name already suggests. This method is preferably used for larger molecules that are more challenging to remove out of dense polymer matrices.

Unlike for the imprinting strategy described before, there is no need for preparing a stamp in bulk imprinting. Pre-polymer and template are mixed before polymerization takes place. Generally, this method is the first choice for MIP synthesis in relation with small molecules. Since the template is evenly distributed in the polymer, it is not solely located at the surface.

Because of the size of the template, it is feasible to travel through the matrix and can get washed out. For biomolecules, it should be checked whether the polymer environment is compatible to them. In other words, too harsh conditions might induce denaturation of several molecules (50). This of course is unwanted and has to be taken into consideration.

Another approach is named sedimentation imprinting (51). Rather than preparing a stamp, the analyte solution is dropped onto a pre-polymer layer. Afterwards, a PDMS or glass stamp can be applied to enforce pressing of the target into the polymer.

At last, epitope imprinting is a valuable alternative for the imprinting of whole molecules. Here, only a subpart of a molecule is imprinted and can recognize this sequence in binding experiments. Generally, a part at the terminal of a sequence is chosen and a polymer is forming a complex around the template. The resulting cavities allow binding of the short sequence as well as the whole molecule through this bond.

1.2.3. Pros and Contras

MIPs are also denoted as plastic antibodies because they possess high selectivity. The question one has to ask is why one would prefer MIPs to biological antibodies. Biomimetic receptors are characterized by many advantages (52, 53): As already explained, they are featured by high selectivity and affinity towards target molecules. They also gain a lot of interest because of their straightforward synthesis and reproducibility. Processing antibodies generally requires more effort. In comparison with proteins, who lose their affinity over time, artificial antibodies may preserve their stability for months to years. Moreover, MIPs are also known for their robustness against severe conditions (i.e. high temperature) and impressive stability (44). In a chemical stability study, Svenson et al. demonstrated that MIPs did not suffer from significant loss of affinity towards the analyte in a broad pH range (54). A brief overview of the advantages accompanied to MIPs is given in Figure 5.

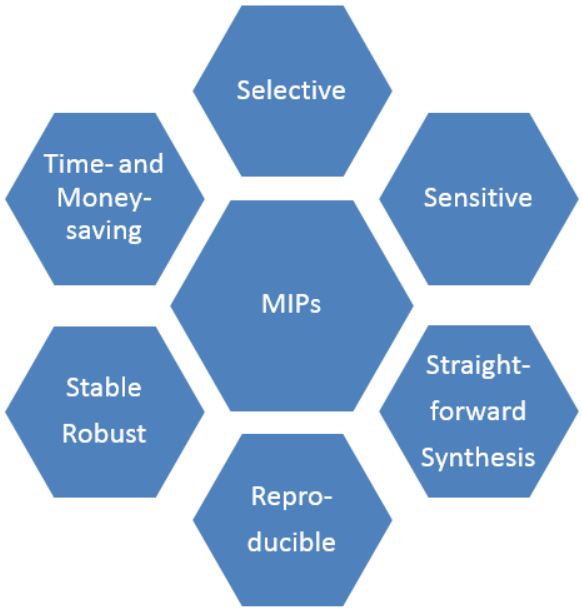

Figure 5: Advantages of molecularly imprinted polymers.

Because of their rigid design, MIP sensors are a relatively cheap solution for analysis of drugs, allergens, toxins, small organisms, etc. Lab analysis on the other hand would be more elaborate, time consuming and especially more expensive. Their low production cost is also of great importance for production on large scale. To end, MIPs can be prepared in different formats such as thin films, blocks and beads.

However, there are also some drawbacks related to molecular imprinting: Molecules such as proteins may denature in the polymer matrix. There also exists a chance that the cavity collapses or ruptures after removing the template. Furthermore, imprinted cavities can differ considerably in behavior regarding their affinity towards respective target molecules. If this interaction is too large, it is very challenging to remove the template. Mass transfer problems can also occur after usage of big amounts of crosslinker or in case of employing bulk imprinting for extensive large molecules. Here, removal of the template is facilitated by utilizing surface imprinting (55).

Nevertheless, diverse challenges are accompanied with the imprinting of proteins. First, one has to keep in mind that these large biomolecules can denature during various steps of the process. Besides, also less drastic modifications can occur. Other objections are everlasting entrapment and discrepancy among binding sites. Sometimes, MIPs suffer from lower catalytic behavior compared to proteins.

1.2.4. Radical Polymerization

Most molecularly imprinted polymers that are currently published rely on free radical polymerization. Formation of polymers out of individual building blocks (monomers) can be separated into three distinct phases (56). The whole process is shown in Figure 6. During the first phase, called initiation, an initiator (R) are split due to heating or radiation, resulting in two radicals (R·). These radicals can interact with the monomers (M) for example by opening/breaking the double bond of alkenes. This action leads to the origin of a new radical, which at its turn reacts with another monomer and thus enables chain growth. This step is also called propagation. When chains with free radicals meet and combine, the process ends. This last step is known as termination. Two types of termination may occur: When two chains combine to form one large complex, it is called recombination. Disproportionation, on the other hand occurs when one chain delivers a radical to another chain. Both chains stay separate according to this approach (57).

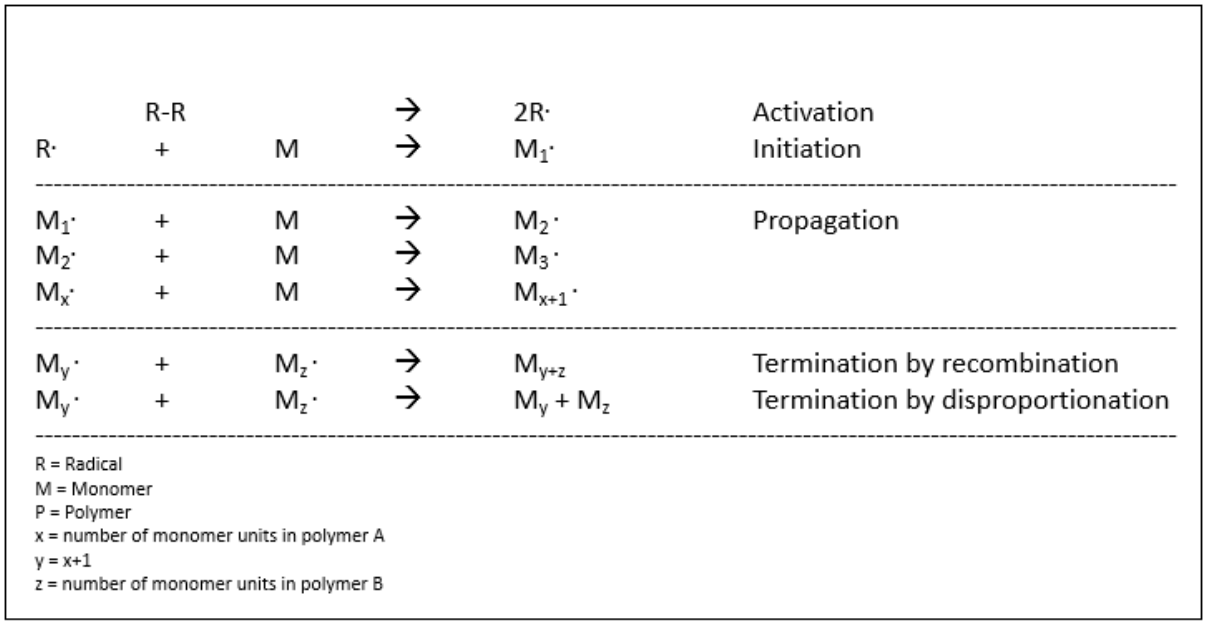

Figure 6: Reaction mechanism of free radical polymerization.

Advantages of free radical polymerization (FRP) include tolerance for a wide range of templates, functional groups and solvents. Moreover, this technique is relatively insensitive to trace impurities. Besides, multiple polymerization processes can be performed even at moderate reaction temperatures. A significant drawback, however, is the lack of control over the chemical reaction, e.g. molar mass distribution. As a result, MIP based on FRP usually reveal broad site heterogeneity. Aside of that, kinetics of the process is sometimes slow.

One way to avoid these problems is to synthesize the MIPs by controlled/living radical polymerizations (CRP) (IUPAC: reversible deactivation radical polymerization (RDRP)) (58). All of them result in more consistent reactions during polymer network growth, which results in more narrow molar mass distributions. CRP combines both the advantages of anionic (narrow molar mass distributions, high definition of end groups, decisive reactivity of polymer chains) and of radical polymerizations (straightforward reaction procedures, practicable in wide range of reaction conditions, various initiation modes, high tolerance towards purity of reagents and functional groups). Key classes of RDRP are atom transfer radical polymerization (ATRP), nitroxide mediated polymerization (NMP) and reversible addition fragmentation polymerization (RAFT). They are all characterized by establishing of a dynamic equilibrium between active and dormant state. During the polymerization process, dormant species are reactivated and single monomers are added to the chain. This is followed by deactivation leading again to the dormant state. The process of switching from active to dormant state can be represented by a seesaw. One end of it represents the active species, the other the dormant. Changing from one state to the other occurs repeatedly and fast. The proportion of dormant species is much larger than the one of active species. Through this, all chains are denoted the same propagation probability. Thus, it is feasible to maintain equal chain lengths for all polymers. Termination events in ATRP and NMP are reduced by instantaneous low radical concentrations. Considering this, it seems that anionic polymerisation conditions are ascertained. For RAFT, however, this is not the case. Here, the total radical concentration stays identical throughout the whole process (57).

The first of all modern approaches to control polymerization was **nitroxide mediated polymerization (NMP)**. It only relies on NMP-initiator, monomer and optionally free nitroxide. In this process, there is an enduring interplay between the growing propagating chain and the nitroxide. This type of polymerization is characterized by its low polydispersity index. It is only executable at high temperatures and is partially very slow. It results in thermally instable products and is infeasible for the use of methacrylates. The most famous mediator is called 2,2,6,6-Tetramethylpiperidinyloxyl (TEMPO) which a radical which can react with dormant species (59).

Atom transfer radical polymerization (ATRP), alternatively named Kharash addition, makes use of interactions between halogenated compounds and alkenes or alkynes. Through this, it is feasible to obtain control over the reaction via catalytic equilibria and redox reactions between active and dormant species. The reaction occurs under influence of light or radical initiators by a free radical mechanism. 2,2-azobis(2-methylpropionitrile) (AIBN) is a very common radical initiator employed in this setting (60).

Discovered in 1998 by Rizzardo and his working group, **reversible addition fragmentation transfer (RAFT)** polymerization now belongs to the most important and commonly used CRPs. Its significance is due to its broad compatibility towards plenty of monomers as well as the fact that the reaction can proceed at moderate conditions. Polymers of low dispersity and specific shape can be obtained this way. The reaction can be controlled with the aid of a chain transfer agent (CTA). This is a chemical in the form of a thiocarbonylthio compound. Dithioesters, thiocarbamates, and xanthates are the most known examples of CTAs. Binding of the propagating chain to the CTA results in the formation of an intermediate radical (61).

Free radical polymerization has many advantages. To start with, it allows for fast chain growth at moderate reaction temperatures. It can also be applied in a large number of polymerization processes. Moreover, it is relative insensitive to impurities and enables rapid irreversible chain termination. Unfortunately, there are also a few limitations coupled to this approach. It is accompanied by poor control over molar mass distribution. Second, it is hard to predetermine the functionality of a final polymer. Last, synthesis of block copolymers is nearly impossible. In summary, conventional FRP is not limited to demanding reaction conditions and shows great potential for the polymerization of various vinyl monomers. Figure 7 describes the different levels of polymerization and its subdivision.

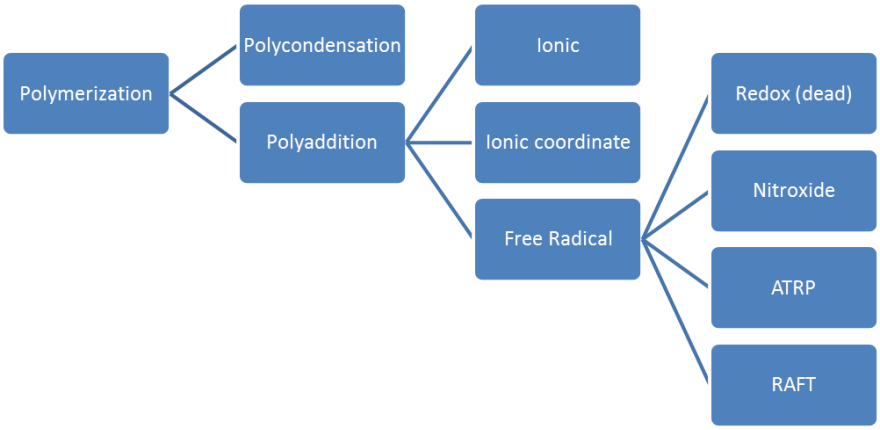

Figure 7: Overview of the different types of polymerization techniques.

1.2.5. Polyurethane Synthesis.

In 1937, Otto Bayer et al. developed polyurethane, which became commercially available in 1952. Nowadays, PU has a broad range of applications such as paints, coatings, elastomers and foams. In this work, various polymer systems were developed for the creation of MIPs. Previous experiments by members of our working demonstrated the applicability of PU in the field of molecular imprinting. The working mechanism of this process is demonstrated in Figure 8. Isocyanate groups combine to obtain urethane bonds. DABCO acts as a reaction catalyst here. It acts by enhancing the nucleophilicity of BPA.

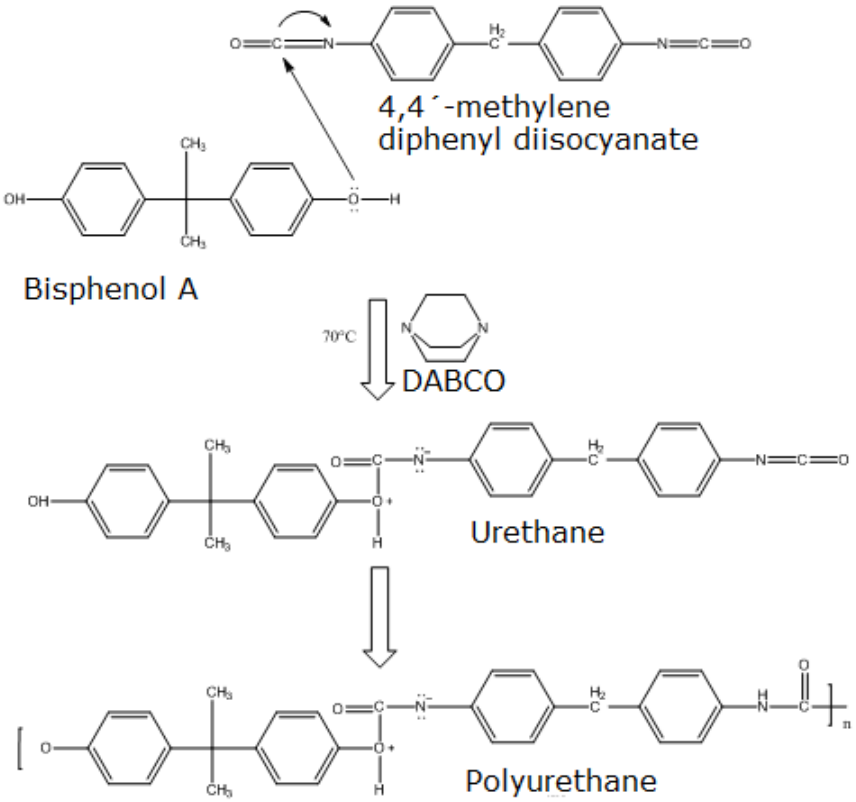

Figure 8: Polyurethane synthesis mechanism.

1.2.6. Nanoparticles

According to IUPAC, a nanoparticle (NP) is defined as a particle of any shape with dimensions in the 1×10^{-9} and 1×10^{-7} m range. They are known for their large surface to volume ratio and its applications are expanding over the last decades (62). In order to bind more analytes onto our sensor surface, synthesis of these particles was considered. These NPs could then be bound onto the electrode by pressing them into a thin polymer layer. After literature research, silica was chosen as material of choice. These structures could then be coated by different polymers which at their turn can be imprinted with our target analytes. In this work, silica (SiO_2) nanoparticles are the preferred candidate to fulfill the core function. They are synthesized using the Stöber synthesis, reported in 1968 (63). Through this sol-gel procedure, it is possible to obtain monodisperse particles of controllable and uniform size (64).

1.3. Quartz Crystal Microbalance (QCM)

1.3.1. Theoretical Background

It took until the mid-eighteenth century when Carl Linnaeus and Franz Aepinus discovered the pyroelectric effect (65). Here, a temperature change induces an electric potential in specific materials. Later on, René Just Haüy and Antoine César Becquerel came up with theoretical propositions claiming the relation between mechanical stress and electric charge (66). These preliminary discoveries motivated Jacques and Pierre Curie to put this comparably abstract hypothesis to the test. In 1880, the two brothers pioneered by truly demonstrating the effect of piezoelectricity (67, 68). Upon application of mechanical stress to certain specific materials (i.e. quartz, topaz, Rochelle salt and tourmaline) leads to the generation of an electrical voltage proportional to this pressure (69). This physical principle is called the piezoelectric effect. More specifically, when subjecting a material to mechanical stress results in a voltage, it is called the direct effect. Likewise, applying an electric field to such a crystal gives rise to a mechanical deformation and is denoted as the inverse piezoelectric effect (65). Piezoelectric crystals have in common their asymmetric build-up. Furthermore, they are characterized by insulating behaviour. Quartz (SiO_2) crystals are the most prominent piezoelectric materials. Besides, it exhibits a large quality factor, being the ratio of frequency to bandwidth. This outlines both stability and accuracy for frequency determination. In addition, quartz is not dissolvable in aqueous solutions. Figure 9 displays the general setup of a QCM. Quartzes perform the action of a crystal oscillator by creating an electrical signal with exact frequency. Requisite for this event is the mechanical resonant behaviour these specific oscillators possess. Applying a voltage to an AT-cut quartz results in a thickness shear formation. Here, the quartz´ electric field is distorted by application of a voltage. Matching the frequencies of excitation and acoustic resonance leads to a large amplitude of the oscillation. Other well-known vibrational modes except for shear-thickness include longitudinal, flexural and face shear mode.

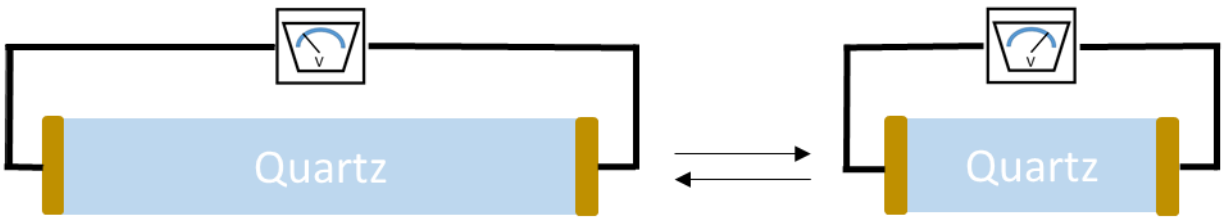

Figure 9: Fundamental principle of a QCM.

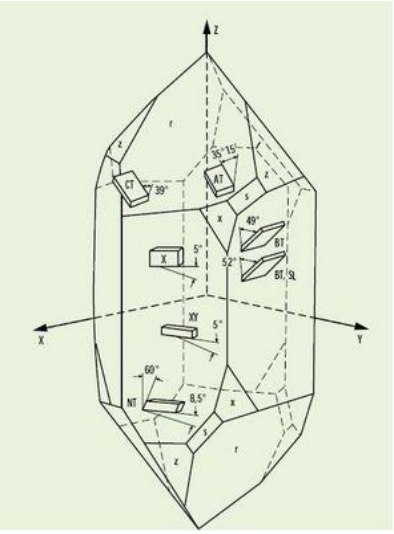

Figure 10: Different cuts of a quartz crystal (70).

Our AT-cut crystals function in thickness shear mode. An important advantage of this vibration mode is its independency for temperature changes beneath 570°C. It almost hast no drift around room temperature. Thereby, its employment is perfect for micro weighing since this mode is the most susceptible for mass addition and release. Take into account that these provided quartzes are blanks, meaning that they are not coated with any material (i.e. metals such as gold, chromium, copper, titanium and many more). Figure 10 gives a visual representation of this most common cuts and multiple distinct-orientated sliced slabs.

As visualized in the picture below, quartz is composed of silicon (Si^{4+}) and oxygen (O^{2-}). In equilibrium, positive and negative charges cancel out each other. Thus, there is no net polarization. After subjecting a quartz crystal to pressure, atoms are displaced. This automatically leads to a shifting of charges ultimately heading to accumulation on contrary faces.
The result is an electrical polarization (P) which is proportional to the dipole moment μ ($Q.h$) between the two borders of the crystal. Q is denoted as the full charge on one side while h is the height of the layer. There also exists a reciprocal relationship $\left(P = \frac{\mathrm{Q.h}}{\mathrm{V}}\right)$ between the amount of polarization and the volume (V) of the quartz crystal slice. The ratio of dipole moment to volume makes quartz a very promising candidate for acoustic measurements. Higher electrical responses compared to other piezoelectric materials are achieved by SiO_2 for the same mechanical strain. Of course, this process also applies in the reverse direction. The process is visualized in Figure 11

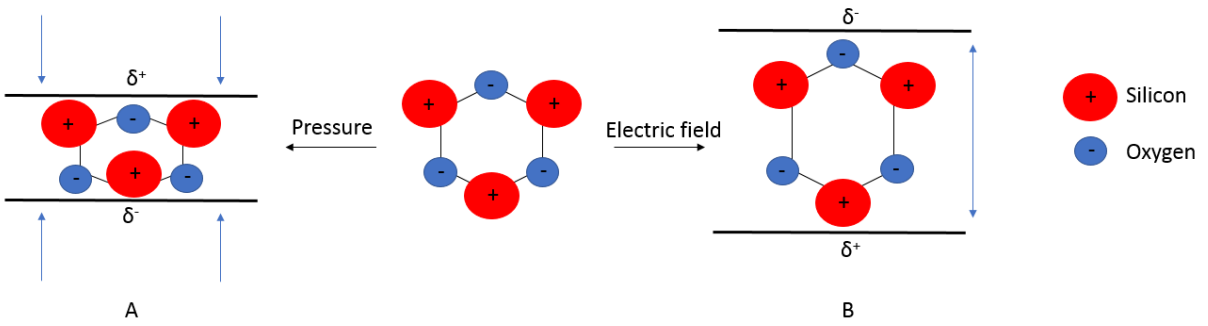

Figure 11: A) Piezoelectric effect versus B) electrostriction (inverse piezoelectric effect).

It is said that applying voltage results in a distribution of charges in a quartz crystal. Whereas charges remain in a fixed position upon application of a direct voltage, charges can redistribute in the case of an alternate voltage. The latter one results an oscillation of the quartz crystal. Mass binding onto it leads to an alteration of this fundamental frequency, the so-called *eigen-frequency*. In the middle of the twentieth century, Sauerbrey indicated the relation between the resonance frequency and the alteration in surface load (71, 72). Equation 1 describes this principle as:

Equation 1: Sauerbrey equation

$$\Delta f = \frac{-2 f_0^2}{A \rho_{crystal} v_{crystal}} \cdot \Delta m = -\frac{\Delta m}{m_0} \cdot f_0$$

Where:

Δf = Frequency change (Hz)

f_0 = Resonant frequency (Hz)

Δm = Mass change (g)

m_0 = Initial mass (g)

A = Piezoelectrically active crystal area (cm^2)	0.5024 cm^2
$\rho_{crystal}$ = Crystal density (g/cm^3)	3 $g.cm^{-3}$
$v_{crystal}$ = Velocity of sound in quartz (cm/s)	33400 $cm.s^{-1}$

It should be noted that the equation above only counts for uniform and rigid deposited films (73). In this work, polymers were rigid enough to ensure that the Sauerbrey equation could be used (74).

It can be seen that the change in fundamental frequency is proportional to the change of mass on the surface. Furthermore, a change in frequency is proportional to the square of the fundamental frequency. This feature has to be considered for the development of sensitive sensors. f_0 is dependent on the thickness of the piezoelectric crystal and is given by Equation *2*.

Equation 2: dependency of quartz crystal on layer thickness.

$$f_0 = \frac{v_{Crystal}}{2d}$$

Where:

f_0 = Resonant frequency (Hz)

$\nu_{crystal}$ = Speed of sound in quartz (cm/s)

d = Crystal thickness

It can thus be deduced that a quartz crystal with a thickness of 168 µm corresponds to a fundamental frequency of 10 MHz knowing that the speed of sound in quartz equals $3.34x10^5$ cm/s. It is also characterized by a nominal sensitivity of 0.226 Hz cm^2 ng^{-1}. Moreover, the Δf/f may not exceed 2% (75).

Because of the breakthrough of the Sauerbrey equation, quartz resonators have found their way into the world of detection platforms. Their function can be described as thin-layered microbalances with high sensitivity for detecting various analytes.

Since the measurements in this thesis are performed in liquids, another equation has to be utilized, namely the Kanazawa Gordon equation (76).

Equation 3: Kanazawa-Gordon equation.

$$\Delta f = -fo^{3/2}.\left(\frac{\eta_L \rho_L}{\pi \mu_Q \rho_Q}\right)^{1/2}$$

f_0 is the oscillation frequency of the free (dry) crystal, ηL and ϱL are the absolute viscosity and density of the liquid, respectively, and µQ and ϱQ are the elastic modulus and density of the quartz. Because of this equation, shear waves in quartz can be connected to a damped shear wave in the fluid.

Acoustic devices can be divided into two main groups: bulk acoustic wave (BAW) and surface acoustic wave (SAW) devices. Their classification is based on the way of wave propagation through the substrate.

Concerning BAW devices, waves, as the name indicates, spread through the bulk of the substrate. In these devices, a piezoelectric element is sandwiched between two electrodes and the acoustic wave propagates vertically through the material. Excitation takes place by means of thin-film transducers. They comprise the whole volume of the excited piezoelectric crystal. BAW compass

frequencies ranging from 5-50 MHz. By far the most known example of this category is the QCM. In this work, 10 MHz QCM substrates are employed. Thereby, a maximal sensitivity of 1 Hz/ng can be accomplished (77). From the previous formula, it can be derived that increasing its fundamental frequency leads to higher sensitivity. However, handling such quartzes becomes very inconvenient since frequency enhancements are paired with reduction in substrate thickness. In layman´s terms, quartzes break very easily (78).

SAW devices differ from the bulk variant in that they transmit their energy convergent on the surface of the material rather than through it. In other words, acoustic waves propagate parallel to the piezoelectric crystal. These devices are also marked by the presence of interdigital transducers (IDTs). These are finger-shaped zinc structures resembling two intertwined fine-toothed combs. Following the working mechanism, subjecting the structure to an alternating electric field leads to a time harmonic periodic deformation of the underlying piezoelectric material. As a result, each finger pair excites an acoustic wave perpendicular to its direction (78).

QCM can be seen as a protrusive technique for uncovering interfacial properties. In order to determine whether or not chemicals bind to the detection platform, quartz crystal microbalance (QCM) can be seen as a protrusive characterization method (77). Its simplicity, cost effectiveness and real time behaviour are only some of the many advantages of this measuring procedure (79, 80). After application of an alternating voltage between the electrodes, blank (uncoated) QCMs undergo mechanical oscillations at their proper eigen-frequencies. At this frequency, the system oscillates in absence of any damping or driving force. Functionalization of these samples results in additional mass and thus in a decrease in natural frequency. After a significant frequency drop, one can state that a binding event has taken place. The extent of the frequency shift dependents on mass size, following the Sauerbrey equation, denoted earlier. This observation allows one to monitor binding events taking place, but only for films that are rigid, homogeneous and sufficiently thin ($\Delta f/f_0 < 0.02$) (81). Energy dissipate to its proximate environment if coatings are too thick.

If microbalance and polymer-analyte complex oscillate independently, the behaviour of the system may deviate from its standard. In some occasions, even positive frequency changes are observed (82). This increase, also known as the anti-Sauerbrey effect, can be assigned to inaccurate imprinting resulting in deficient geometrical fit. This way, unimpeded motion of target molecules on the crystal surface occurs. Therewith, superabundance of analytes over available binding pockets may also result in this positive frequency shift.

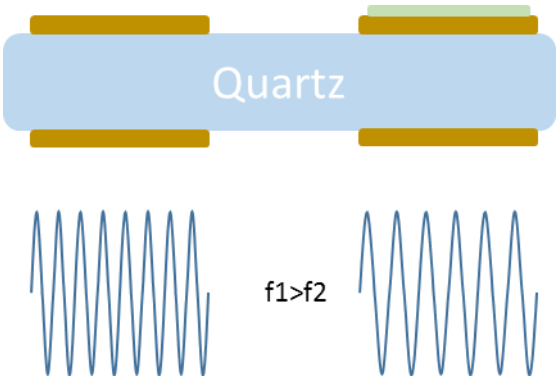

Figure 12: Influence of mass loading in fundamental frequency of a QCM crystal.

In numerous cases, however, the absorbed films cannot be considered rigid or homogeneous, causing other parameters to be of relevance as well; the film's viscoelastic properties, thickness and density should then also be taken into consideration. Viscoelastic films tend to dampen the sensor's oscillation, a phenomenon referred to as *dissipation*, which can be assessed through QCM-D analysis. Here, however, one deals with rigid layers comprising polyurethane. Therefore, QCM without dissipation monitoring is employed.

1.3.2. Challenges Related to QCM Experiments

Anti Sauerbrey effect

As already demonstrated, mass increase on a QCM surface results in a decline of fundamental frequency according to the Sauerbrey equation (72). Also note that this statement is only valid in case of homogeneous rigid layers (83). If quartzes are coated with polymers, these macromolecules have to oscillate synchronously with the crystal for the condition to hold. Here, addition of a certain analyte leads to frequency increases. This peculiarly effect is appointed to as the anti-Sauerbrey effect and can be considered the result of various causes (82). If binding sites are too wide, molecules are not able to bind in a tight fashion. Because of this surface mobility, molecules move freely in imprinted cavities and ultimately leading to frequency enhancements. Alterations from this frequency can also end up in anti-Sauerbrey behavior. Same conditions are required for analytes after their addition onto the sensor surface. Therewith, interfacial slippage between multilayer and liquid medium can also result in this behavior. At last, there might also be influence due to acoustic film resonance deriving from a sufficient thick film.

Drift

QCM measurements generally start after the system reaches stable baseline. Depending on the experiment, this may take some minutes, but can also last for hours. Aside from sinusoidal wave stabilization, it can also happen that the signal increases or decreases in a particular fashion. This typical behavior is called drift. Usually, it is present from the beginning of the experiment but in rare cases it may also originate during the measurement. At the end of a measurement, when the analyte is washed out completely, the baseline may not be at the starting frequency. One can correct this by drawing a slope through the curve of the measurement.

Temperature differences during the measurement

Since the exact frequeny in an oscillator circuit is temperature dependent, changing conditions have a possible influence on the measurement. Keeping the climate constant over the length of the measurement is crucial.

1.4. Atomic Force Microscopy (AFM)

1.4.1. Theory

Scanning probe microscopy (SPM) is useful for obtaining information about surface properties such as morphology, adhesion or magnetism using a probe to scan the specimen locally. Atomic force microscopy (AFM) is widely considered one of the most notable SPM subtypes. Gerd Binning invented this technique and together with his colleagues, he introduced it in 1986. As its name suggests, it is possible to image the surface topography with extremely high magnifications down to the atomic level. It results in 3D information, whereas electron microscopes cannot provide any details about the vertical dimension. Figure 13 depicts the general working mechanism of AFM.

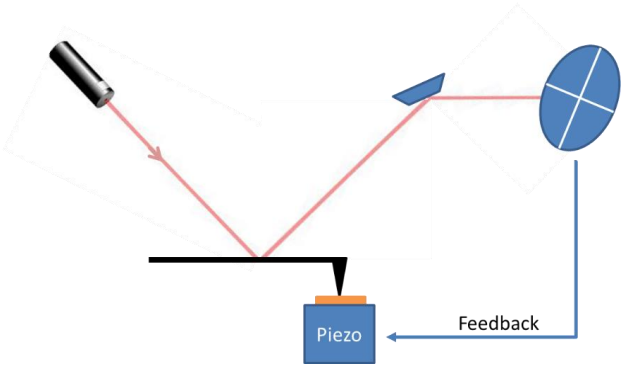

Figure 13: Schematic illustration of the AFM working principle.

The cantilever, featured by a sharp tip, scans the surface. This extremity is typically made of silicon or silicon nitride. It is possible to scan the surface by means of three different modes. In contact mode, the cantilever tip is in constant contact with the surface when scanning over it. Characteristic for this operating mode is the close vicinity of the tip to the top layer. The disadvantages of contact mode include that both brittle samples as well as the cantilever tip are easily damaged because of permanent contact. In non-contact mode, as its name indicates, the cantilever probe oscillates just above the surface rather than making contact with it. At last, tapping mode can be seen as the most commonly used operating mode and as the golden mean between contact and non-contact mode. Here, the cantilever tip encounters attractive and repulsive forces intermittently leading to minimal sample damage accompanied with high resolution. The working range of all three modes is shown in Figure 14. When the cantilever is far away from the surface, no interactions between tip and surface are observed. At a certain distance, attractive forces start to increase. At this point, it is feasible to measure by the non-contact mode depicted by the green part of the figures. There exists no contact between tip and surface. Approaching the cantilever towards the sample increases the attraction even more. This tapping mode principle (salmon rose part of the graph) allows to repeatedly touch the surface and pull

away the tip. Scanning in permanent contact with the surface is called contact mode and can be seen in the blue part of the graphs.

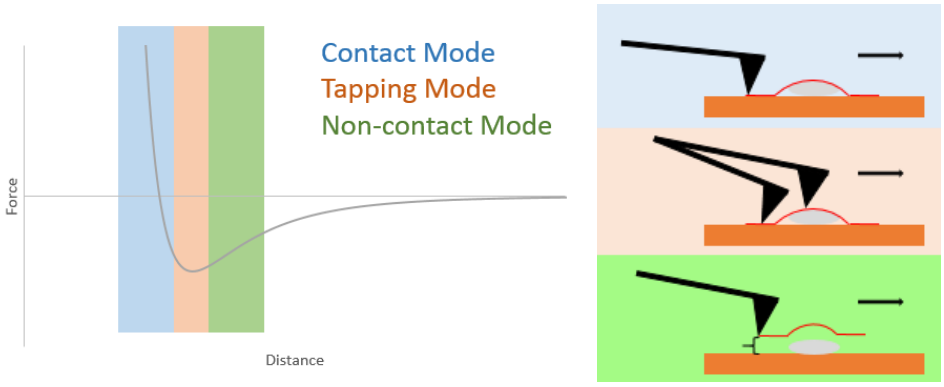

Figure 14: Different modes of AFM.

Varying shapes of the surface results in different deflections of the cantilever. By irradiating the cantilever using a laser beam, it is possible to determine the actual structure of the scanned top layer. A photodiode is used in order to perceive the beam sent out by the laser. The deflection of the laser beam is characteristic for the shape of the surface. When the tip is located "far" from the surface, forces between the two are negligible. Though, if the tip approaches the single atoms, the cantilever experiences an attractive movement because of Van der Waals, Coulomb and binding forces. There is a polarizing interaction between atoms. However, at a certain moment when the tip is too near to the atoms, a repulsive force (blue line) overrules the attractive component (orange line). These exchange reactions happen because the electron orbitals of the two atoms begin to overlap and is called Pauli's principle. This method is not only valid for single atoms but can also be applied to molecules. For simplicity, there will only be referred to interactions between two particles in the following explanation. Figure 15 demonstrates this behavior.

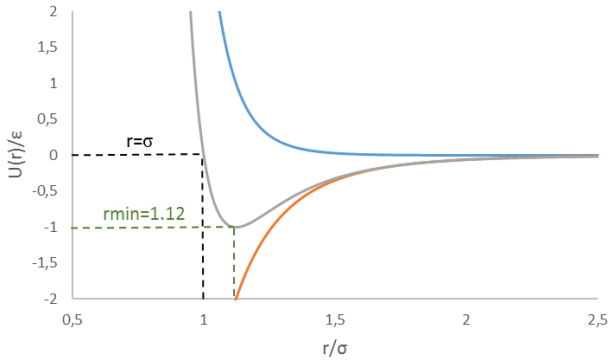

Figure 15: Lennard-Jones potential.

1.4.2. Contact Mode

Figure 16 represents a detailed picture of the AFM setup where the cantilever makes contact with polystyrene beads. In case of contact mode measurements, the probe is drawing near the surface until it experiences repulsive force. In constant-height mode, sample and probe are moved towards each other. Out of the various deflections of the cantilever, a surface profile (topographical map) is established. However, there is the risk of probe and/or sample damage. The cantilever height is readjusted continuously when benefiting contact mode with constant force. Here, the surface profile is obtained simply by readjustment of the cantilever. Advantageous for this method is the conservation of probe and sample.

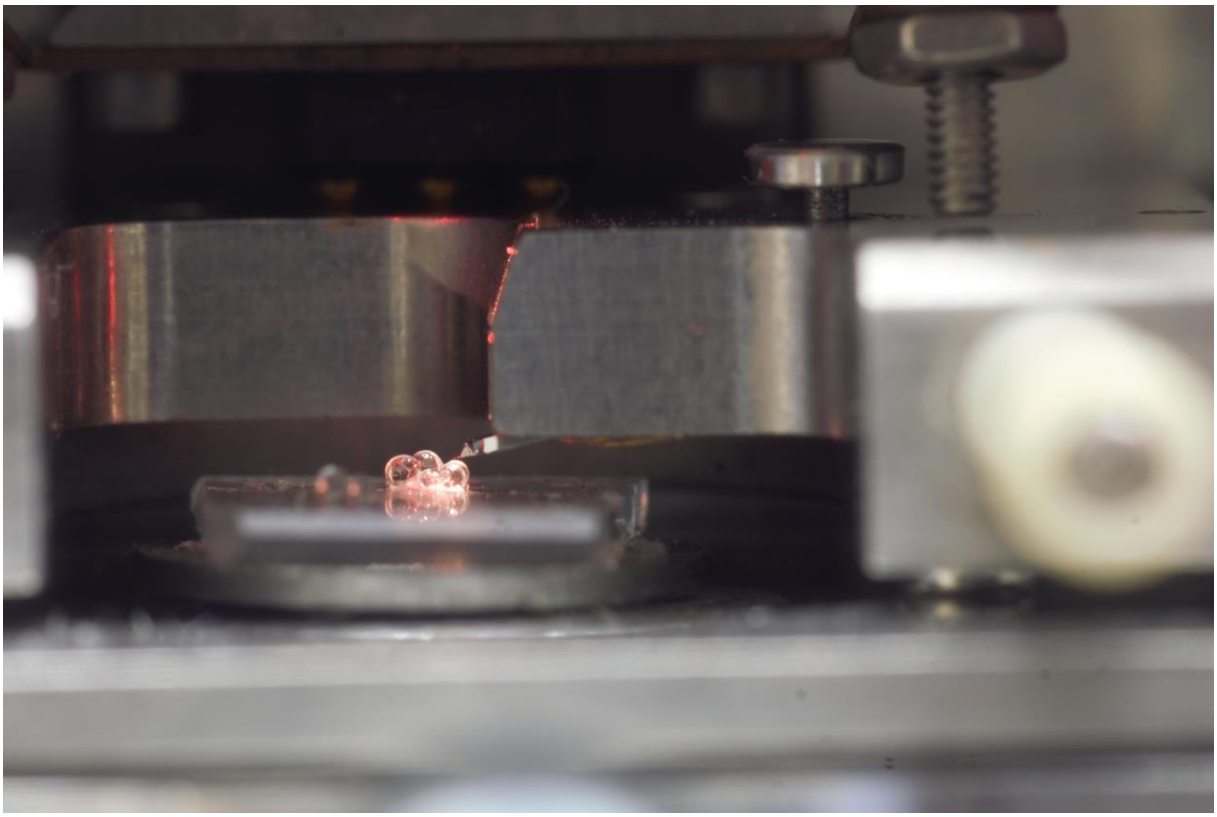

Figure 16: High-resolution image of polymer beads on a sample for AFM characterization.

1.4.3. Non-contact Mode

The non-contact mode is a dynamical mode where the cantilever functions as a harmonic oscillator. Under the influence of external forces, a resonance frequency deflection occurs. Conversely, this frequency shift is indicative for the working force. Cantilever and tip are stimulated to oscillate over a piezoelectrical element. Exclusively VDW interactions are taking place. Actions of the tip on the sample are ruled out. Different heights between tip and sample result in distinct resonance deflections.

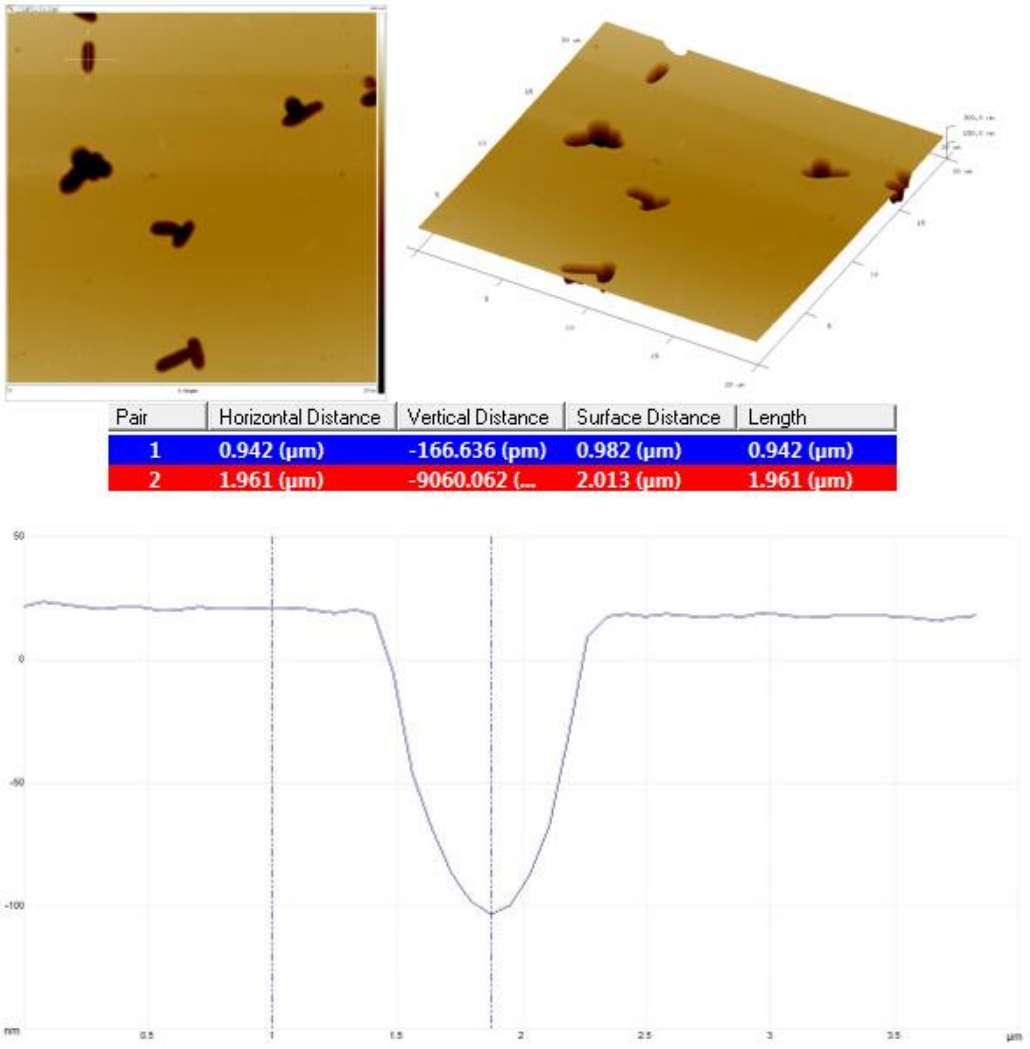

Figure 17: Profile of E. coli imprints in polymer matrix

This section shows a few examples of atomic force microscopy pictures taken by members of our working group. *E. coli* Bacteria are visualized on picture Figure 17. These gram-negative organisms are characteristically rod-shaped with a length of 2 µm and a diameter of 1 micron. Because of their size, it is also feasible to detect them by conventional light microscopy. In order to differentiate between the bacteria as such and imprints, AFM can be very helpful. Additionally, the depth of imprinting can also be visualized. From the picture profile, it can be stated that the bacterium imprint has a depth of around 120 nm. Moreover, AFM may provide additional information such as fimbriae and pili, which are too small to detect by the naked eye.

Tobacco mosaic viruses (TMV) deposited on glass slides are visualized in Figure 18. These pathogens have large variations in length from 80 until 400 nm and are typically 18 nm in diameter. Values found in literature confirm our results. Gold nanoparticles with a size of 50nm in diameter are displayed in Figure 19.

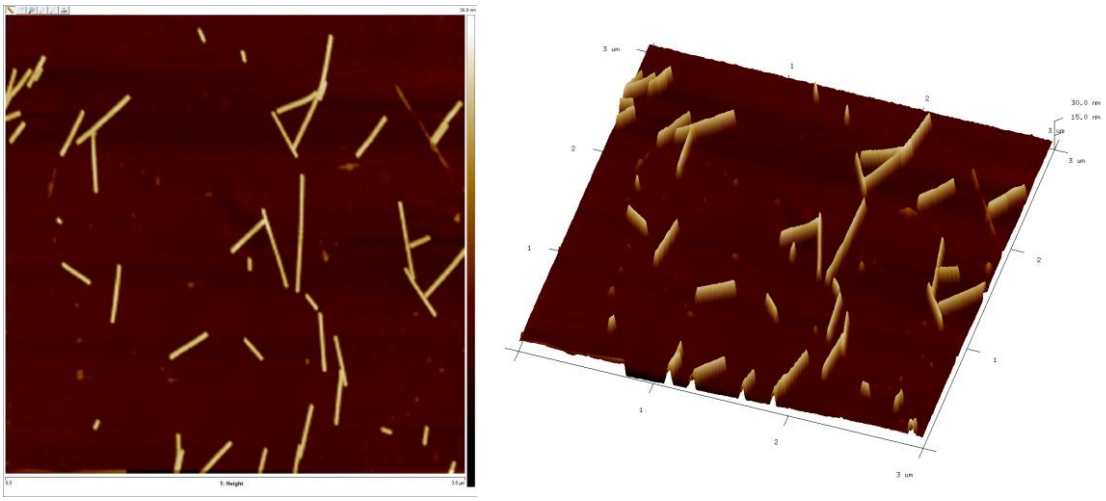

Figure 18: AFM image of tobacco mosaic virus (TMV) on a glass slide.

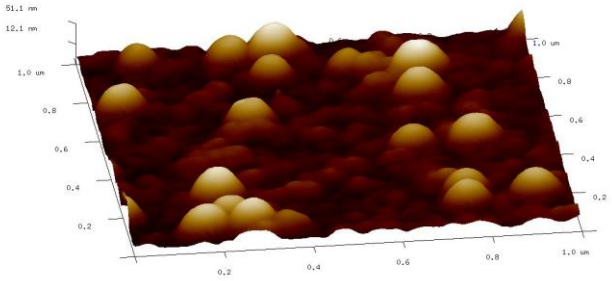

Figure 19: AFM picture of 50 nm large gold NPs on a silicon wafer functionalized by APTES.

1.5. Scanning electron microscopy (SEM)

Light microscopy cannot depict small molecules accurately because their resolution limit is around 200 nm lateral. Smaller particles (sub-nanometer size) can be characterized by other techniques such as AFM and SEM. Compared to conventional (light) microscopy, SEM relies on electrons as source of illumination rather than photons. Thereby, it circumvents the wavelength limitations. A schematic overview of SEM build-up and mechanism is given in Figure 20. During such an experiment, an electron gun illuminates the specimen with electrons in a high vacuum. When the beam hits the specimen, this results in two different types of electrons: The first type is known as secondary electrons (SE). In this case, atoms at the surface absorb the energy and emit their own electrons. These electrons can be detected by a positively charged Faraday cage. If they reach the detector, the information of the electrons results in an image. The second type of electrons are called backscattered electrons (BSE). SE originate from the electron source of the microscope and arise from atoms at the surface, whereas BSE originate from deeper parts of the surface. Its detector is vertically above the stage where the specimen is located, at the pole piece. If atoms are ionized, they may emit X-rays, which can be used to determine the composition of the sample.

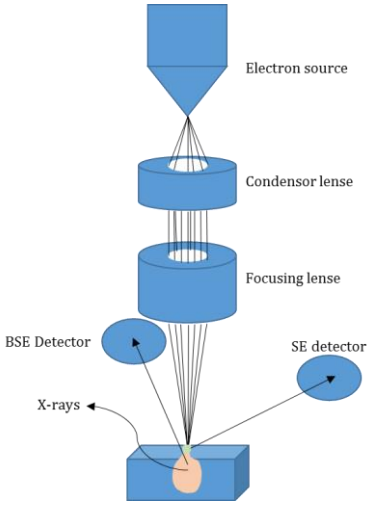

Figure 20: Schematic build-up of a scanning electron microscope (SEM).

Comparing both AFM and SEM, both are excellent candidates providing three dimensional nanometer-scale information about a sample. Smooth surfaces may benefit the use of AFM, giving highly detailed information about a certain material. SEM, on the other hand, is in favor for rough surfaces because of its intrinsic large depth of field. In addition, SEM also provides information about a sample´s composition through X-ray detection. AFM at its turn has the capacity to reveal compositional parameters such as adhesion, stiffness, modulus, magnetism, conductivity, phase and so on.

1.6. Analytes

1.6.1. Serum Albumin

Serum albumin is known to be the most abundant blood plasma protein in all vertebrates (84). Synthesis of this polypeptide takes place in the ribosomes of hepatocytes in the liver where it is formed as preproalbumin. Before arrival out of the endoplasmic reticulum, an 18 amino acid long N-terminal peptide is cut off by signal peptidase resulting in the origin of proalbumin. A further modification takes place in the Golgi apparatus, where proalbumin is cleaved by furin leading to the production of serum albumin and a six amino acid long extension (hexapeptide) (85, 86). Albumin is immediately released into the serum. The whole process is visualized in Figure 21.

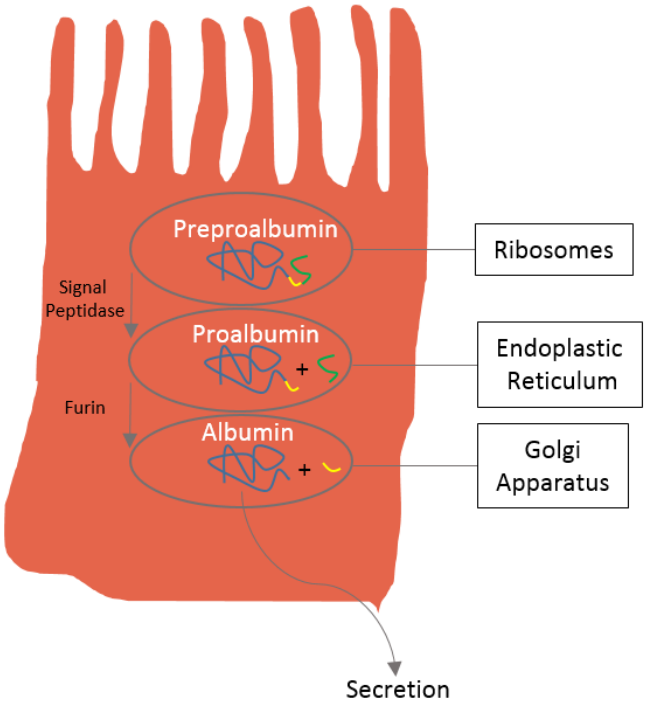

Figure 21: Graphic representation of serum albumin synthesis in a hepatocyte.

It circulates through blood for maintenance of the osmotic balance, more precisely the oncotic pressure. Despite of homeostatic regulation, it is also known for their outstanding ligand binding properties (87). Both endogenous and exogenous compounds can become coupled. SA is able to bind hydrophobic steroid hormones, nutrients and many other molecules in its hydrophobic cleft. Moreover, transport of haemin and fatty acids can be established. Deeper understanding about protein-ligand interactions between mammalian serum albumins is inevitable in order to obtain the full picture of their transport mechanism. Because of its wide availability, it can be bought at a reasonable price and its structure is one of the most studied ones.

Deviations from clinically normal albumin levels may be an indicator for the particular diseases related to kidney, liver or even the heart (9, 21, 88-90).

Every species has its own characteristic amino acid sequence for serum albumin. This work only highlights on bovine serum albumin and human serum albumin. These are the two proteins we worked with and are also the most clinically relevant for research and development.

Bovine serum albumin (BSA)

Laboratory experiments usually utilize bovine serum albumin (BSA) rather than human serum albumin. Both structures share 76% complementarity in amino acid sequences and also its functions are very akin. However, they differ in binding affinity towards certain molecules. BSA is a 66.4 kDa globular protein derived from cows (*bos bovis*) and is a major component of fetal bovine serum (91, 92). Its active form is a single polypeptide chain comprising 583 amino acid residues. Its three-dimensional structure is visualized in Figure 22 (93). Three homologous domains, labelled I-III, can be identified from the picture below. Each domain, at its turn consists of two subdomains (A and B). The whole complex is held together by 17 disulfide bridges. Comparing the amino acid sequences of BSA and HSA, a change in the subdomain IIA can be observed. BSA displays a larger amount of positively charged amino acids. Additionally, the active surface of this subdomain is more exposed in the case of HSA, resulting in alternative binding properties (94). Aside from different binding affinity, both molecules also differ in flexibility. BSA appears to be more rigid in solution than HSA. Literature frequently mentions the fact that HSA possesses only one tryptophan residue whereas BSA contains two (84, 94).

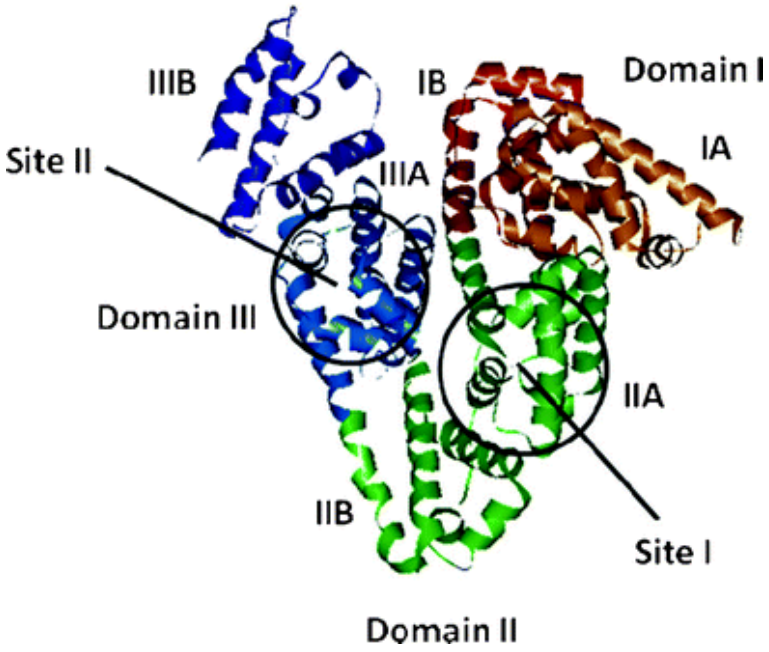

Figure 22: 3D crystal structure of bovine serum albumin and a subdivision showing all domains (93).

As already mentioned for albumin in general, the main function of this slightly acidic protein is to maintain osmotic blood homeostasis. Moreover, BSA also establishes transport of various ligands in the blood, both endogenous and exogenous. BSA, alternatively called Factor V, plays a significant role in biochemical applications (e.g. ELISAs, immunohistochemistry, etc.) (95). It can fulfil the role of universal blocking agent or stabilizer (of restriction enzymes) by binding nonspecific binding sites (96). It is also used as the model protein for protein–ligand binding studies(93). Furthermore, the indirect anti-globulin test (IAGT) employs the possibility of BSA to deduct negative charges of erythrocytes (97). In daily life, BSA is used as a culture medium during vaccine production (98). Due to its potential allergy-evoking behaviour, the WHO enacted a limitation of 50 ng BSA per dose (99). Interesting is the fact that BSA is related to both milk (100) and beef allergies(101).

BSA is characterized by excellent solution stability, leading to increased signals in assays. It is also praised for their absence of effect in many biochemical reactions. Another benefit is its low cost so as its multifunctional binding characteristics. It is also relatively resistant to digestion.

Attention has to be paid concerning the usage of BSA together with high temperatures and/or radiation. Heating above 50 °C results in the formation of hydrophobic aggregates. These complexes do not revert to their original conformation after cooling. UV C (100-280 nm), at its turn, induces protein aggregation. Tryptophan (Trp), tyrosine (Tyr) and phenylalanine (Phe) absorb UV because of their aromatic built-up. This results in electron generation followed by

recombination. As an outcome, disulfide bridges break ultimately leading to conformational changes.

As already stated, MIPs are synthesized at 70 °C. In order to preserve full shape and functionality of BSA, it is appointed not to include the protein as template in the (pre-) polymerization process. It starts to denature at temperatures above 40 °C. However, here one is still able to fully recover initial structure. Further increment of heating leads towards irreversible damage of helical structure. This way, it is our purpose to produce polymers followed by imprinting with heat-sensitive proteins at acceptable temperatures. Needless to say, selective recognition and reproducibility stay guaranteed.

Human Serum Albumin

HSA is encoded by the *ALB* gene located on chromosome 4 in locus 4q13.3 (61). **Fehler! Verweisquelle konnte nicht gefunden werden.** in the Appendix section visualizes the complete sequence of HSA. With a concentration of 3.5–5 g/dL and constituting more than 50% of the total protein content, serum albumin is known to be the most abundant blood plasma protein in humans (102). It has a molar mass of approximately 66.5 kDa and consists of a 585 amino acid long single strain. Its synthesis (10-15 g/day) is established by hepatocytes (103) and the serum half-life amounts about 20 days. It is marked by the highest solubility and lowest isoelectric point (4.7 at 25 °C) of all major plasma proteins.

Its structure can be described as a globular, unglycosylated complex. Its form is somehow heart-shaped with dimensions of around 80x80x80 Å. Approximately two-third of the conformation appears as α-helix and no β-sheets are present. Three homologous domains (I-III), all comprising two subdomains (A&B), can be differentiated. Due to the large presence of acidic and basic residues such as glutamic acid, aspartic acid, lysine and arginine, it is highly water-soluble. Having an overall net charge of approximately -15, the protein is of acidic nature. Its structure is displayed in Figure 23.

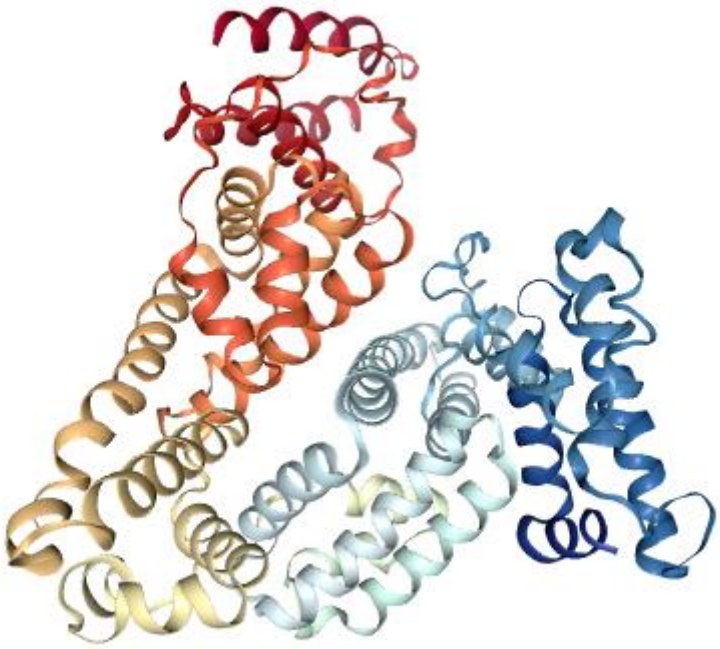

Figure 23: 3D structure of human serum albumin (HSA) (104).

Analysis is carried out to assess the nutritional status in individuals (105). Underexpression of this molecule is mainly due to liver function disorders such as cirrhosis (106), cancer (88), hepatitis, alcohol-related liver disease, and fatty liver disease (90). In addition, renal (9) and heart (90) failures may also lead to hypoalbuminemia. Finally, enteropathy and malnutrition can also result in reduced albumin levels. Treatment is possible by intravenous administration of albumin but also medication and changing nutritional behavior have an effect to increase the albumin amount in blood. Since prevention is better than healing, monitoring HSA levels in blood is major interest. Low numbers can be an indication for a certain disease. Early identification enhances chances for healing to take place.

Nowadays, detection of HSA is mainly established by electrophoresis or dye binding (107). But also immunological precipitation, salt fractionation and even color reaction measurements between albumin and hemin can be done. The latter method is not possible for BSA since it does not react with hemin the same way as HSA does. The first method is considered precise and is known as the golden standard for serum albumin measurement. Although this technique was accurate, it suffered from time-consuming steps and could not be automatized enough. A way to obtain quicker results was achieved in 1965 through the onset of an inverse colorimetric dye binding method, utilizing bromocresol green (BCG) (108). At present, this is the standard technique for identification of SA. In order to avoid over- and underestimations of protein, which

tended to occur by this technique, a similar method relying on bromocresol purple (BCP) rather than BCG was developed (109). It combines the benefits of the BCP method with greater selectivity towards albumin. Moreover, it is less responsive to other interferences in the sample. A thorough study showed that albumin detection performed by three different approaches (SPE, BCP and BCG), showed significantly different results. Therefore, the need for a reliable and standard method is of great interest. With the combination of molecular imprinted polymers and QCMs, we aim to obtain this goal.

1.6.2. Lysozyme

Accidentally discovered by Alexander Fleming in 1922, lysozyme gave rise to one of the most notorious breakthroughs in science (110).The observation that his own nasal mucus impeded a certain bacteria strain´s growth triggered great interest. While he was suffering from a cold, he must have dripped onto an agar plate resulting in the disappearance of the bacteria. He linked this phenomenon to the presence of a certain protein in his mucus. This protein causing bacterial cell lysis is from then on known as lysozyme. Intrigued by this fact, he started to deepen in the subject of antibacterial agents and ultimately led to the discovery of penicillin. For this achievement, he was awarded with the Nobel Prize in 1945 (111). Lysozyme is the first enzyme ever to be determined using X-ray crystallography in 1966 (112). It even is the first enzyme reported containing all 20 amino acids (113). Its crystal structure is given in Figure 24.

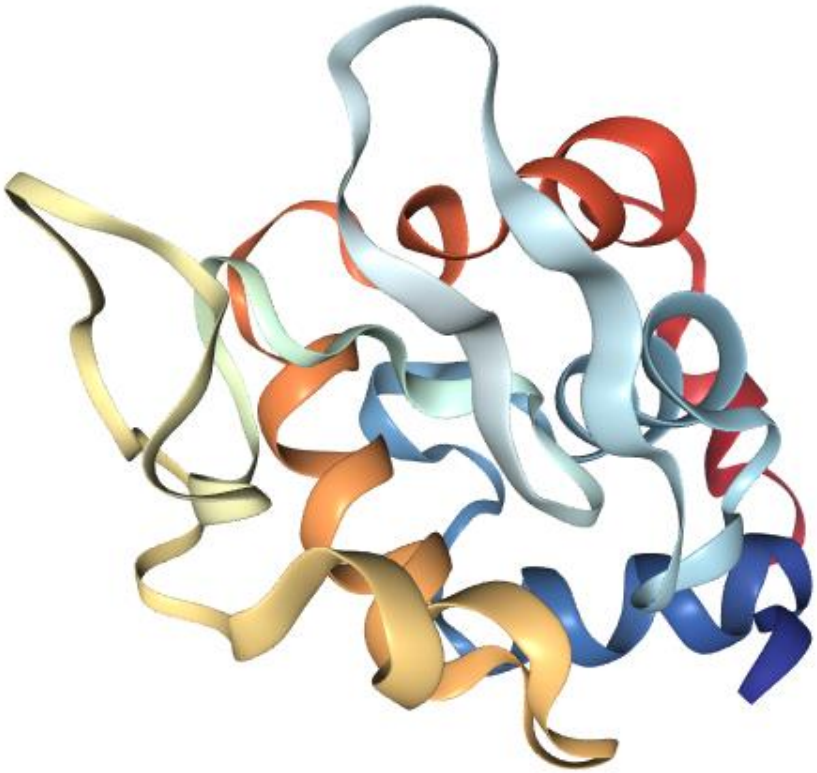

Figure 24: 3D structure of lysozyme. (114)

Lysozyme is bearing five α helices as well as five β-sheets. To sum up, lysozyme is a globular protein marked by a deep cleft forming the active site. It has a hydrodynamic radius of around 1.89 ± 0.025 nm (115). The protein possesses its maximal stability at pH 5 (116). Its melting point at this pH is located at 73 °C (117) whereas its isoelectric point is 11, thus being positively charged at neutral pH (118).

It is an antibacterial enzyme belonging to the innate immune system. Humans, animals, plants, bacteria and viruses all contain it in secretions such as mucous, tears, blood and saliva. Tears for example, contain 1.2 to 4.6 mg of lysozyme per mL (119). Its principal role is to hydrolyze glyosidic bonds in peptidoglycans of Gram-positive bacteria hence contributing in host defense (110). Since presence of this alkaline protein is inevitable for human life, it is necessary to identify lysozyme content in secretions or blood.

Possessing antimicrobial activity, lysozyme has the power to sabotage the cell wall of gram-positive bacteria by means of hydrolyzing β-1,4- linkages between N-acetylmuramic acid and N-acetyl-D-glucosamine residues in peptidoglycan. The protein therefore receives an alternative name, namely N-acetylmuramide glycanhydrolase. As a hydrolytic agent, lysozyme consumes water to cleave the bond. The enzyme acts as a catalyst by decreasing the activation energy of this process. Disruption of the cell´s boundary leads to lysis. On the other hand, the bond between C-1 of NAG and C-4 of NAM cannot be attacked (120). The antibacterial process is visually described in Figure 25.

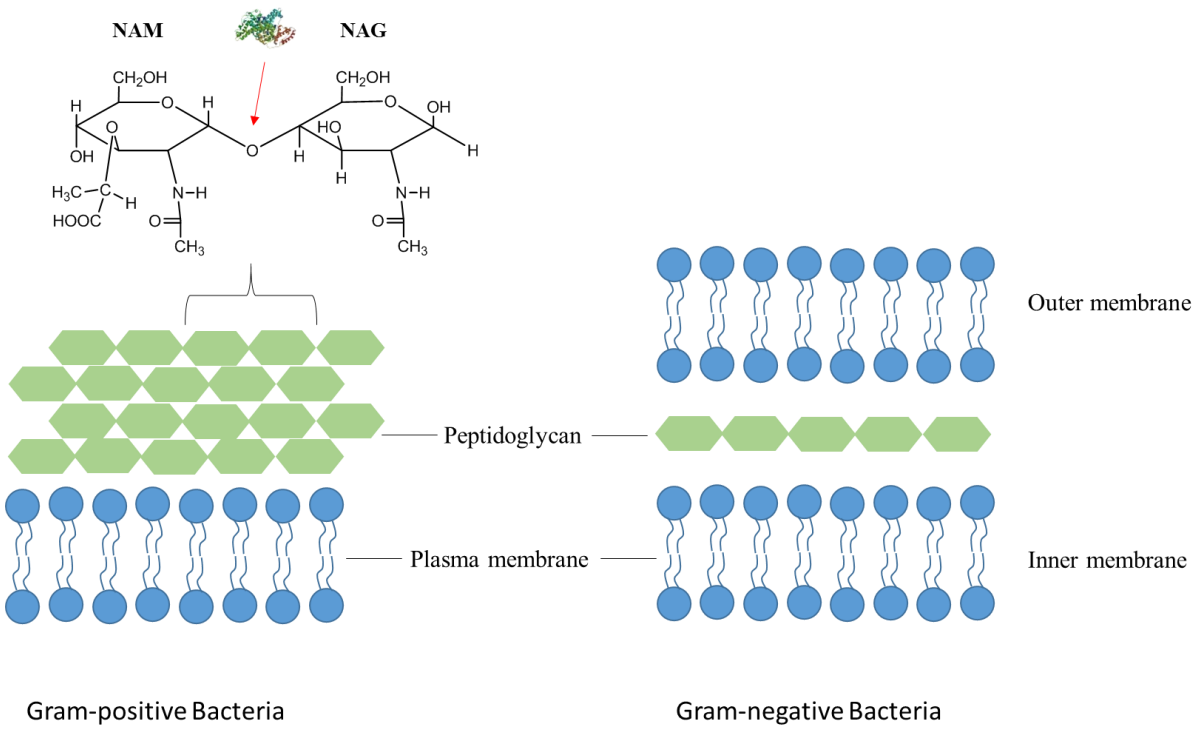

Figure 25: Scheme depicting the reaction mechanism of lysozyme towards the cell wall of Gram-positive bacteria.

For our research, lysozyme from chicken egg white was used. The active site of this protein consists of six subsites (A-F). It is widely accepted that cleavage occurs at the glyosidic bond between the D and E subsites. The amino acids corresponding to these units are glutamine and

aspartate at position 35 and 52 respectively. Acting as an electrophile, Glu35 donates a proton to the glyosidic bond. Aspartate at its turn then acts as a nucleophile by a backside attack on the C1 of NAM. This can only be achieved because lysozyme folds NAM to a half-chair conformation. Water acts as a nucleophile and attacks the C1 of NAM breaking the bond between NAM and aspartate. This mechanism is visualized in Figure 26. Weakening the integral structure of the cell wall can then result in bacterial death.

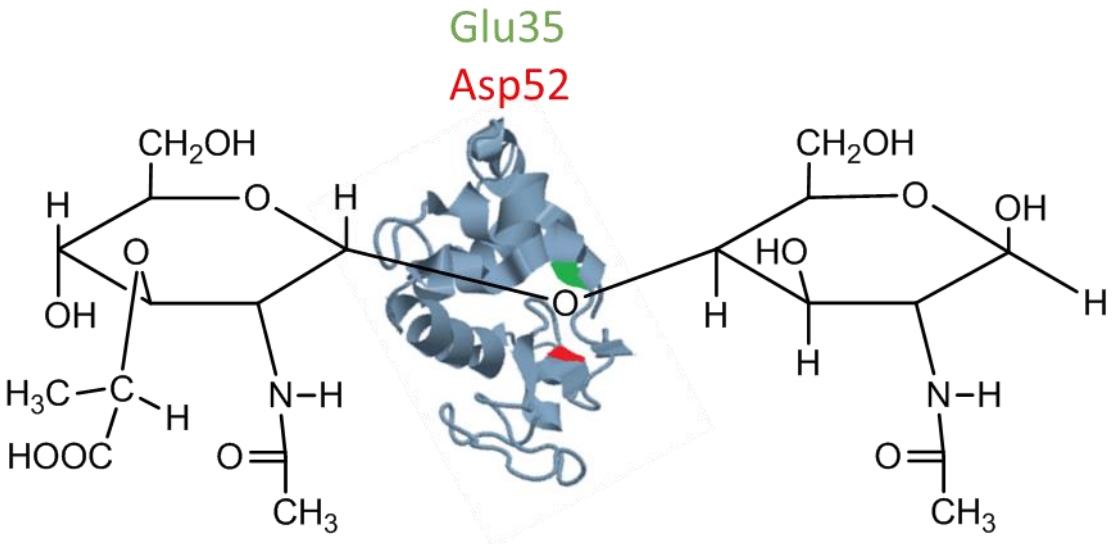

Figure 26: Hydrolysis mechanism of lysozyme in glyosidic bonds.

Lysozyme plays a vital role in food industry (121). Through its adoption, the usage of chemical antibiotics, e.g. nitrates and sulfites can be avoided. Moreover, food adulteration can be impeded this way. It is also used for food preservation and food safety by augmenting shelf life. It can be used in the cheese factory to prevent late blowing but also fulfills an antibacterial role in beer and wine production (122, 123).

Aside from nutritional advantages, the presence of lysozyme is also of considerable value for human kind. Protecting us against microorganisms, lysozyme acts like a guard in our life. This "body´s own antibiotic" acts as a boost for the immune system. Figure 27 shows various clinical examples where a concentration of lysozyme out of the healthy range can be used as a biomarker related to particular disorders. Shortage of the protein is related to a chronic lung disease in babies called bronchopulmonary dysplasia (124, 125). This disorder appears in infancy, mostly lightweight and/or early-born children are affected. Those youngsters are treated with extra oxygen in the beginning of their life since their lungs are not developed. Another example is conjunctivitis. It is familiar that our skin protects us from chemicals, pressure, radiation and so on. On our eyes, however, there is not such protective layer. Nonetheless, a small layer called

conjunctiva covers our eyes. Here, proteins (lysozyme and defensin) fulfill the role of protecting guards eliminating unwanted organisms from entering the human body. Lack of lysozyme in the human body may give rise to chronic irritating conjunctivitis (126). High concentrations of the antibacterial protein are found in TBC (127) and leukemia (128, 129). It also plays a role as biomarker in breast cancer (130), rheumatoid arthritis (131) and Alzheimer´s disease (132).

Albeit being beneficial for human kind, excessive numbers of lysozyme are usually not considered to be a good sign. In case of some cancers, maleficent cells tend to produce exorbitant amounts of lysozyme. This may eventually lead to kidney failure and low concentrations of potassium in the blood.

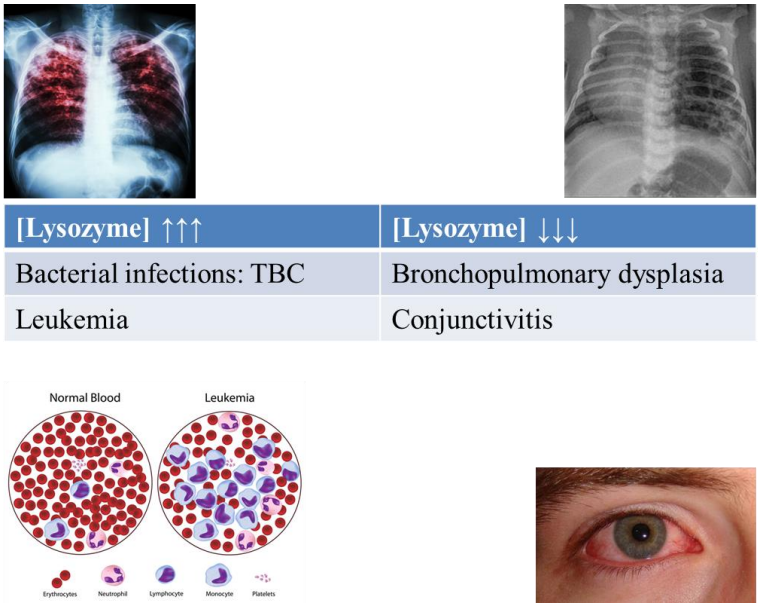

[Lysozyme] ↑↑↑	[Lysozyme] ↓↓↓
Bacterial infections: TBC	Bronchopulmonary dysplasia
Leukemia	Conjunctivitis

Figure 27: Lysozyme as a biomarker for various diseases (pictures from Google images).

Currently, there are some widely used characterization methods for lysozyme. One of them is based on *micrococcus lysodeikticus* cells (133, 134). These cells are used as substrate and the presence of lysozyme evokes lysis. During this process, the absorbance at 450 nm is constantly monitored to determine the concentration of lysozyme available in the sample. An LOD of less than 2 µg/mL is reached by this method.

Determination of lysozyme can also be achieved by chromatography or by ELISA immunoassays (135). Although immunoassays benefit high sensitivity, they often suffer from cross reactivity and interference with other matrix components.

In the last years, a method is developed for lysozyme detection using aptamers (118). The mechanism is based on the fact that free lysozyme and lysozyme-coupled magnetic beads compete

for anti AptLysTRAN-Bio in solution. The approach reached a limit of detection of 10 nM with linearity 5–140 nM for Lys. Approximately full recovery (99%) was obtained using this procedure. It also demonstrated significantly higher selectivity towards lysozyme compared to casein, BSA or cytochrome C.

Also graphene field-effect transistor (GFET) functionalized with selectively designed single-stranded probe DNA (pDNA) is proven successful for the detection of lysozyme in the concentration range from 10 nM to 1 μM.

2. Experimental

2.1. Materials

2.1.1. Chemicals

4,4'-methylenediphenyl diisocyanate (alternatively denoted as diphenylmethane 4,4'-diisocyanate (DPDI)), phloroglucinol (PG), 1,4-diazabicyclo[2.2.2]octane (DABCO), Ethylene glycol dimethacrylate (EGDMA), methyl methacrylate (MAA), acrylic acid, toluene, hydrogen peroxide (H_2O_2), ethanol, sulfuric acid (H_2SO_4), and sodium hydroxide (NaOH) were used as received from Merck KGaA. Divinyl benzene (DVB) was stabilized by 4-tert-butylcatechol and also purchased from Merck, 4,4′-Isopropylidenediphenol (Bisphenol A, BPA, ≥95%), azobisisobutyronitrile (AIBN) and (3-Aminopropyl) triethoxysilane (APTES, ≥98%) were purchased from Sigma-Aldrich. Polyvinylpyrrolidone (PVP, MM: 58 kDa) was purchased from Alfa Aesar GmbH&Co KG. THF was delivered both by Merck and Sigma Aldrich. Most monomers were stabilized by monoethyl ether stabilizer (>50 ppm). All untreated solvents used for synthesis were of HPLC/Analytical grade and were used as received. APTES was stored under argon gas pressure prior to use. Milli-Q grade water was used unless otherwise specified.

For preparing phosphate buffered saline (PBS), sodium chloride (NaCl), potassium chloride (KCl), disodium phosphate (Na_2HPO_4), monopotassium phosphate (KH_2PO_4) and distilled water dH_2O were needed. Table 2 describes the preparation of 10mM PBS. NaOH and HCl allowed for achieving a pH of 7.4.

Table 2: 10mM PBS preparation.

Component	Concentration [g/L]	Concentration [mmol/L]
NaCl	8.0	137
KCl	0.2	2.68
Na_2HPO_4	1.44	10.1
KH_2PO_4	0.24	1.76

2.1.2. Proteins

Bovine serum albumin (BSA) was delivered by both Amresco as well as Alfa Aesar. The purity exceeded 98%. Human serum albumin (HSA), on the other hand was obtained from Merck.

Lysozyme, egg white from chicken (CAS No. 12650-88-3) is delivered by VWR. We also received hen egg white lysozyme from Sigma Aldrich (>95% pure). Both revealed activity of >23000 U/mg.

Pepsin was obtained from Sigma Aldrich with a protein content of 99.7% and a purity greater than 98%.

2.1.3. AFM Tips

For contact mode experiments, silicon nitride (SNL-10) cantilevers were used. Tapping mode measurements, on the other hand were executed by RTESPA or TESPA-V2 cantilevers. All cantilevers were purchased from Bruker Metrology. The properties of both types of cantilevers is given in the following boxes. Table 3 and Table 4 display the properties of contact and tapping mode tips respectively.

Table 3: Contact mode tip.

SNL-10	Wafer: A041/01	
Cantilever T	600 nm	
	f_0 (kHz)	**k (N/m)**
A	50-80	0.35
B	16-28	0.12
C	40-75	0.24
D	12-24	0.06
Coating front	/	
Coating back	Ti/Au 45 nm	

Table 4: Tapping mode tip.

TESPA-V2	Wafer: A003/12
Cantilever T	3.8 µm
L	127 µm
W	35 µm
f_0	320 kHz
D	42 N/m
Coating front	/
Coating back	40 nm Al

2.1.4. Quartz Crystals

AT-cut quartz crystals were obtained from Great Microtama Electronics, Indonesia (Order number TRD 00198 BZ/009223). They have a fundamental frequency of 10 MHz (9.970-10.030 MHz) corresponding to a thickness of 168 μm. Their diameter equals 14 mm. Furthermore, they are characterized by a cutting angle of 35°15'±3° in respect to the optical z-axis orientation.

2.2. Techniques

2.2.1. Sieve Pattern Manufacturing

Sieves patterns are tailor-made and synthesized by means of photolithography. Figure 28 shows a picture of the in-house-made sieves.

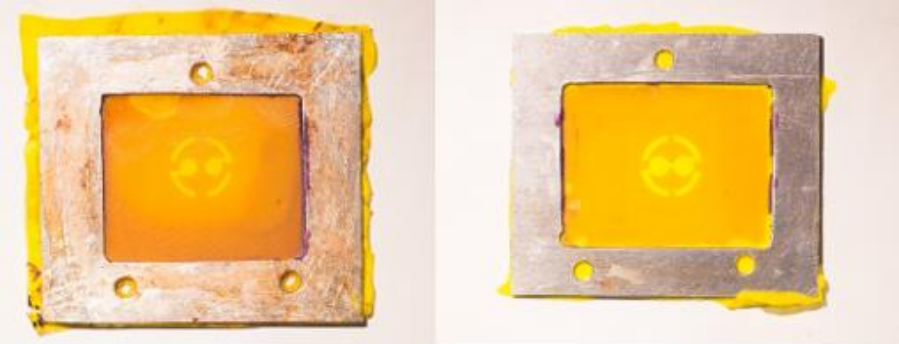

Figure 28: Picture of the sieves used for screen-printing. Left) Sieve with the pattern for the "back" side of the quartz which is in contact with air. Right) Sieve with the pattern for the "front" (i.e. sample) side of quartz which is in contact with liquid.

Sieves with 21 µm are affixed onto a metal frame by means of superglue. Next, the sieves surface was homogeneously covered with UV Photo lacquer (Azocol Poly-Plus, KIWO). The unit is dried for 30 minutes in darkness. UV-transparent film containing the desired electrode structure is adhered to the UV-lamp table. Here, two different sieve patterns are established. One template exhibits 5 mm diameter electrodes while the other is characterized by 4 mm diameter electrodes. The sieve is placed over the template and UV-lighted for 30 seconds. This way, light is blocked at regions displaying the electrodes. Photo lacquer exposed to the light hardens. The whole is washed with water in order to remove the unhardened material from regions representing the electrode structure.

2.2.2. Screen Printing

Figure 29 demonstrates the whole screen-printing procedure. To print electrode structures onto QCM, we used brilliant gold paste (GGP 2093, 12% gold, from Heraeus) stored in the fridge at 4 °C. Quartz crystals are kept in place by a vacuum pump. After patterning one side, crystals are baked in an oven at 400 °C for four hours to remove organic residues and to reveal homogeneous gold layers. Thereafter, the other side is screen-printed using the other template.

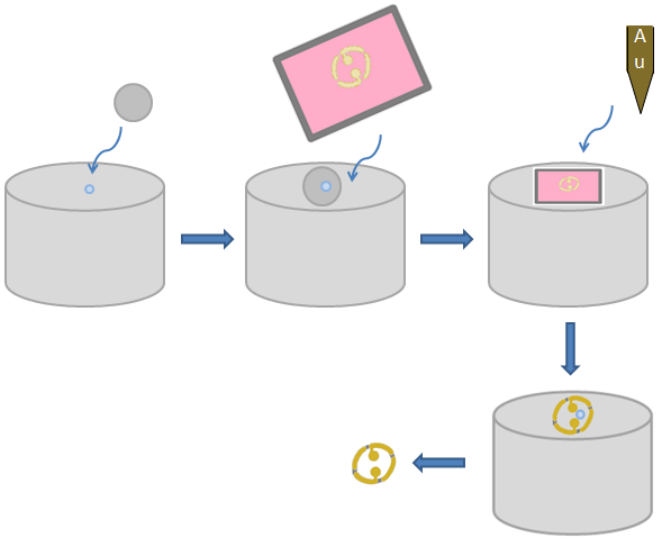

Figure 29: Graphic representation of the screen-printing process.

Quartz crystals before and after printing are depicted in Figure 30. Measurements are executed benefiting the use of dual electrodes. In this structure, one electrode serves as a reference compensating for physical interferences such as temperature alterations. Chemical composition of the analyte solution can be kept constant using this technique. In addition, viscosity effects can be reduced and plausibly eliminated in this way. Measurement errors depending on the environment are therefore the same for both channels. The quartz surface is now featured by electrodes with a diameter of 5 mm on one side while the other side is marked by electrodes having a diameter of only 4 mm. This enables us to address conductivity changes arising while measuring in liquid solutions. This effect needs to be minimized because it has an influence on the parallel capacity of the quartz, which at its turn affects the resonance frequency. Coating happens on the larger electrodes and these surfaces evidently stand in contact with the liquid phase during the measurement. The smaller electrodes are not exposed to the analyte solution and are required to complete the electronic circuitry.

Figure 30: Left) Schematic drawing of QCM electrodes; Right) Picture of a quartz crystal before (left) and after (right) gold electrode coating (screen-printing).

2.2.3. AFM Setup

AFM measurements were performed on a Bruker Multimode apparatus, Nanoscope VIII. Figure 31 shows the setup of our AFM device. Image analysis and adjustments were established by both the instrument software as well as through Gwyddion (GNU General Public License 2.53; http://gwyddion.net/download.php).

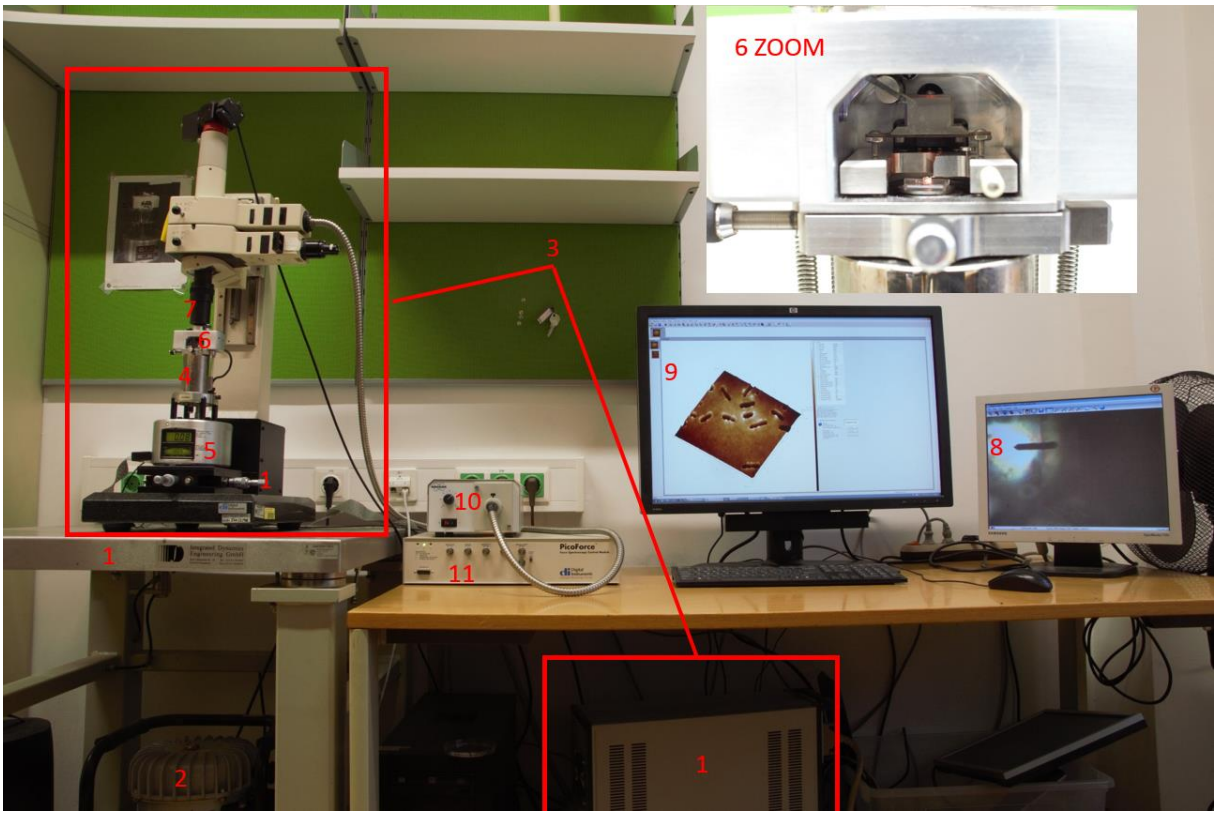

Figure 31: AFM set up consisting of different components: 1) air table, 2) compressor, 3) AFM device, 4) sample table, 5) piezo scanner, 6) sample compartment, 7) optical microscope, 8+9) screens, 10) lamp, 11) Pico Force device.

2.2.4. QCM Setup

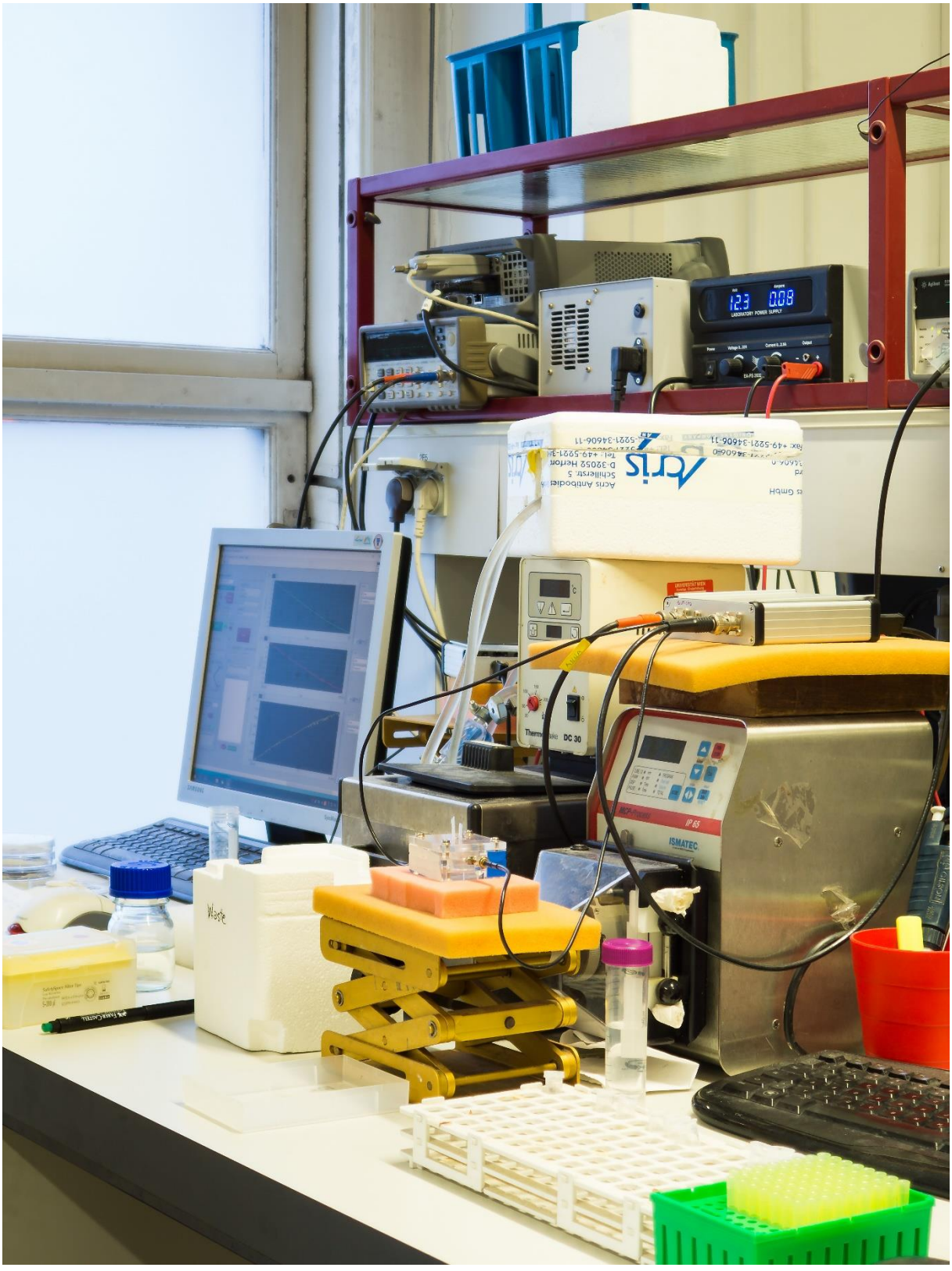

Figure 32: QCM setup in the lab.

Figure 32 presents the QCM set-up. It consists of following parts: 1) a measuring cell, 2) an oscillatory circuit, 3) a frequency counter, 4) a power supply, 5) a computer with Labview software. For some measurements a 7) peristaltic pump was used.

The QCM setup consists of many parts such as:

1) Preventing the measurements cell for unwanted vibrations and to ensure better shielding, it can be placed on a cushion, in a Plexiglas box or even in a Faraday cage. A picture of the measuring cell is given in Figure 33.

2) The oscillation circuit is custom-made and comprises two amplifier circuits, one for operating the quartz and the other one for signal amplification.

6) An MCP peristaltic pump of ISMATEC was utilized for flushing liquids through our measurement cell. The flow rate was set at 0.2mL/min.

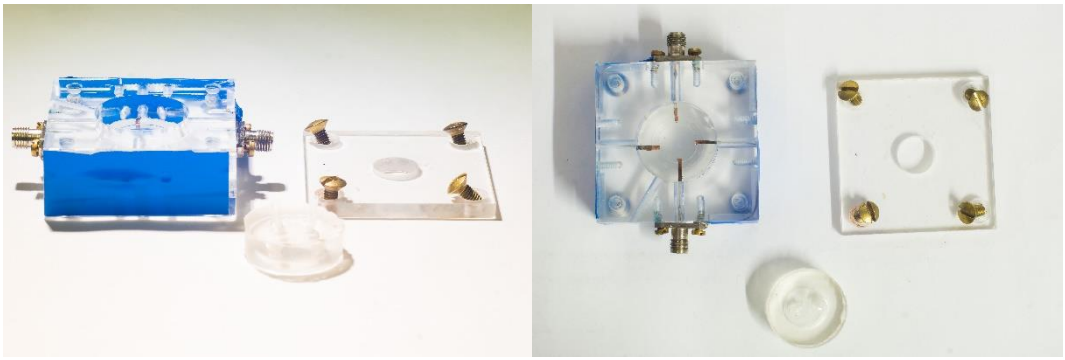

Figure 33: Photo of the measurement cell with its two SMA jacks, the closing lid and a PDMS stamp with inlet and outlet.

Experimental set-up of QCM measurements

Exploitation of QCM crystals takes place using a tailor-made oscillator circuit. Frequency measurements are carried out with a 2-channel frequency counter (Agilent Technologies 53131A, 225 MHz) and a laboratory power supply (EA-PS 2032-025). Data acquisition is performed using homemade software, a program relying on Labview software.

Two types of QCM experiments are executed in this thesis. During the first, measurements were done under stop-flow conditions. Each time a different solution was injected into the measurement cell, the measurement is paused. After some time, the signal reaches a rather stable signal under normal conditions. On the other hand, the second type of experiment was accomplished through the use of a peristaltic pump. The latter one allows for continuous and constant flow through the system. Nonetheless, this insurmountably leads to noisier signals. QCM measurements were begun at the moment when a stable baseline was achieved. Figure 34 shows the onset of this phenomenon.

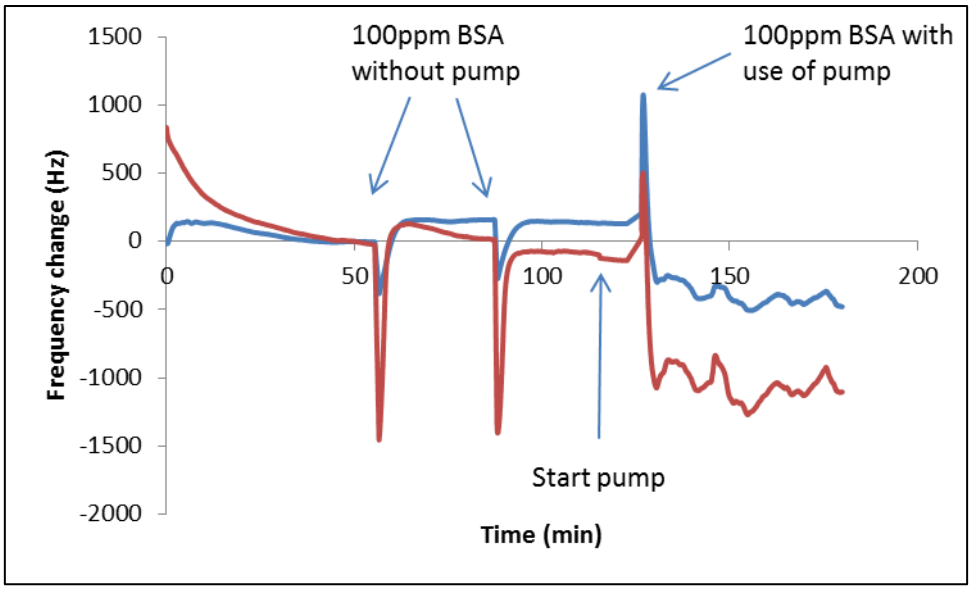

Figure 34: Influence of peristaltic pump on stability of QCM signal.

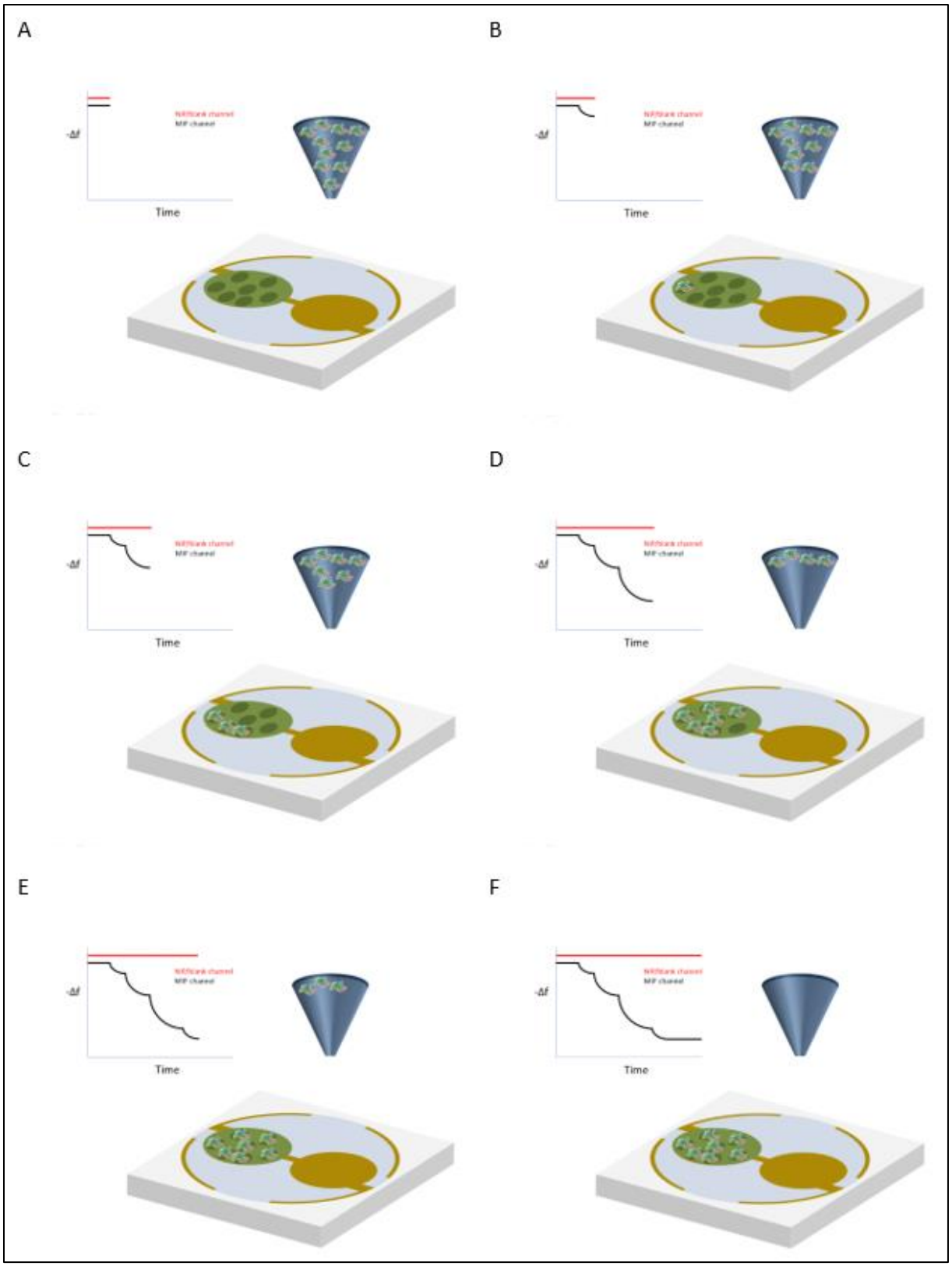

Figure 35: Working mechanism of a QCM measurement; A) Start of the measurement. B) Addition of analyte. C+D) Further addition of more concentrated analyte solutions. E) Saturation level is reached. F) Stable frequency signal due to saturation.

Figure 35 shows a graphical representation of the QCM working mechanism. A two-electrode quartz oscillates at its fundamental frequency. One side (green with holes) is covered by a MIP towards a certain analyte whereas the other electrode (gold) represents a blank/NIP-coated reference channel. A) At the start of the measurement, the frequencies of both channels are stable. B) Addition of analyte results in binding into binding pockets of MIP. Ideally, no analyte binds on the reference side (blank or NIP coated electrode). This can be seen in the graph located in the upper left corner of each figure. The black line describes the sensor response of the working electrode. Similarly, the red line depicts the signal of the reference side. Binding leads to a decrease in frequency in case of MIP. The reference side, however, stays unchanged. C+D) Increasing the concentration of the analyte leads to more prominent frequency decrease on the working electrode. Ideally, it should not have any influence on the signal of the reference. E+F) At a particular concentration, all accessible cavities are filled. This state is known as saturation and larger concentrations do not result in significantly bigger responses. It should be noted however that this representation is pure theoretically and does not fully reflect the real outcome of an experiment. Due to unselective binding, the analyte also produces a signal on the reference side. Since we operate these double-electrode QCMs, it is possible to cancel out unwanted binding effects. Furthermore, it does not always occur that the signal is as straight as represented. More on this topic is described in the section of QCM theory.

2.2.5. Network Analyzer

An Agilent 8712ET RF network analyzer was used to determine the frequency changes of quartz crystals before and after coating the electrodes with polymer. Additionally, removal of the analyte from the polymer surface was also monitored this way. Figure 36 shows a picture of this network analyzer in our lab.

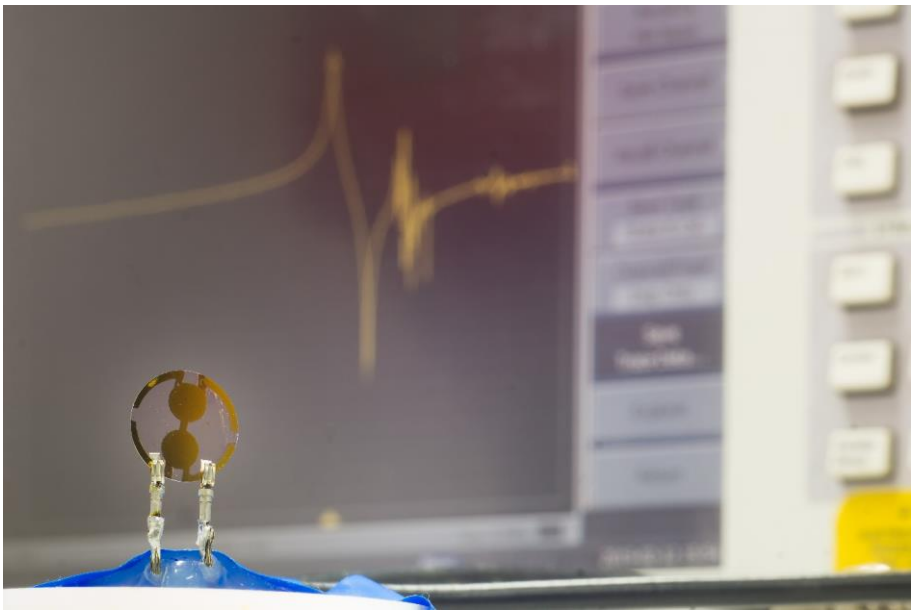

Figure 36: Quartz connected to network analyzer and its corresponding frequency/damping spectrum faded in the background.

Mass addition onto the electrodes leads to decreases in resonance frequency. Likewise, frequency changes can be coupled back to alterations in layer height, washing out of analyte, etc. After coating with a polymer and analyte, the frequency (and damping) decreased. Out of this frequency change, layer thickness and thus mass addition can be calculated. Washing out of the analyte results in an increment of the frequency signal, now located between the two previous curves. In addition, the damping of our platelets was investigated. Quartzes characterized by excessive damping values (large negative dB values) indicate inhomogeneous surfaces and most probably give rise to unstable QCM measurements. Network analysis allows therefore for a quick test in order to remove these samples with intrinsically high noise. This way, long waiting times are avoided and the QCM can be removed.

Filename List	Legend Name	Frequency [MHz]	Damping [db]	Calculate Thickness
A1A.CSV	blank electrode	9.874109	-3.10	☑
A1AC.CSV	coated electrode	9.867730	-3.55	☑
A1AW.CSV	washed	9.868668	-3.78	☑

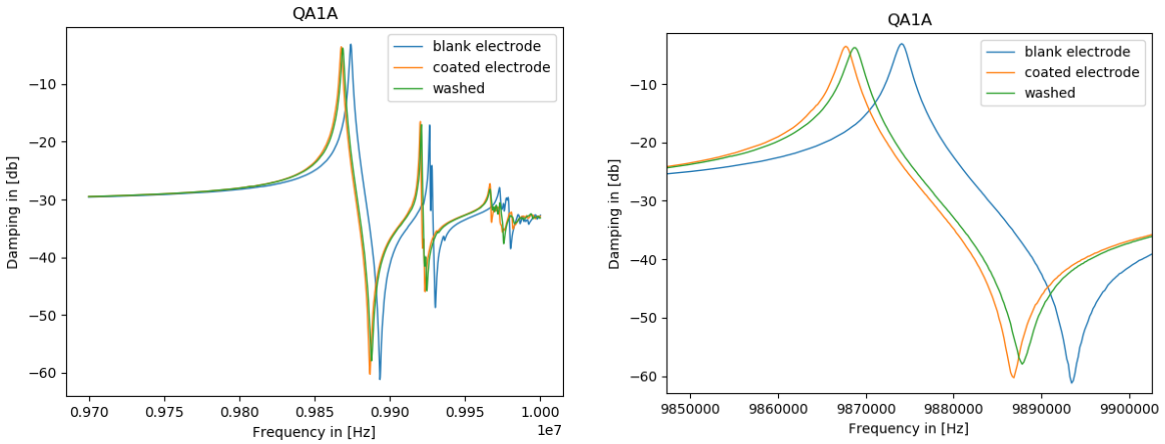

Figure 37:Network analyzer spectra of a QCM before (blue) and after (orange) imprinting as well as after removal of the template (green).

Figure 37 shows the network analysis spectrum of a quartz electrode before (blue line) and after coating (orange line) with a polymer. Three distinct clusters of resonance signals can be observed here. The main interest lies in the larger of three visible peaks here. When zooming in at this frequency, it can be seen that the curve shifted to a lower frequency after coating. By using the Sauerbrey equation, it is possible to calculate the layer thickness of the polymer. Depending on the density of the polymer, in this case polyurethane, the thickness changes. For this measurement, we obtained a value of 251.29 nm assuming a density of 1.15 g/cm^3. Also since this electrode now contains polymer as well as analyte, washing out the analyte results in an increase of 96 Hz. Except for the frequency, this graph gives us also information about damping, a measure of the homogeneity of the surface. Flat, rigid surfaces are characterized by low damping values (close to 0 dB). If the surface gets rougher however, for example in case of coating with a polymer, this value changes. Also placement of the quartz in a liquid leads to a damping alteration since liquid molecules settle on the quartz and form an insulating layer where dissipation may appear. The graph here displays a damping value of -3 dB in air. Likewise, it is also feasible to determine the layer height for the non-imprinted channel. However, after the washing step, no or little frequency change should be observed since no analyte is present in the matrix. A rise in frequency might indicate unwanted removal of polymer.

2.2.6. Fourier-transform Infrared Spectroscopy (FTIR)

FTIR is a technique to enlighten the structure of molecules by determining their functional groups. In this work, a Perkin Elmer Spectrum 100 spectrometer was used to monitor the progress of the polyurethane formation. The goal was to determine the moment when isocyanate and diol groups form urethane bonds due to heating. 5 µL of polymer solution was pipetted onto the ATR crystal to perform the analysis. Spectra were taken every five minutes in the range of 4000 to 600 cm^{-1}. Each measurement, eight scans were performed and averaged to become reliable results. A picture of the setup can be found in Figure 38.

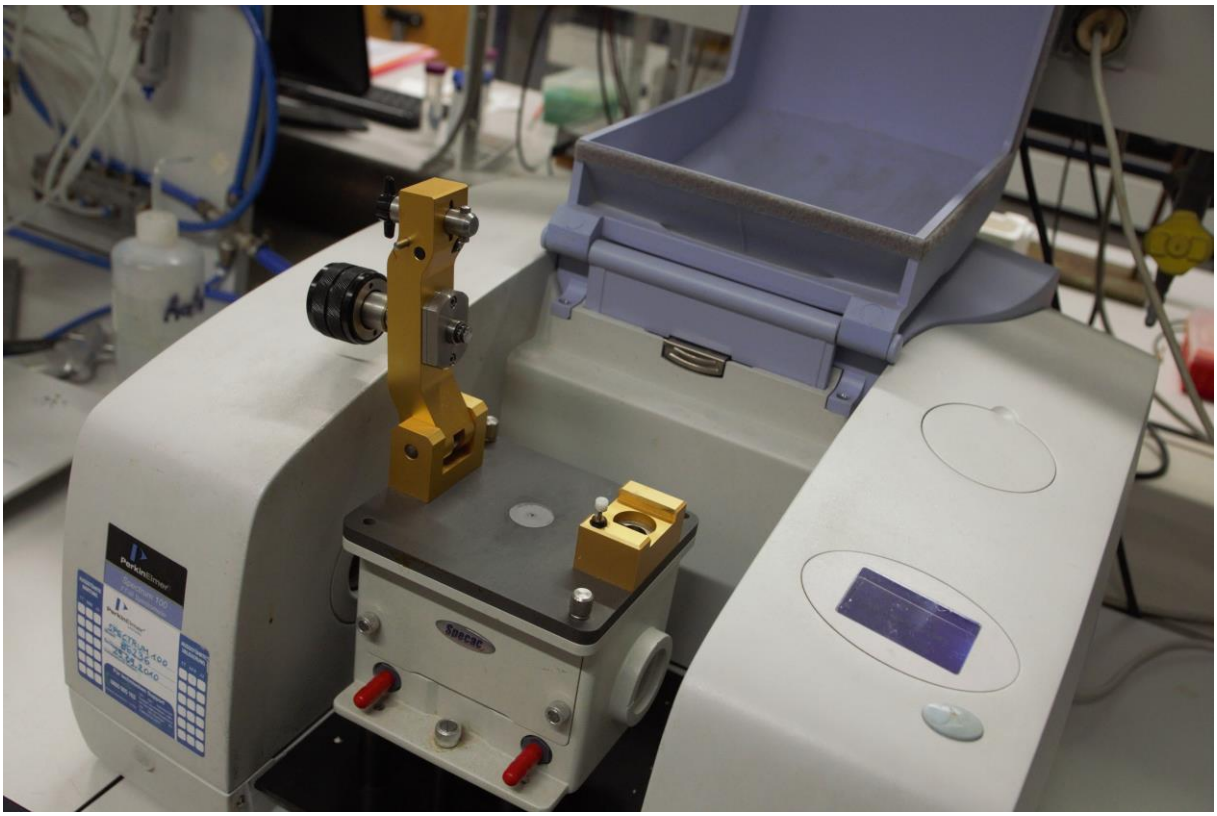

Figure 38: Picture of Perkin Elmer Spectrum 100 spectrometer.

2.2.7. Scanning Electron Microscope (SEM)

SEM measurements were carried out by administering few microliters of our sample onto silicon wafer. All samples were carried out by the Zeiss Supra 55 VP Scanning Electron Microscope. The standard settings for the SEM were an acceleration voltage of 5 kV, a working distance of circa 7 mm and an aperture size of 30 µm. All measurements were performed with the SE2 detector.

2.2.8. Dynamic Light Scattering (DLS)

The Zetasizer Nano (Nano-S) particle-size analyser from Malvern Instruments measures the size distribution of small (sub-micrometer) particles in solution. It uses the dynamic lights scattering technique to obtain this result. Here, a monochromatic light source is passed through a first polarizer and the sample. After being scattered by the presence of molecules in the sample, the light is collected by a photomultiplier after being passed through a second photomultiplier. A speckle pattern is created and out of this, the system can relate it to particle size. The principle relies on Brownian motion stating that large particles move slower compared to small particles. The rate of fluctuation in scattering intensities is determined by the size of the particles. In our case, we were interested in the average size of TEOS particles, before and after functionalization. DLS measurements lead to an average particle size (Z-average) and a polydispersity index (PDI). Values below 0.05 correspond to monodisperse samples whereas values above 0.7 represent broad size distribution. As a result, values leaning towards 0.05 are preferred.

2.2.9. Spincoater

Spincoating results in homogeneous layers by spreading the initial droplet over a flat surface using centrifugal force. In this work, the spincoater is used to deposit our pre-polymer onto the quartz electrodes. To achieve this, we used a PI-KEM LTD G3P-8 spin coater. One can set various settings such as speed (rpm), time (s) as well as ramp time. The latter parameter describes the time needed to approach the maximum speed. All these functions can be modified individually to obtain the desired layer thickness. Spincoating results in homogeneous layers by spreading the initial droplet over a flat surface using centrifugal force.

Figure 39: Working principle of a spincoater.

2.2.10. Xanthoprotein Reaction

In order to determine the amount of protein in a solution, the xanthoprotein reaction can be used. More specifically, aromatic amino acids consisting of a phenyl ring (phenylalanine, tyrosine and tryptophan) can be detected by nitration using a concentrated nitric acid solution. Nitration of the ring structure leads to the yellow (xantho) colour of the mixture. This test gives a qualitative idea about the presence of protein in a sample but can also be used to distinguish between AAs with and without a phenyl group. Because phenylalanine is difficult to nitrate, its presence is not as visible as the other two aromatic amino acids.

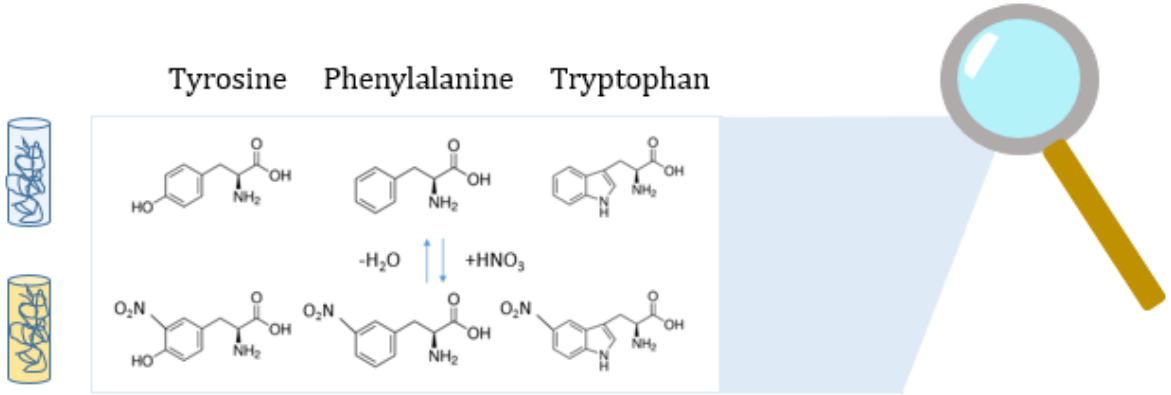

Figure 40: Graphical representation of the xanthoprotein test.

2.3. Synthesis

This section focuses on the various synthesis procedures employed in this work. As already discussed in the introduction, there exist multiple types of imprinting (bulk, stamp, sedimentation, …). For all these methods, even more distinct polymer systems can be used. The most known polymers in combination with QCMs are polyamides, polyesters, phenol-methanal plastics and polyurethanes. These are all made by condensation polymerization. On the other hand, there are a lot of polymers formed by addition polymerization. Think of polyvinylchloride (PVC), polystyrene (PS) and polymethyl methacrylate (PMMA). Here, we enlighten several procedures of polyurethane, DHEBA-MAA/AA(-VP) and HEMA-EbAM synthesis for BSA and lysozyme imprinting. If not stated otherwise, templates were removed using dH_2O only.

2.3.1. Polymer Synthesis for BSA

For any template, an optimal choice of monomers and crosslinkers has to be selected in order to obtain highly sensitive and selective imprints. Other groups have already demonstrated the great affinity of acrylamide and acrylic acid towards the protein in molecular imprinting (136). Looking at the structure of methacrylic acid (MAA) in Figure 41, it is considered to establish hydrogen bond formation with lysozyme. Additionally, coulomb interactions with the cationic residues of lysozyme can also be evoked. Acrylamide is capable to attach to lysozyme through hydrogen bonds as well. Also methyl methacrylate and ethylene glycol dimethacrylate were used as functional and cross-linking monomers, respectively in the past (137). Acrylates (such as 2-(dimethylamino)ethyl methacrylate for example) are also able to form hydrogen bonds with the protein. They can also create coulomb interactions with the anionic residues of lysozyme.

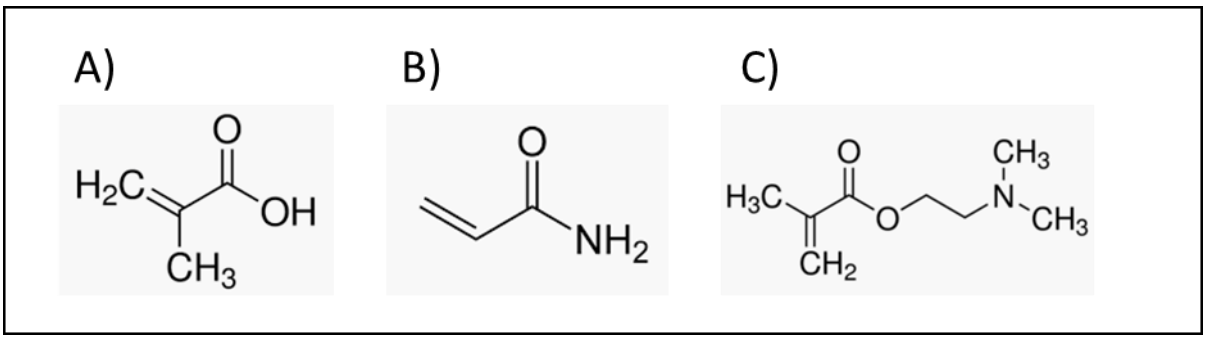

Figure 41: Chemical structures of methacryalic acid, acrylamide and 2-(dimethylamino)ethyl methacrylate.

Our group already published MIP sensors comprising of acrylic acid, N-vinylpyrrolidone and N,N´-(1,2-dihydroxyethylene) bisacrylamide. Several combinations for synthesizing BSA-imprinted polymers were tested (137).

DHEBA-MAA

60 mg (30 mmol) N,N′-(1,2-Dihydroxyethylene)bis-acrylamide (DHEBA), 12 mg (14 mmol) methacrylic acid (MAA) and 24 mg (14 mmol) dimethylamino propyl methacrylamide (DMAPMA) were dissolved in 3 mL of a 2 mg/mL sodium persulfate (in 10 mM PBS) solution. The structures of the monomers can be found in Figure 42.

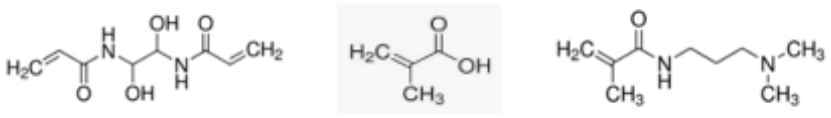

Figure 42: Structures of: Left) N,N′-(1,2-Dihydroxyethylene)bis-acrylamide (DHEBA); Middle) acrylic acid (AA) and Right) dimethylamino propyl methacrylamide (DMAPMA).

The mixture was polymerized at 70 °C for 30 minutes. 100 µL of a 20 mg/mL BSA solution was dissolved in 900 µL of prepolymer to obtain the MIP solution. The NIP solution is established by adding 100 µL of PBS (10 mg/mL) to 900 µL of prepolymer. 10 µL of each solution is pipetted onto the respective electrode and spin-coated for five seconds at 3000 rpm. The sensor was left in the oven for polymerization overnight at 37 °C. In order to remove the template from the MIP surface, three washing steps were performed. First, the sensor was placed in a bath filled with PBS (10mM) followed by an SDS washing step (0.1%). Lastly, the QCM was rinsed with distilled water. All steps were performed for half an hour.

DHEBA-AA-VP

25 mg (12.5 mmol) DHEBA, 6 mg (54 µmol) 1-vinyl-2-pyrrolidone (VP) and 4 mg (55.5 µmol) acrylic acid (AA) are dissolved in 1 mL of buffered sodium persulfate solution (2 mg/mL in 10 mM PBS; pH 7.4). Similar to the previous procedure, the mixture was polymerized at 70 °C for 30 minutes. One part of BSA solution was added onto 9 parts of prepolymer to prepare the MIP solution. The NIP was produced by the combination of 1 part of a PBS solution onto nine parts of prepolymer. After addition onto the quartz (10 µL each side), the QCM was spincoated for ten seconds at 3000 rpm followed by placement in the oven at 37 °C overnight. The chemical structure of 1-vinyl-2-pyrrolidone is represented in Figure 43.

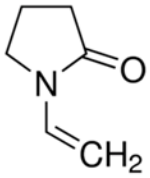

Figure 43: Chemical structure of 1-vinyl-2-pyrrolidone (VP).

The polymer system described above was employed for synthesizing BSA imprinted polymers by bulk imprinting. Aside of this approach, stamp-imprinted BSA sensors were developed as well. The same monomers and crosslinking molecules were utilized for preparation of these stamp imprinted polymers. However, different ratios and solvent were used. AA and VP were mixed in a ratio of 2:3. 7.5 µL of this solution is added to 17.5 mg (8.75 mmol) DHEBA and 7.5 µL of a sodium persulfate solution (400 mg/mL). The whole was dissolved in 600 µL DMSO followed by prepolymerization for five minutes at 60 °C. The MIP side is produced by application of 10 µL prepolymer followed by coverage with a BSA glass slide (50 mg/mL in dH_2O). Analogous to this procedure, the NIP is made without applying a BSA stamp though. Spincoating was performed at 3000 ppm for 25 seconds. Incubation took place overnight at 50 °C. Washing was performed in four steps. In a first step, the sensor was placed in a pepsin solution (0.2 %; pH 2) for 45 minutes at 45 °C. Pepsin is capable of breaking proteins down to smaller fragments. It could thus also cleave bovine serum albumin. This step is followed by five minutes washing in a PBS solution (10 mM). Next, the QCM was placed in a 0.1% SDS solution for another five minutes and finally washed with dH_2O for five minutes.

HEMA-EbAM

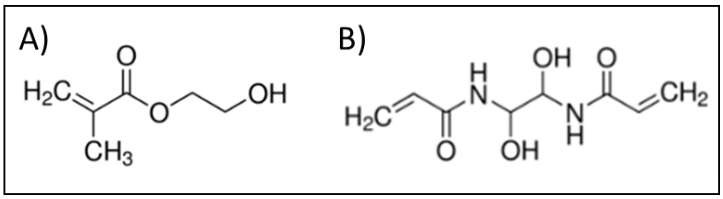

Figure 44: Chemical structures of: A) hydroxyethylmethacrylate (HEMA) and B) N,N′-(1,2-Dihydroxyethylene)bisacrylamide (EbAM).

For synthesizing this polymer system, 2 vials were prepared. Vial 1 contained 20.1 mg (154.45 µmol) 2-Hydroxyethylmethacrylate (HEMA) and 48.27 mg (243.52 µmol) of N,N′-(1,2-Dihydroxyethylene)bisacrylamide (EbAM). For vial 2, the amount is doubled for both monomer and crosslinker. Next, the two systems were dissolved in PBS (25 mM; pH 7). After ten minutes of sonication, they were exposed to argon for 15 minutes followed by 10 minutes of polymerization under UV light at 312 nm.

Viscosity started to increase after 30 minutes leading to the pre-polymer, an oligomeric mixture. At this time, we call the mixture “prepolymer” since it is not polymerized fully but already made oligomer chains in an appreciable way. Vial 2 on the other hand completely polymerized after 10 minutes indicating that the concentration of functional molecules was too high

For preparing MIP, 900 µL of our pre-polymer solution of vial 1 was added in a new vial. Additionally, 100 µL of template solution (100 mg/mL BSA in 25 mM PBS) was administered. This mixture was left untreated for one hour in order to accomplish bond formation between the oligomers and the protein. Synthesis of the NIP mixture followed a similar procedure. However, instead of adding an template solution, 100 µL of PBS (25 mM) was added.

HEMA-EbAM via RAFT polymerization

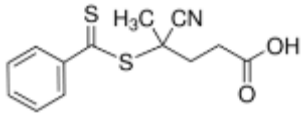

Figure 45: Chemical structure of 4-Cyano-4-(phenylcarbonothioylthio)pentanoic acid.

In order to gain more control over the polymerization, RAFT agent was administered onto the reaction. The polymer described in procedure 1 served as a starting point for the synthesis of this reaction. 20.2 mg (155.21 µmol) HEMA and 44.0 mg (222 µmol) of EbAM were added together in a glass vial. Next, RAFT agent was added to the mixture. We tried two different ratios: using 40 and 80 µL (222 and 444 µM respectively) of RAFT agent respectively. In our case, 4-Cyano-4-(phenylcarbonothioylthio)pentanoic acid was used to fulfil this role. Its structure is displayed in Figure 45. 6,2 mg (22.19µmol) of the chemical was dissolved in 1mL of DMSO of which at 50 µL was dissolved in 1mL of PBS (25 mM, pH 7). Depending on the amount of RAFT solution added, different volumes of PBS solution were used to obtain a total of 1 mL (PBS + RAFT solution; volumes of HEMA and EbAM excluded). The mixtures were purged with argon for 30 minutes on ice followed by UV polymerization at 312 nm for 30 min. 10 µL of pre-polymer solution was applied onto the respective electrodes. Spincoating lasted 5 seconds at a speed of 1000 rpm. Thereafter, a BSA-coated glass slide was pressed onto the MIP side. The NIP channel was covered by a blank glass slide as a reference. The quartz was placed in the oven at 37 °C for overnight. In the washing step, the QCM was rinsed with distilled water for 30 minutes.

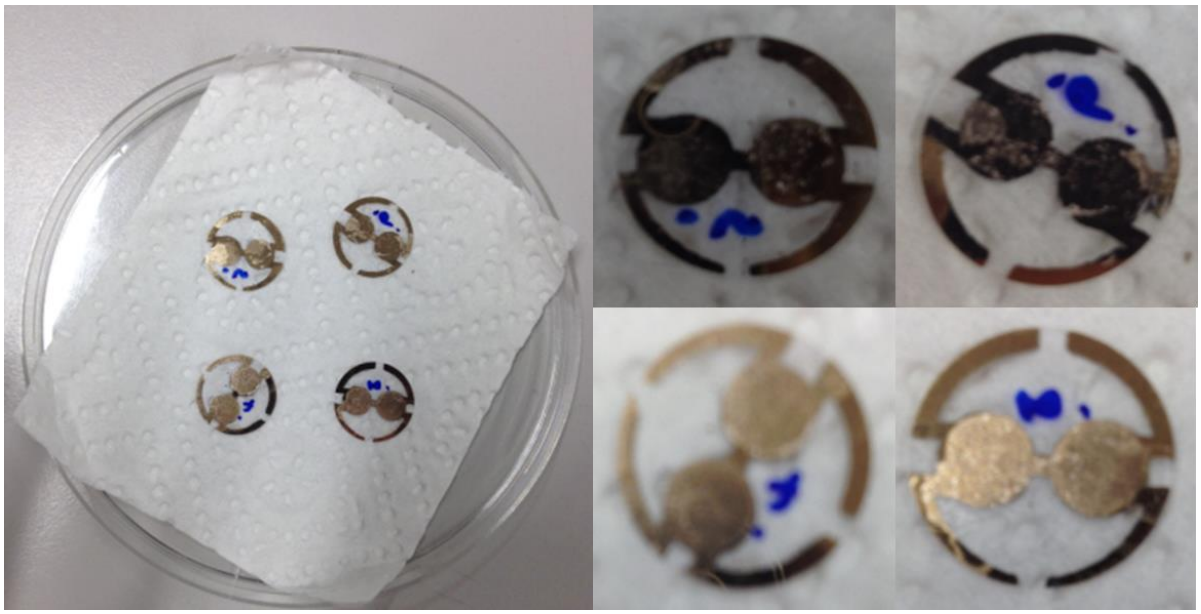

Figure 46: Quartzes coated according to the HEMA-EbAM procedure containing different amounts of RAFT reagent.

Figure 46 shows the outcome of the polymer coating onto the QCM. It can be said that quartzes number 5 and 6, the ones on top, exhibit more clumping polymer islands whether Q7 and 8 appear to have more homogeneously distributed polymer layers. The first two samples were prepared with lower [RAFT] concentration. All QCM were characterized by the network analyser and the frequencies of the electrodes decreased by 1-2 kHz after coating. This corresponds to roughly 80nm homogeneous layers.

2.3.2. Polymer Synthesis for Lysozyme

EGDMA-AA Synthesis

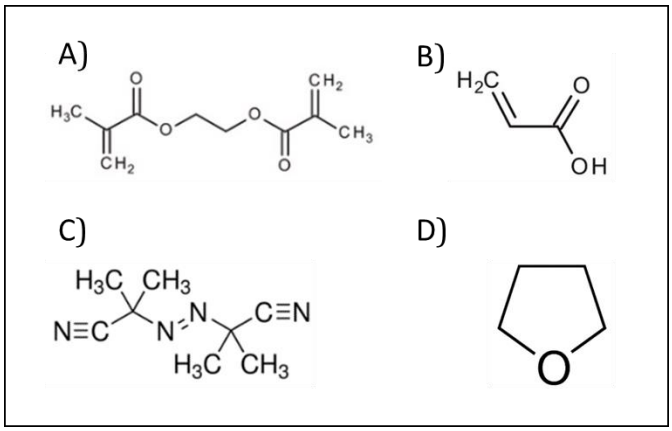

Figure 47: Chemical structures of A) Ethylene glycol dimethacrylate (EGDMA), B) Acrylic acid (AA), C) 2,2′-Azobis(2-methylpropionitrile) (AIBN) and D) Tetrahydrofuran (THF).

For the synthesis of this polymer, EGDMA and acrylic acid were used as crosslinking molecule and functional monomer respectively. AIBN fulfills the role of initiator in the reaction. 150 mg (756.74 µmol) EGDMA, 100 mg (1.39 mmol) AA and 2 mg (12.18 µmol) AIBN are dissolved in 500 µL THF. Chemical structures are displayed in Figure 47. Each batch was polymerized at 70 °C. Three different polymerization times were selected: 30 minutes, one hour and one hour and 40 minutes respectively. The latter one resulted in too thick layers (approximately 3 µm) with bad damping values after hardening. Therefore, this quartz is not further used for QCM experiments. After prepolymerization, the mixture was diluted ten times with THF. Aside of that, a solution containing 10 mg/mL lysozyme in a 0.02 M TRIS buffer (pH 7.5) was prepared. For the formation of the MIP, one part of the protein solution and four parts of the diluted polymer are combined. Here, the method of choice was bulk imprinting. As a reference, a NIP was established by only using the polymer solution, thus without the addition of protein. 2 µL of MIP and NIP solution were pipetted onto the respective gold electrodes. The quartz was spin-coated for 30 seconds at a speed of 2000 rpm. Afterwards, the sensor was placed in the oven at 50 °C for further polymerization. Previous experiments demonstrated that this is beneficial compared to drying at room temperature. A visual representation of these sensors after coating is given in Figure 48.

Table 5: Components and amounts of chemicals for EGDMA-AA polymer synthesis.

Compound	Amount (mg)
EGDMA	150.5
AA	99.6
AIBN	3
THF	499

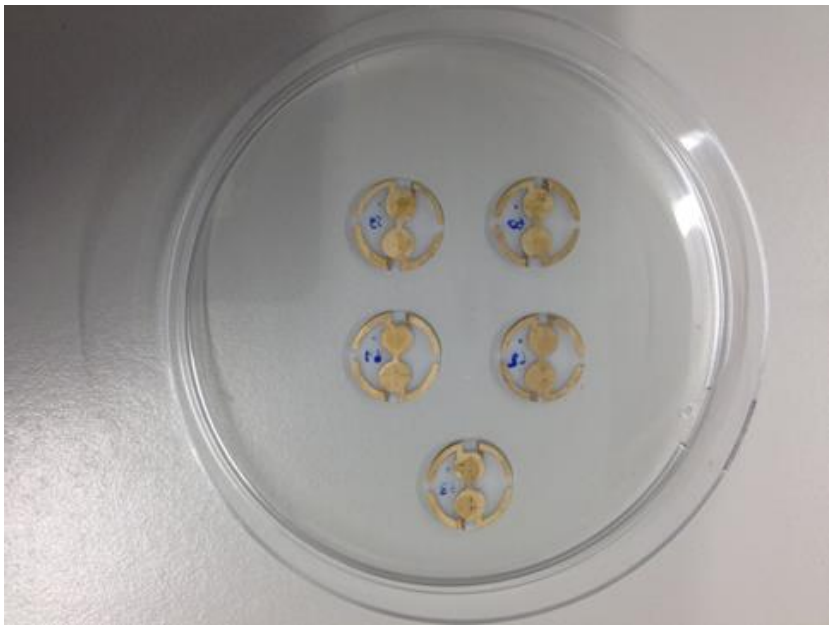

Figure 48: QCMs after coating with EGDMA-AA. The upper two are polymerized for 30 min, the middle two for 1 hour and lowest one for 1 hour and 40 minutes.

Alternative EGDMA-AA Synthesis

Here, the polymer is prepared in a similar fashion compared to the standard EGDMA-AA protocol. However, the lysozyme is dissolved in acrylic acid rather than in TRIS buffer and polymerization took 35 minutes. Only 2 mg of AIBN is used to initiate the reaction. 10 mg (700nmol) of lysozyme was combined with 40 mg (555.09µmol) acrylic acid for preparing the protein stock solution. An equivolumnar solution of diluted polymer and protein solution are mixed together. For the preparation of the MIP side, 10 µL of polymer-protein mixture was added onto the working electrode. 10 µL of polymer only was pipetted for creation of the NIP side. Spincoating was performed for ten seconds at 3000 rpm. After drying, the MIP side was characterized by a frequency drop of 2 kHz. After washing, the signal rose for about 900 Hz obtaining a total difference of about 1.1 kHz.

PU Synthesis

Polyurethane formation is based on a polyol reacting with a diisocyanate. For synthesis, we added 100 mg (400µmol) of 4,4'-methylenediphenyl diisocyanate (DPDI), 200 mg (877µmol) of bisphenol A (BPA), 20 mg (159 µmol) of phloroglucinol (PG) and 200 µL tetrahydrofuran (THF) together in an Eppendorf tube. BPA and DPDI fulfill the role of monomers whereas PG acts as a crosslinker. The mixture was homogenized by placing it into a sonication bath for 15 min. When all components were dissolved, 100µL of this solution was adjusted into a new 1.5 mL Eppendorf tube filled with 880 µL of THF. Then, 20 µL of a 178 mM DABCO solution (in THF) was pipetted to complete a 1 mL starting solution. Pre-polymerization proceeds at 70°C in a water bath. A stirrer bar was placed in the water bath to avoid incorrect temperature monitoring. After 30 minutes, the sample was taken out of the water bath and cooled down to room temperature (RT). The reaction was also monitored by FTIR analysis.

In a first bulk imprinting attempt, we tried to reduce the relative amount of polymer present in the sample by taking one unit of a 10x diluted prepolymer, one unit of a 20 mg/mL lysozyme solution and eight parts of THF. The NIP side was covered by a polymer mixture dissolved in THF (1:9). This is given in Table 6.

Table 6: Alternative PU bulk synthesis.

Component	MIP preparation	NIP preparation
Polyurethane Prepolymer	1 part of a 10x diluted stock solution	1 part of a 10x diluted stock solution
Lysozyme solution	1 part of [20mg/mL] in dH_2O	x
THF	8 parts	9 parts

In order to optimize our results, we went from bulk imprinting strategies only towards a comparison of three possible imprinting strategies: bulk, stamp and sedimentation imprinting. This way, it is more significant to compare the outcome of both techniques. If two different batches would have been used, differences in sensor response could also have been due to small changes in polymer composition, polymerization status and so on.

Table 7 lists five different procedures for sensor production using PU. The first and last quartz are made by stamp imprinting whereas number 2-3 are prepared by bulk imprinting. Bulk imprinting procedures differ by the fact that the lysozyme solutions added to the prepolymer are less concentrated (10 instead of 20 mg/mL). Number 4 is prepared by sedimentation imprinting. In case of the first one, the prepolymer has not been diluted before applying it onto the electrode. The last one, on the other hand, is diluted ten times before being pipetted onto the quartz

electrode. For these two procedures, 5 µL has been selected as volume of choice. The second quartz is prepared by dissolving 1 mg (70 nmol) of lysozyme powder into a diluted PU solution. Afterwards 5 µL of this mixture was applied onto the working electrode. 5 µL of diluted polymer only has been used as a reference channel. All samples are stored overnight at 37 °C and washed for two hours with distilled water to remove the protein. Next, the sensor is available for QCM measurement.

Table 7: List of optimized PU sensor protocols.

Strategy	Channel	PU dilution	Method
1	MIP	/	5µL PU + lys stamp (20mg/mL; pH 7.6)
	NIP		5µL PU
2	MIP	10x	100µL PU
	NIP		5µL PU
3	MIP	10x	5µL of [90µL PU + 10µL lys sol (10mg/mLin dH_2O)
	NIP		5µL PU
4	MIP	10x	lys sol (10mg/mL in dH_2O)
	NIP		5µL PU
5	MIP	10x	5µL PU + lys stamp (20mg/mL; pH 7.6)
	NIP		5µL PU

Selectivity Test

Since molecularly imprinted polymers are known for their specificity and selectivity towards the imprinted molecule, a test was performed to evaluate the binding of denatured versus fresh lysozyme onto MIP and NIP. To make sure our protein was denatured, it was placed in a water bath at 100 °C for 15 minutes. According to literature, the melting temperature T_m equals 74.6 °C. Higher temperatures thus result in transition to a different conformation. A change in structure is also thought to have an effect on the binding towards the lysozyme-imprinted cavities. In 1986, Makki postulated that heating of milk above 70 °C resulted in the destruction of lysozyme. Additionally, if the protein is exposed to temperatures of 100 °C or above, it only retains 3% of its activity (138). This allows us to conclude that we have deactivated lysozyme significantly before executing the test.

NP Synthesis

MIP Core

MIP cores were established by the conventional Stöber synthesis (63, 64). Here, tetraethoxy silane (TEOS) and ammonium hydroxide (NH_4OH) are dissolved in ethanol. NH_4OH fulfills the function of catalyst.

Aside of using silica as the core of our NPs, it is also possible to use other materials (magnetic, polymer, …). Afterwards, measurements performed by DLS gave an indication about the size and size distribution of the synthesized particles.

Two solutions were prepared, A and B. Solution A: contains 34.56g of ethanol and 3.38g (96.57 mmol) NH_4OH (30-33%) which was weighed and directly put in a 200ml reactor. Solution B: 3.95g ethanol and 700mg (3.37 mmol) TEOS which was weighed and put in a 100ml plastic barrel. Solution B was added to solution A in de reactor under stirring at 500 rpm. The mixture is stirred overnight.

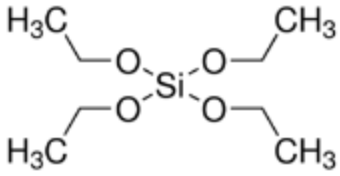

Figure 49: Structure of Tetraethyl orthosilicate (TEOS).

MIP Shell

In the next step, the silica cores can be modified by various chemical groups. The choice of coating depends on the template molecule because of the chemical interactions that have to established between polymer and template. A visual representation of the nanoparticle synthesis process is given in Figure 50. As an example, styrene and methyl methacrylate can be employed as monomers in this system. They are drawn as green chains in the picture. Black dots represent potassium persulfate which functions as initiator. Sodium dodecyl sulfate is used as a surfactant and characterized by their amphiphilic behavior. These molecules appear as orange tadpole-like structures. The whole is dissolved in blue colored distilled water. A distinction between imprinted and non-imprinted NPs is due to the presence or absence of a template molecule in the mixture in this step. Polymerization can take place at 40-70 °C. In this work, TEOS NPs were functionalized with 3-trimethoxysilyl-propyl methacrylate at TNO in Eindhoven.

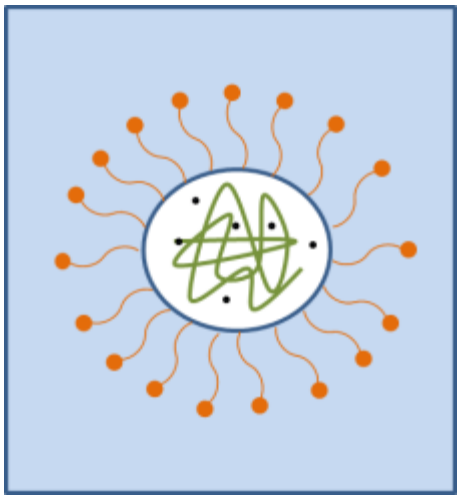

Figure 50: Visual representation of polymer nanoparticle synthesis.

Xanthoprotein reaction

In our case, the xanthoprotein test is used to determine if protein is still present after a washing step. The quartz/lysozyme coated glass slide is placed in a glass vial followed by pouring 1 mL nitric acid (65%) into it. As a result, the mixture turns yellow. The vial was heated into a water bath at 90°C. Thereafter, it was cooled down and 2 mL of NaOH was poured onto it. This leads to a colour change from yellow to orange.

3. RESULTS & DISCUSSION

In order to evaluate the outcome of the results, this section consists of two major parts. The first one describes the results of experiments related to BSA. Various polymer systems are evaluated in combination with the fetal protein. Free radical polymerization procedures as well as RAFT polymerization are executed and discussed here. The main focus lies on the QCM experiments since they give an indication of the sensitivity and selectivity of the sensor. In the second part, QCM outcome for the detection of lysozyme are evaluated. Frequency shifts of the imprinted channels are always characterized by a blue color, while the non-imprinted channel is marked in orange color, unless stated otherwise. Finally, a small side project concerning the synthesis of polymer nanoparticles is discussed.

3.1. BSA MIP SENSORS

3.1.1. Sensitivity Measurements

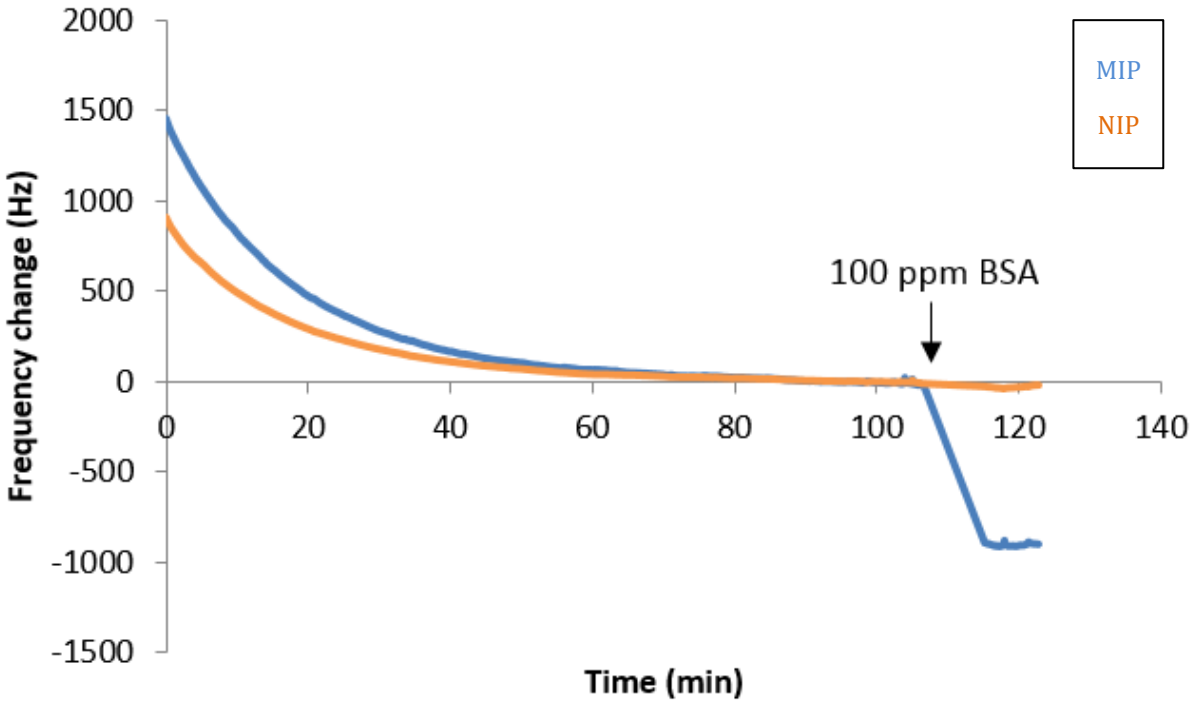

Figure 51: QCM response after application of 100 ppm BSA solution to a BSA imprinted QCM synthesized following procedure 2.3.1.

To continue the work of a predecessor, we designed a sensor for the detection of BSA. Due to literature and working experience in our group, the DHEBA-MAA polymer system (described in 2.3.1) is chosen as the starting point. From Figure 51, it can be observed that addition of a 100 ppm BSA solution evokes a pronounced response of approximately -850 Hz on the MIP channel, whereas the signal on the NIP side remains unchanged. The protein solution was added once a stable frequency signal was obtained, i.e. after 100 minutes. Afterwards, we tried to wash away the protein (from the MIP side) using a 10 mM PBS solution followed by water. However, this led to a steep decrease in frequency signal. The large salt content present in the buffer most probably was not completely washed away by the multiple water rinsing protocol. Ultimately this mass addition due to salt accretion might have induced the frequency drop. It is also feasible that electrostatic effects are the reason. Also 0.1% SDS is used to remove the protein from the surface. Unfortunately, this resulted in a signal not only returning back to baseline, but far above. Presumably, this solution is strong enough to it may help removing parts of the polymer or unreacted mono-/oligomers. From network analyzer measurements, it can be said that the layer thickness after washing out the incorporated template out of MIP amounts 70 nm. The layer thickness of the NIP side was approximately 40nm.

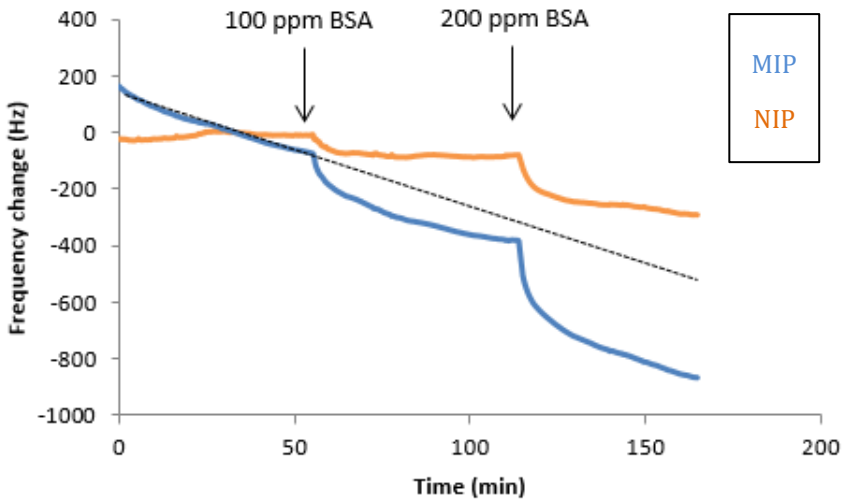

Figure 52: BSA-imprinted sensor using the DHEBA-MAA polymer system and its response to 100 and 200 ppm BSA solutions.

Table 8: Frequency changes after addition of 100 and 200 ppm BSA onto MIP and NIP coated sensor.

Sensor Response (Hz)	Concentration	
	100 ppm	200 ppm
NIP	-50	-250
MIP	-50	-350

A dual electrode quartz for the detection of BSA is prepared by the procedure described in the experimental section 2.3.1. The polymer system consists of acrylic acid, DHEBA and vinyl-pyrrolidone. As can be seen from Figure 52, adding the 100 ppm BSA solution leads to minor differences between MIP and NIP signal. At a concentration of 200 ppm BSA, however, a significantly larger difference could be observed between the two channels. The problem faced here is that the starting signal of the MIP channel is rather unstable. In order to obtain correct results, the signal was corrected for drift. The blue slope line indicates the trend underlying data in the channel. This has to be considered when relating frequency drops to certain concentrations. After taking into account the drift, the difference between working and reference electrode amounts approximately 100 Hz (350 Hz vs 250 Hz) for 200 ppm BSA. The values are compared in Table 8.

Figure 53 displays the outcome of a QCM experiment of a 2-electrode quartz where one side is covered by HEMA-EbAM polymer (for synthesis see section 2.3.1). Because the solution containing the larger amount of monomer and crosslinker fully hardened, the less concentrated solution was selected for the experiment. Addition of BSA in distilled water resulted in a significant decrease of the frequency (-1250 Hz) of the MIP side, whereas it remained almost unchanged on the NIP side after addition of 200 mg/L BSA in dH_2O. The reference channel, however, showed some remarkable behavior. Here, addition of the analyte gave rise to a small frequency increase, the so-called anti-Sauerbrey behavior. Reasons for it are listed in 1.3.2. The washing step also was successful since the signal reaches the baseline again for both MIP and NIP side. Water was used as a washing solution because it guarantees that all changes are due to the binding reactions of BSA to the surface. The experiment is performed twice in order to ensure a correct estimation of frequency drop related to this concentration. The graph shows that the experiment is repeatable, at least when performed in a short time gap. Note also that this measurement was performed in water using a peristaltic pump at a flow rate of 0.2 mL/min.

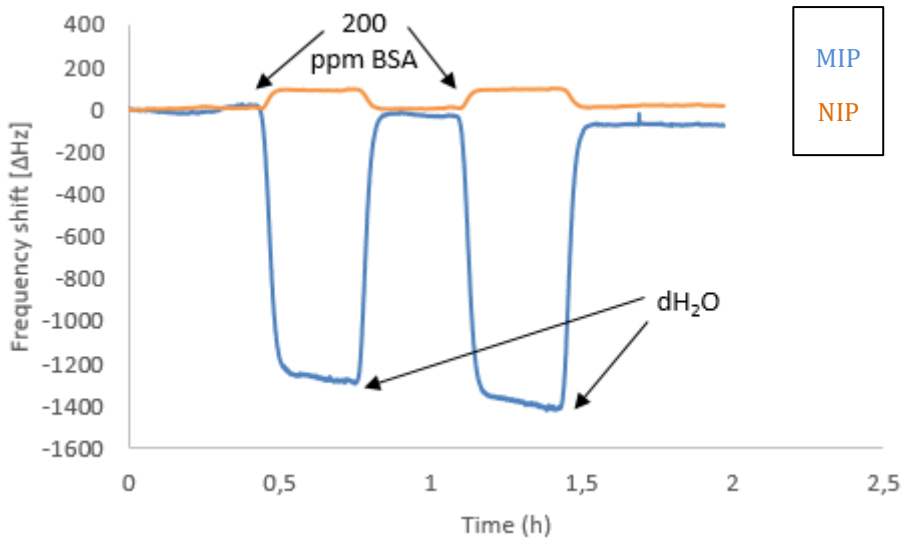

Figure 53: QCM measurement showing the response after application of a 200 mg/L BSA solution. The experiment is repeated for confirmation. The blue line describes the signal on the MIP side whereas the red line displays the response on the NIP side. It can also be seen that the sensor response of the NIP side slightly increases. This is the already previously mentioned anti-Sauerbrey effect.

In Figure 54, a 100 ppm BSA solution was added onto the same polymer resulting in a shift of approximately 400 Hz. To remove the protein from the surface, a washing step with SDS was performed before rinsing with distilled water. Apart from the drift in the signal, it was possible to reach the baseline after washing.

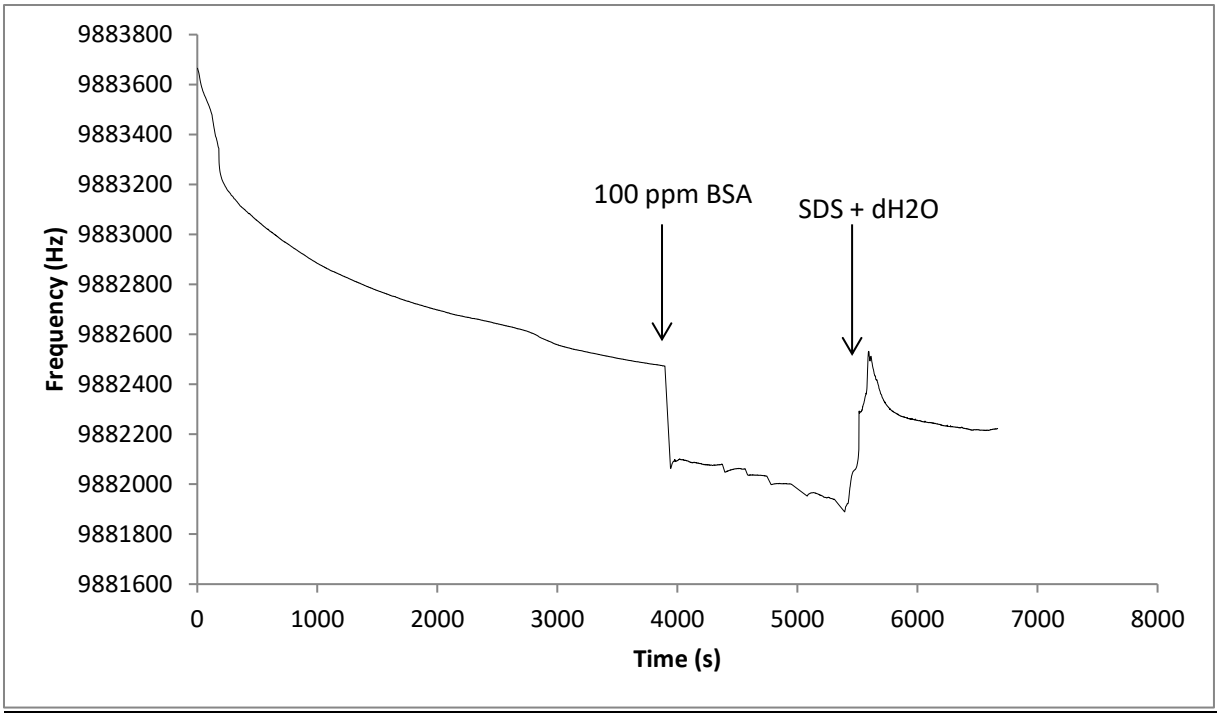

Figure 54: Sensor response after injection of 100 ppm BSA. Washing with SDS followed by water allows the signal to return to baseline.

Addition of 100 ppm BSA solution led to a sensor response of -400 Hz. After washing with SDS followed by water, the signal returned back to baseline.

3.1.2. Selectivity Measurements

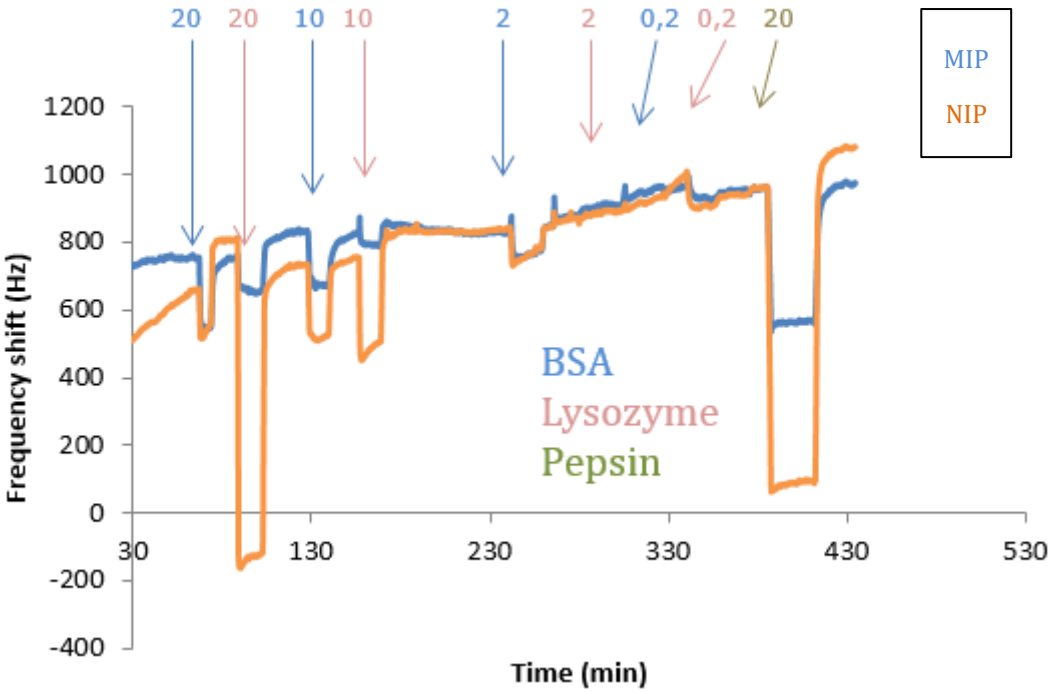

Figure 55: QCM outcome of selectivity measurements (lysozyme (pink), pepsin (green) and BSA (blue)) at different concentrations (0.2-20 mg/mL) for a lysozyme-imprinted sensor.

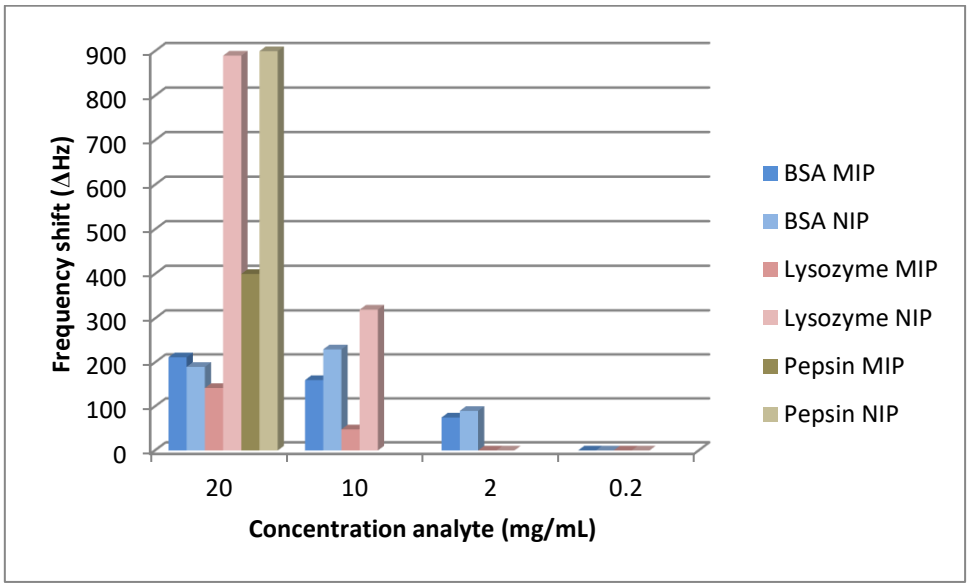

Figure 56: Bar graph displaying the frequency shifts towards three different proteins at four different concentrations.

Figure 55 shows the outcome of a selectivity measurement carried out with BSA imprinted sensor synthesized by RAFT polymerization. 4-Cyano-4-(phenylcarbonothioylthio)pentanoic acid is especially suitable for polymerizing methacrylates and methylamides but can also be used to polymerize other classes of amides. Therefore, this RAFT agent is selected as optimal candidate to control the polymerization of our polymer. The sensor used here is described in 2.3.1 and displays a sensor prepared with larger [RAFT, 88.8 μM]. For better visibility, Figure 56 summarizes the outcome of the QCM measurement shown in Figure 55. From the figures above, it can be seen that the NIP side of the sensor towards BSA displayed greater a six times larger response towards lysozyme at large concentrations compared to BSA. The response towards pepsin is also fivefold compared to the original template. Considering the signals on the imprinted side towards concentrations above 10 mg/mL, little distinction can be made between all three analytes. Exposure leads to a significant response at all times. However, one cannot discriminate between the different proteins. A possible reason therefore is that all three analytes favor (unselective) binding onto the polymer surface. At a concentration of 2 mg/mL however, the QCM almost showed no reaction towards lysozyme whereas BSA could be detected. Despite that, no difference between MIP and NIP channel could be observed. Washing steps have proven to be successful for all analytes at all concentrations. Note the large responses of lysozyme and pepsin on the NIP channel of the sensor.

3.1.3. Working at flow conditions

Previous measurements are performed under stop-flow condition. This means that once the analyte or washing solution is added into the measurement cell, the resulting signal response is measured. To state more clearly, there is no continuous flow of solution through the measurement cell. Aside of this technique, continuous administration using a peristaltic pump is feasible as well. In order to test the influence of a peristaltic pump on QCM measurements, a separate experiment was set up. The preparation of this quartz is given in the alternative section of 2.3.1. Starting the pump resulted in much more fluctuating signals (up to 400Hz) as can be seen in Figure 57 and Figure 58. However, when not using the pump, no clear discrimination between imprinted and non-imprinted side could be made after injection of a 100 ppm BSA solution. The MIP channel barely responds to adding 100 ppm BSA solution (ca. 15 Hz). The signal on the NIP side decreased by approximately 100 Hz. With the addition of the peristaltic pump, on the other hand, it became feasible to differentiate between both channels. When not using a pump, more unselective binding of proteins onto the surface can occur. Permanent flow of protein over the surface acts like a constant delivery of molecules to both the imprinted and non-imprinted side of the quartz. This enduring availability of new proteins, enables the molecules to bind to the cavities whereas BSA just passes over the NIP-coated electrode. These reactions on the MIP side are weak and short-

lasting (44). A permanent administration most probably facilitates this process of binding and rebinding. After 200 minutes, the sensor was rinsed with 0.1% SDS followed by multiple washing steps using dH_2O. However, washing out all SDS molecules was not successfully since the sensor signal dropped drastically with approximately 15000Hz.

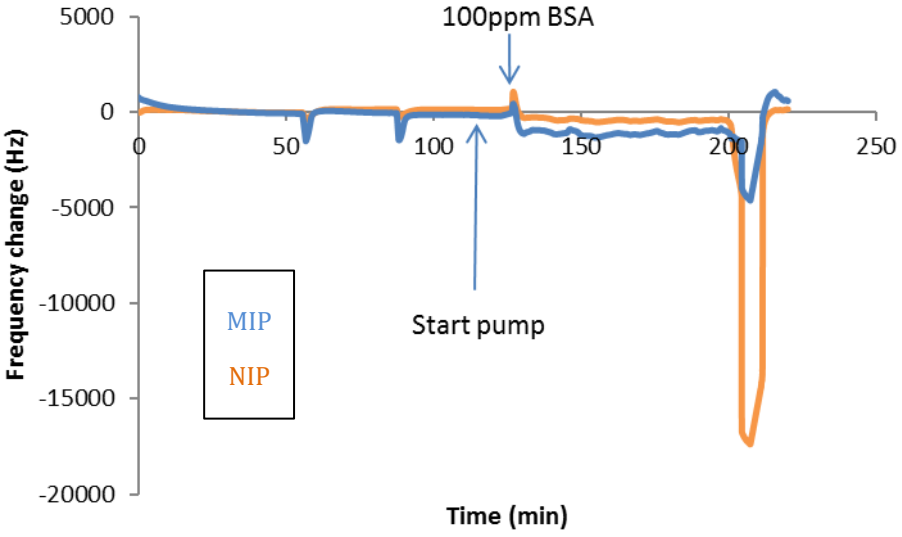

Figure 57: Influence of the peristaltic pump on a QCM measurement.

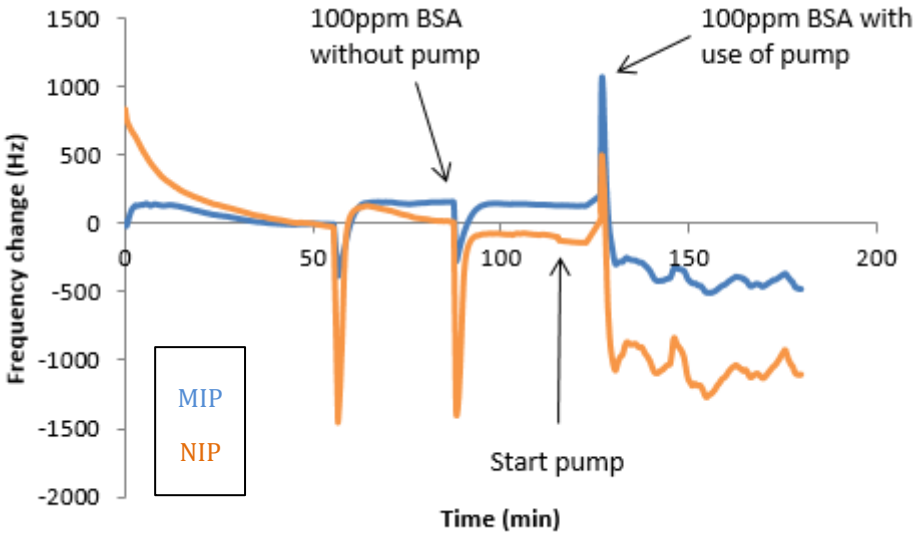

Figure 58: Measurement indicating the difference between flow conditions and stopped flow conditions.

3.1.4. AFM Images of Bovine Serum Albumin Stamps

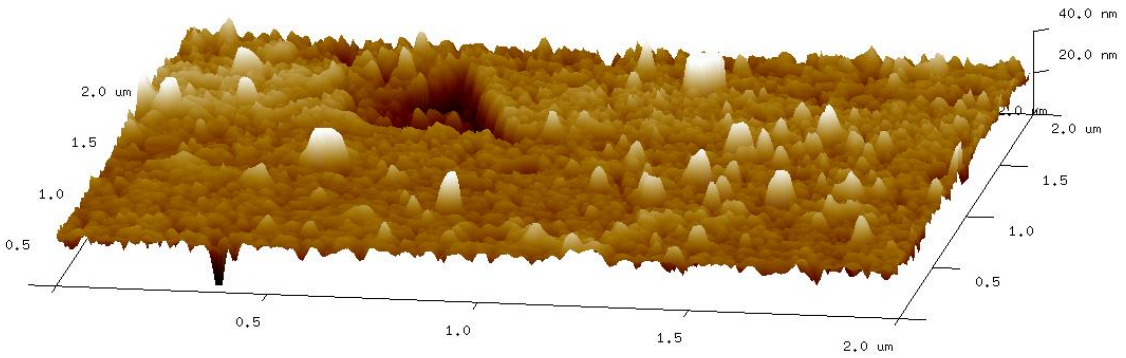

Figure 59: AFM image showing the topography of a BSA coated glass slide.

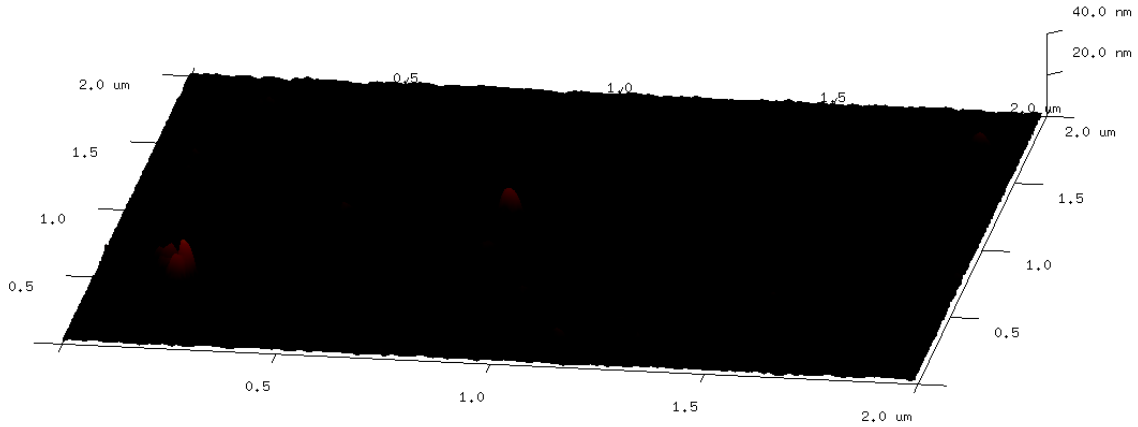

Figure 60: AFM picture displaying the surface of a clean glass slide.

Figure 59 shows the presence of BSA molecules on a glass slide. Firstly, a strongly diluted BSA solution was prepared (0.00001 mg/L). Out of this solution, 2 µL were pipetted onto a thoroughly cleaned glass slide. After drying in the fridge for 24h, the glass slide was subjected to AFM measurement. To make sure that we were not dealing with impurities, a cleaned glass slide without BSA solution was measured as well. This can be observed in Figure 60. The topographical profile shown in Figure 59 can fully be related to the protein molecules since no buffers and thus salts are involved. To make both figures comparable, we adjusted both z-axis to 40 nm. On the glass slide, nothing significant can be observed whereas the BSA coated glass slide clearly displays the presence of the protein, clustered or individually.

To put it in a nutshell: various polymers are tested for their potential as BSA imprinting candidate. All in all, the HEMA-EbAM system without the RAFT agent leads to the most stable and repeatable signals. Additionally, a significant distinction between MIP and NIP side is observable (-1300Hz compared to +100Hz at 200 ppm BSA for MIP and NIP respectively). The attempt to obtain more control over the reaction by administration of the RAFT agent does not result in a satisfactory outcome. The sensor developed for BSA cannot distinguish between the template and two other proteins (pepsin and lysozyme) at the same weight concentrations.

Moreover, signals on the NIP side appear larger compared to the imprinted channel for 20 mg/mL. The polymer recipe containing DHEBA and EbAM, developed by a predecessor, shows a significant response towards 100 ppm BSA on the imprinted side whereas the reference channel does not react. Unfortunately, the quartz broke after the measurement and the successful trial could not be repeated again. A sensor consisting of acrylic acid, DHEBA and vinyl-pyrrolidone was imprinted with BSA as well. Administration of 100 and 200 ppm of the protein solution leads to significant frequency responses on the MIP channel of -50 and -350Hz for the two concentrations respectively. At 100 ppm, the signal on reference channel does not differ from the one on the MIP side. However, at 200 ppm, the MIP side responds with an additional 100Hz compared to the NIP side. Protein removal can easily be achieved by multiple rinsing using dH_2O only. Also washing with SDS is possible. However, thorough rinsing with distilled water is necessary in order to remove any remaining detergent molecules. Applying a peristaltic pump for the QCM measurement allows to discriminate between MIP and NIP side at 100 ppm which is not feasible for this sensor without the external help. However, switching on the pump leads to more fluctuating signal up to 400Hz. From the AFM image, it is undisputed that a layer of BSA molecules has formed and is present on the surface. This is proven by comparing it with a blank glass slide. Since the BSA was present in dH_2O rather than any salt-containing buffer, the topography visible on the AFM image is the outcome of protein accretion.

3.2. LYSOZYME MIP SENSORS

3.2.1. Preliminary Studies for MIP synthesis

Monitoring of Polyurethane Synthesis

FTIR is utilized to observe the polyurethane polymerization process. By this approach, it is possible to monitor the PU chain formation in an online manner. Figure 61 displays the full PU spectrum from 4000 until 600 cm^{-1}.

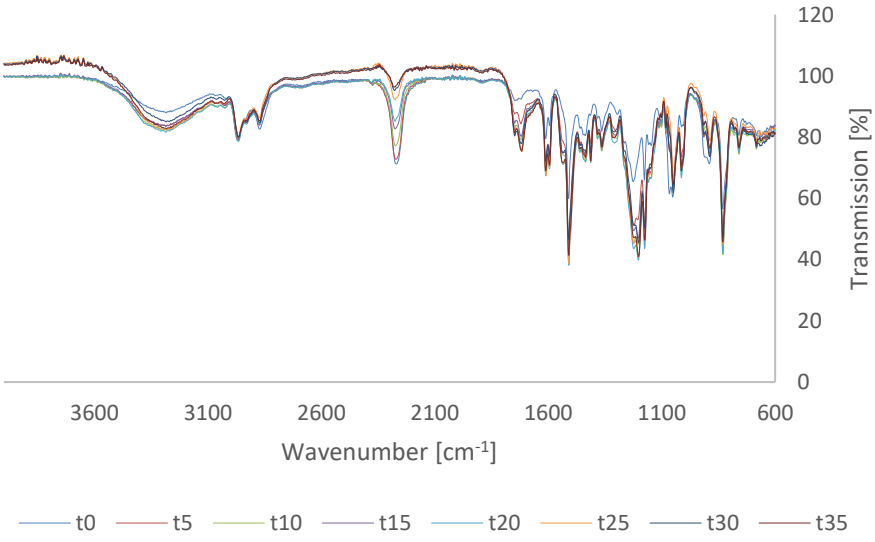

Figure 61: FTIR spectrum of polyurethane from the polymer synthesis start until 35 minutes of polymerization.

Over time, the proportion of isocyanate (R–N=C=O) and hydroxyl (-OH) groups declines. At the same time, peaks corresponding to the origin of urethane bonds arise. The (broad) isocyanate peak can be found at 2275-2250 cm^{-1} (139). This peak declines quickly near reaching the gel point. The newly formed peak related to urethane (C-O-C) establishes at approximately 1100 cm^{-1}. The peak at 1700 cm^{-1}, describing the carbonyl group and also known as the urethane peak, becomes larger over time. The PU synthesis process is monitored for 35 minutes. At that moment, the polymer is considered to be polymerized adequately enough.

Looking at the reaction, the isocyanate, hydroxyl, tertiary amide and C=O free peaks should decrease. C-O, C-N and secondary amine peaks should become more present. Since, N-H and O-H absorb around the same wavenumber, it is not feasible to discriminate between the two. Therefore, the focus of differentiation is at the disappearance of the isocyanate peak.

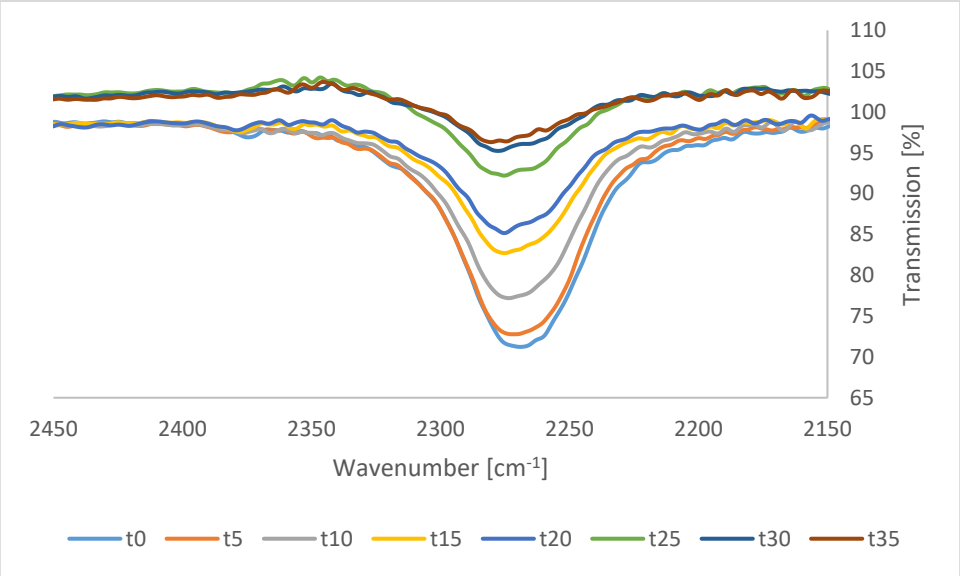

Figure 62: FTIR spectrum of the isocyanate peak intensity, monitoring the polyurethane synthesis for 35 minutes.

Figure 62 displays a segment of the entire FTIR spectrum of PU from 2450 until 2150 cm^{-1}. Increasing the polymerization time leads to a disappearance of the isocyanate peak. This is the most obvious way to monitor the PU process. Therefore, it can be stated that BPA and DPDI monomers are forming polyurethane bonds. After 35 minutes, the measurement was stopped since visible oligomers started to become formed in the solution. The experiment was performed in a water bath at 70 °C. FTIR spectra of all individual components (or dissolved in THF) in the process are displayed in *Table 9*.

Table 9: Major chemical groups of polyurethane and their respective wavenumbers.

Functional Group	Pure PU film (cm-1)	Composite PU films (cm-1)
N-H or O-H stretching	3372	3444
C-H stretching	2934	2962
C=O stretching of urethane	1730	1741
OC-NH stretching	1526	1539
C-H in-plane bending	1459	1461
C-H out of plane bending	1380	1386

Obviously, Fourier transform infrared spectroscopy is not limited to monitoring PU synthesis only. In our work, for example, it is also employed for confirming the presence of lysozyme in a sample. Typically for the existence of lysozyme are the peaks corresponding to the amide I (C=O stretching) and II (NH-bending) regions of the protein. These bands can be found between 1700 and 1500 cm^{-1}. The amide I band, located at the higher wavenumber side can be found around 1650 cm^{-1}. Infrared absorption is evoked by various components of which two are dominant. On the one hand, the random coil (1645 cm^{-1}) contributes to this signal. Additionally, the α-helix (1652 cm^{-1}) is also responsible for this peak (140). The slightly smaller peak at 1540 cm^{-1} originates after presence of an amide II band. The small bump at 1100 cm-1 arises because of the glycosidic C-O-C bridge. Figure 63 shows the FTIR spectrum of lysozyme in water.

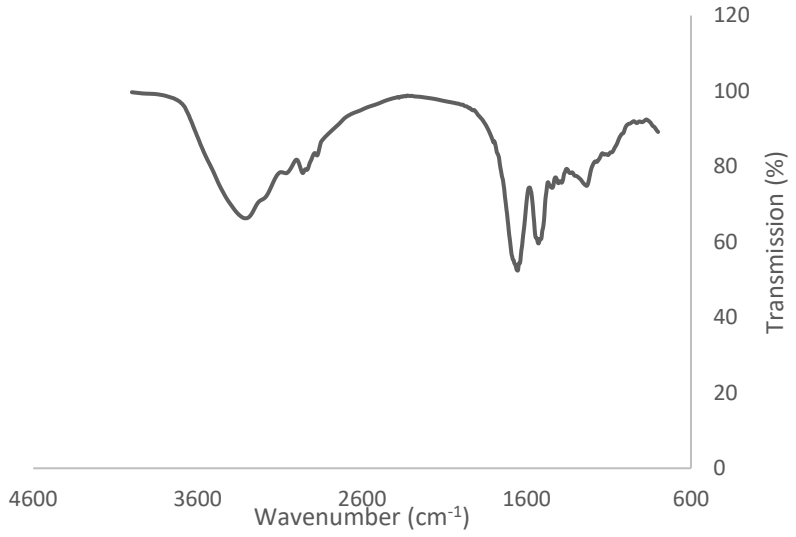

Figure 63: FTIR spectrum of lysozyme displaying the amide I and II regions present around 1700 cm-1.

FTIR can be used as a verification method to determine if washing out of the protein was successful or not. Removal of lysozyme leads to vanishing of the amide I and II bands in the 1700-1500 cm^{-1} region.

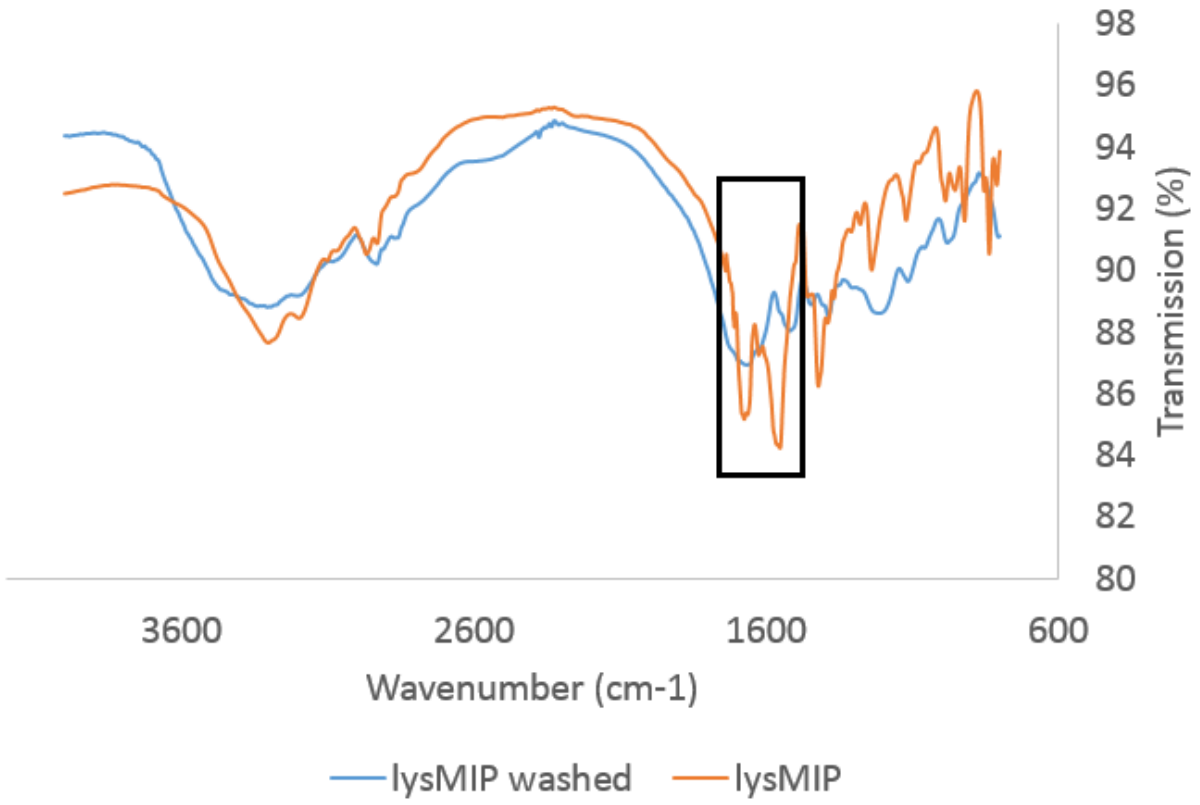

Figure 64: FTIR spectra of lysozyme MIP: orange line) before and blue line) after washing. After washing the lysozyme MIP, the amide bands at 1650 and 1550 disappear.

The polymerization reaction of DHEBA/MAA/VP is followed by means of Fourier transform infrared (FTIR) spectroscopy. Figure 64 represents the FTIR spectrum of the polymerization reactions. Samples are taken every two minutes for eighteen minutes. At that time, pipetting was no longer feasible because the sample had turned gel-like. Out of the reaction course, no significant modifications can be observed in the transmission profile. This uniformity indicates that no alterations of functional groups have occurred. Methacrylic acid combines with 1-vinyl-2-pyrrolidinone by cleavage of the double bonds. In the end, a dense network is established by crosslinking of DHEBA with the polymer strands.

Monitoring of the PU process could also have been expanded to the other polymer systems. However, implementation in polymer systems where double bounds are broken and single bonds are formed is quite challenging. Therefore, we only presented the online monitoring for the two polymer systems above.

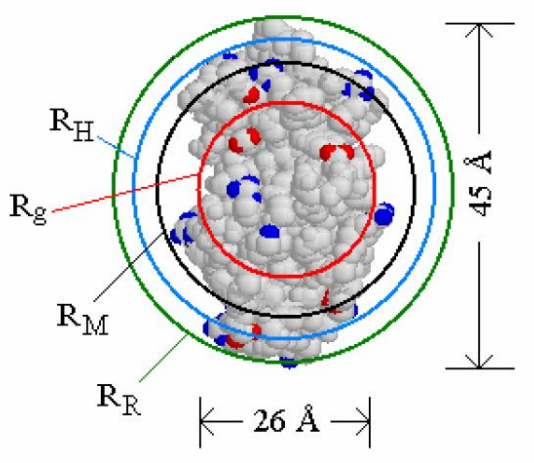

Figure 65: Graphical representation of lysozyme and its theoretical radii (141).

When trying to determine the presence of certain molecules, it is crucial to understand the size and shape of the specific target. As already mentioned, lysozyme is a protein with a molar mass of approximately 14.6 kDa. Looking at the crystal structure of lysozyme, it can be considered an ellipsoid with dimensions of 26 x 45 Å, see Figure 65. Its axial ratio amounts 1.73. There exists more than one formula to illustrate the radius of proteins. R_M describes the radius of a rigid sphere having equal mass and density as lysozyme. R_H, on the other hand, takes into account solvent (hydro) as well as shape (dynamic) effects. R_g, finally, is specified as the mass weighted average distance from the core of a molecule to each mass element in the molecule. When rotating lysozyme around its geometric center, it is possible to determine R_R. It has to be noted however that lysozyme was measured on glass slides after drying. This means that they might have a different conformation compared to when one would measure it in liquid state AFM.

This section is included to clarify the size dimensions concerting lysozyme. Since we are dealing with fairly small molecules, <10nm in diameter, it is challenging to get high resolution images out of it. In order to detect single molecules rather than large protein aggregates, the lysozyme solution was diluted significantly (1 million times). For molecular imprinting, stamps bearing 10-20 mg/mL lysozyme solutions are synthesized. In the future, it could be of interest to make benefit of these low-concentrated protein stamps. Further research has to reveal if this approach leads to more beneficial imprinting and thus recognition.

In literature, many stamp imprinting procedures rely on stamps bearing large amounts of analyte onto its surface. By substantially diluting the protein solution (10^{-5} mg/mL), it was possible to obtain individual proteins onto the glass slides rather than large agglomerates. Additionally, the surface appears more homogeneous. This is confirmed by the AFM images given in Figure 66 and Figure 67. More detailed information about the preparation can be found in section 3.2.1.

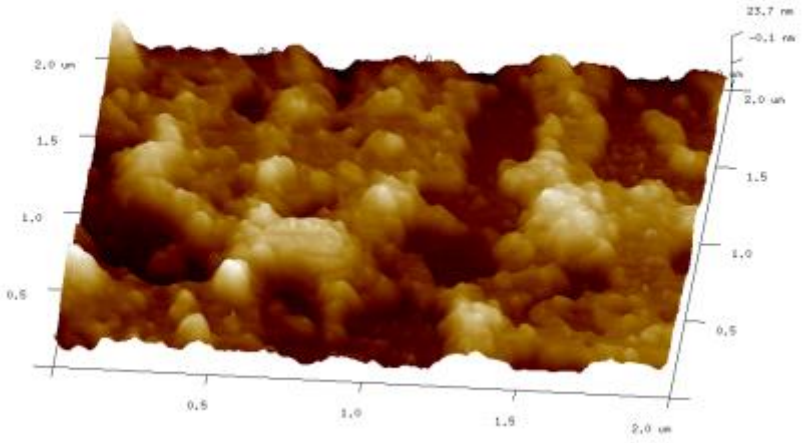

Figure 66: Atomic Force Microscopy image of lysozyme on a glass slide (20 mg/mL lysozyme solution).

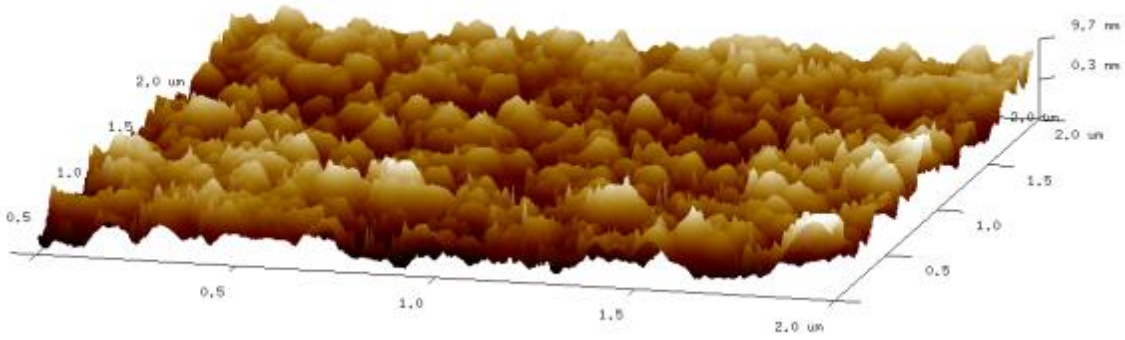

Figure 67: Atomic Force Microscopy image of lysozyme on a glass slide (0.00001 mg/mL lysozyme solution).

As a reference, Figure 60 shows the topography of a blank glass slide. Looking at the z-axis, it can be seen that the surface is relatively smooth (less than 1nm). From its structure depicted in Figure

65, it can be deduced that the hydrodynamic radius of lysozyme amounts 1.85 nm. A study has shown that the radius increases in the presence of ethanol. Since we are dealing with lysozyme dried on glass slides, we should consider possible deformational alterations as well.

Xanthoprotein Reaction

As already indicated in 2.3.2, the xanthoproteic reaction can be used to determine the presence of proteins (benzol-containing amino acids) in a sample. To determine if our washing step was successful, this method can be used as a quick confirmation tool. Figure 68 demonstrates the presence of protein by a yellow-orange color on glass. On gold, a darker yellow-brown color appears. Trying this test for lysozyme in combination with polyurethane gave rise to a white powder-like structure. A drawback is that rather high concentrations of protein are required to be able to detect it.

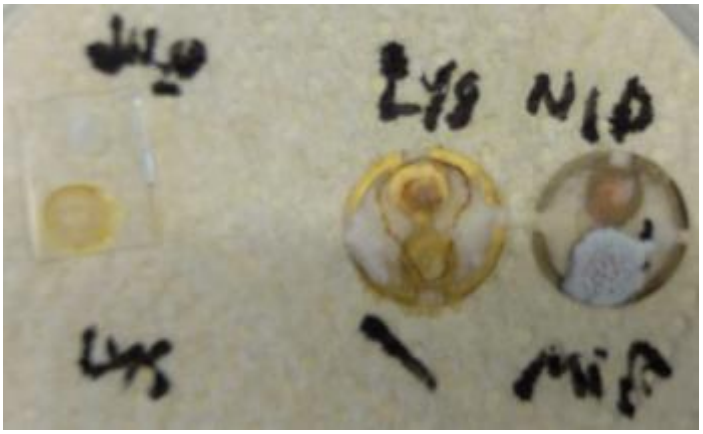

Figure 68: Left) Glass slide indicating the presence or absence of lysozyme; Right) Two quartzes: left up: lysozyme solution on gold electrode, left down: blank gold electrode, right up: polymer on gold electrode, right down: imprinted polymer with lysozyme molecules on surface.

3.2.2. Sensitivity

EGDMA-AA

In a first successful attempt, we synthesized a lysozyme-imprinted polymer comprising EGDMA and AA as monomers. This is done by first diluting 10 mg of lysozyme in a TRIS buffer (0.02 M; pH 7.5). The protein was dissolved in the buffer to stabilize its conformation. In preliminary trials, lysozyme was added as such or dissolved in water which did not lead to acceptable results for this particular recipe. Next, one part of the protein solution us mixed with four parts of EGDMA-AA prepolymer. Three different prepolymers were prepared, meaning they only differ in prepolymerization time: 30, 60 and 100 minutes respectively. However, as already explained in the materials section, prepolymer subjected to 100 minutes of heating were not suitable for coating.

Figure 69 shows the outcome of a concentration dependent QCM experiment for this lysozyme bulk-imprinted quartz. Its precise synthesis procedure is given in section 2.3.2. Note that prepolymerization takes thirty minutes and that the amount of AIBN equals 3 mg. Figure 70 describes the effect by subtracting the signal on the reference electrode from the imprinted side. The concentration range spans 10 to 2000 ppm lysozyme. For concentrations up to 20 ppm, no significant difference between both channels could be observed. Starting from 50 mg/L lysozyme solutions, the discrimination between MIP and NIP became more pronounced (ΔMIP-NIP = 30Hz at 50 ppm, 220Hz at 2000 ppm). The imprinting factor from 50-2000 ppm is approximately 3 in this range. Precise frequency shift values corresponding to each concentration can be found in Table 10. Figure 71 plots the corresponding sensor characteristic, i.e. the differences between MIP and NIP signal as a function of concentration.

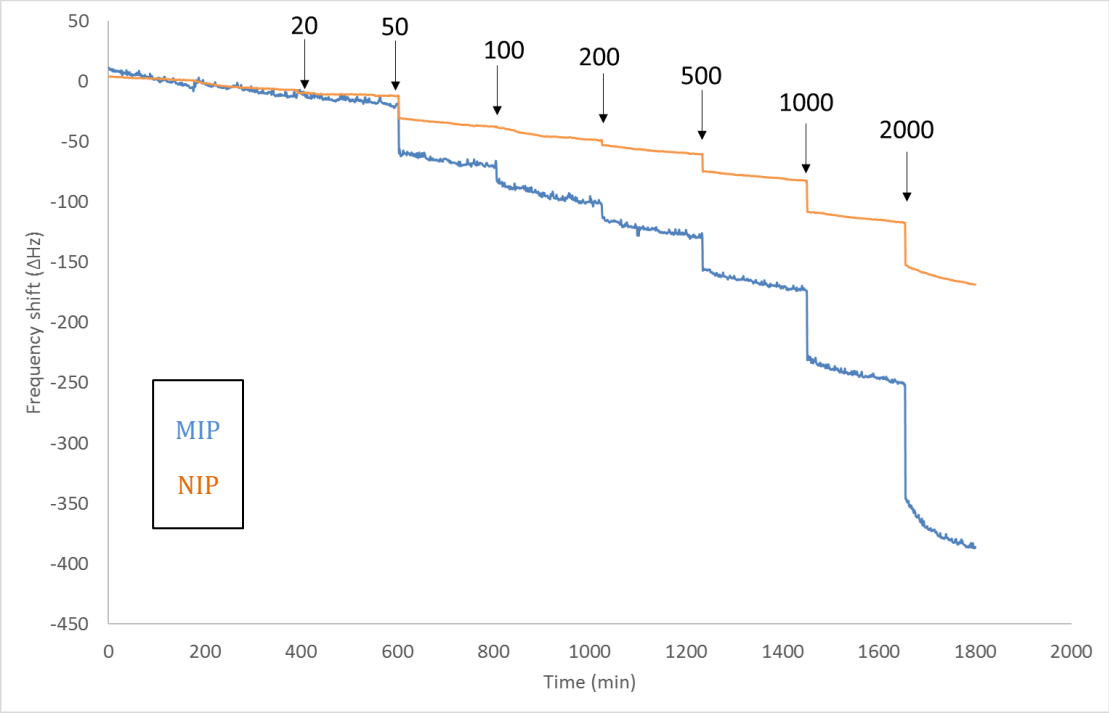

Figure 69: Sensor response of lysozyme-imprinted QCM after addition of increasingly concentrated lysozyme solutions. The blue curve displays the response of the imprinted side (MIP), whereas the red line depicts unselective binding towards the NIP side.

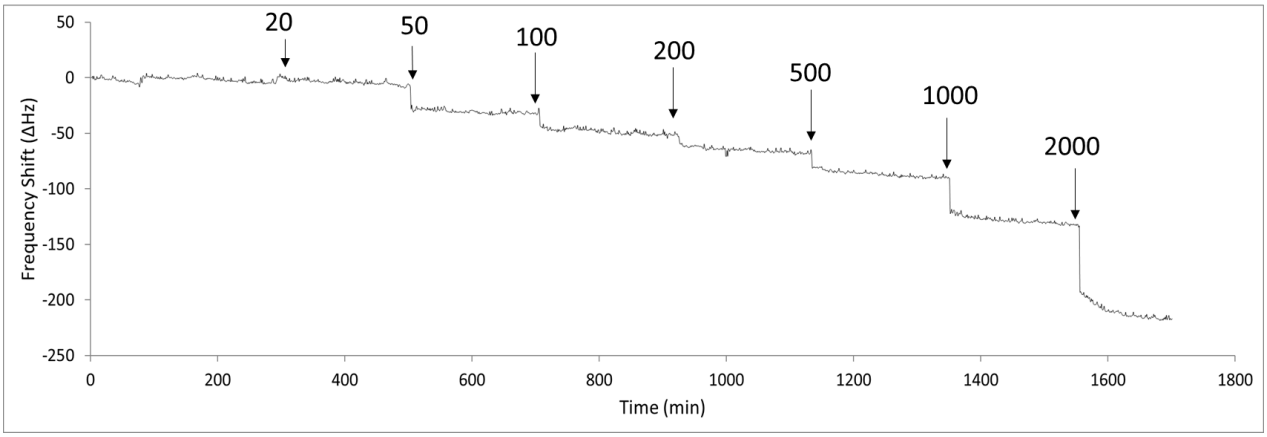

Figure 70: Difference of MIP-NIP response.

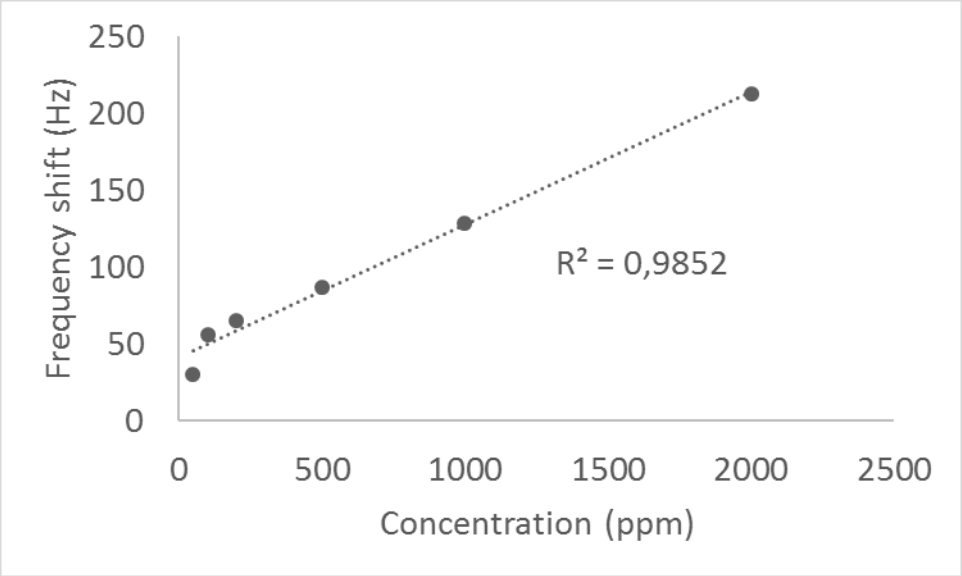

Figure 71: Lysozyme MIP sensor characteristic on QCM.

In the range of 10 till 2000 ppm, a linear behavior could be observed. This was proven by a R^2 of 98.52 %. This strongly indicates that this EGDMA-AA polymer gives rise to successful imprinting. The reasons for this may be that the original conformation of the protein stays preserved since it is dissolved in TRIS buffer.

Table 10: Sensor response for respective concentrations of lysozyme.

	Concentration (ppm)	Sensor Response; MIP-NIP (Hz)
1	10	1
2	20	4
3	50	30
4	100	56
5	200	65
6	500	86
7	1000	128
8	2000	213

Unfortunately, repeating the experiment did not lead to distinctions between MIP and NIP signal. This can be observed in Figure 72. In a second experiment, concentrations of lysozyme ranging from 10-500 ppm did not lead to significant frequency changes. At the application of 1000 ppm lysozyme, the signal did decrease significantly. However, the distinction between MIP and NIP side was negligible. This could be due to insufficient washing out the lysozyme after the first trial. In the end, we washed out the protein successfully using TRIS buffer.

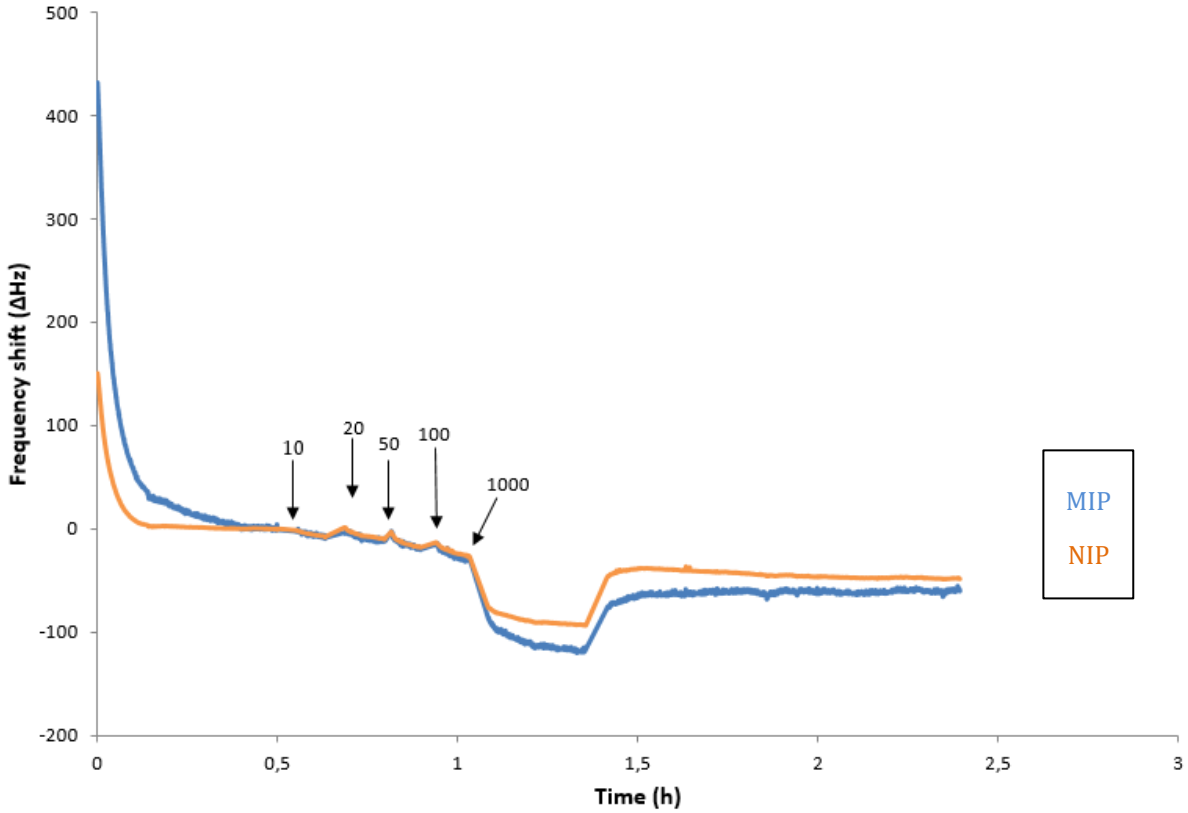

Figure 72: Second trial for lysozyme EGDMA-AA imprinted sensor. No significant difference between MIP and NIP side can be observed.

Aside of stepwise addition of increasingly concentrated protein solutions, an experiment is carried out where a washing step follows after addition of a particular protein solution injection. Figure 73 shows the outcome of an EGDMA-AA lysozyme imprinted sensor washed with TRIS buffer. This leads to removal of the protein molecules from the surface. Nonetheless, complete clearance is not achievable in this case. Note that this sensor is not the same as the one from the previous experiment, however it was made by the same conditions.

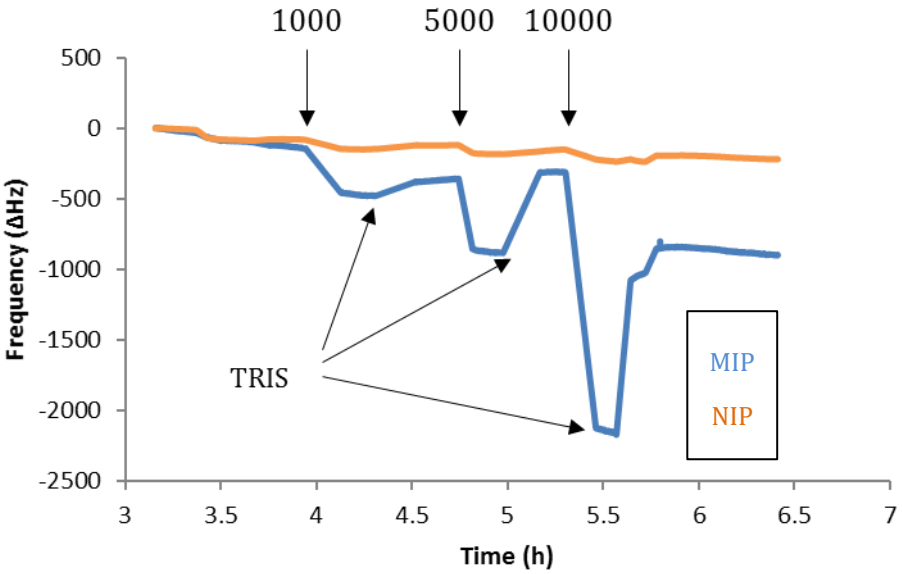

Figure 73: Washing out lysozyme from an EGDMA-AA sensor using TRIS buffer.

Sensors prepared with prepolymer exposed to heating for 60 and 100 minutes did not result in a satisfactory product. They are characterized by too much mass addition proven by network analyzer measurements. Furthermore, they have extremely poor damping values below -15dB, making further acceptable QCM measurements close to impossible.

Alternative EGDMA-AA

Because the repeatability of the standard recipe is not satisfying, an alternative approach is proposed. Moreover, it is also possible to test if successful imprinting is due to the fact that lysozyme´s structure is stabilized by a buffer. For the alternative method, monomers and their ratio stay the same. However, instead of dissolving lysozyme in TRIS buffer, it is dissolved in acrylic acid. The exact procedure of this bulk imprinting approach can be found in 2.3.2.

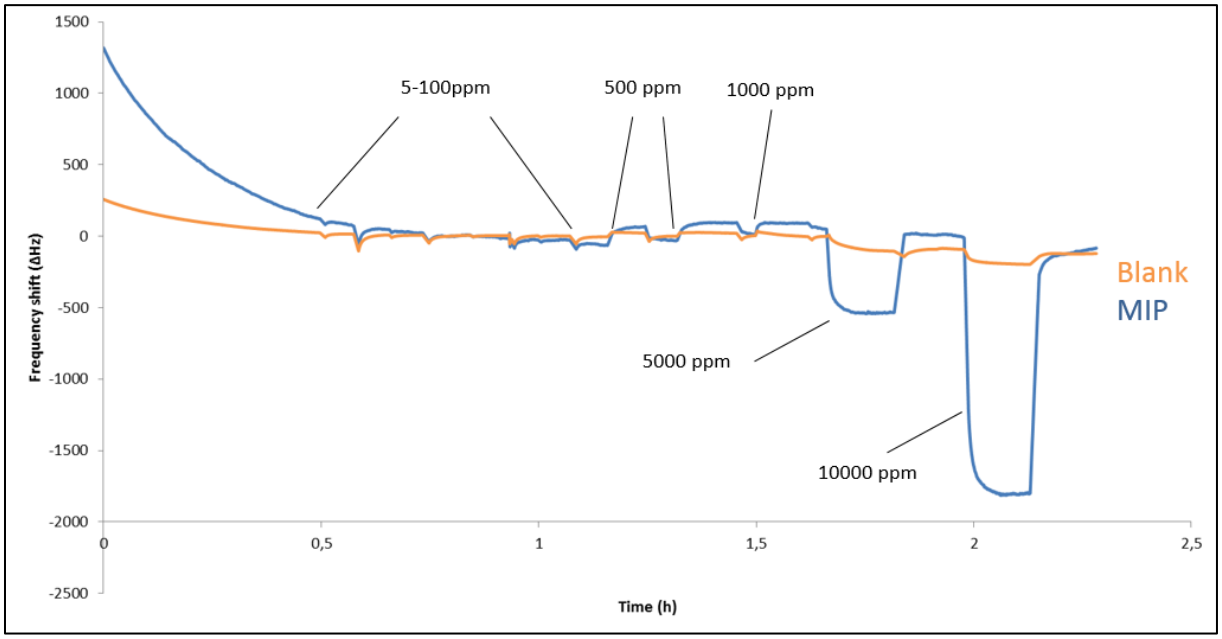

Figure 74: QCM measurement for lysozyme imprinted polymer using the alternative EGDMA-AA approach.

Figure 74 gives the frequency responses of a dual-electrode QCM after exposing it to increasing concentrations of lysozyme. The quartz is coated with an EGDMA-AA polymer according to the alternative sedimentation explained in 2.3.2 using only 2 mg of AIBN. Only at really high concentrations, starting from 5000 ppm, significant frequency changes (-600 vs -100 Hz) can be observed between MIP and blank side. Administration of 10 mg/mL lysozyme solution even produces a signal on the MIP side 18 times as large as the signal on the uncoated channel. Figure 75 reveals a more detailed image of the low-concentrated area of Figure 74. At lower concentrations, discrepancies between both sides can be seen when zooming in on this region. Applying 500 and 1000 ppm BSA solutions into the measurement cell leads signals on the MIP channel twice as high as on the reference side.

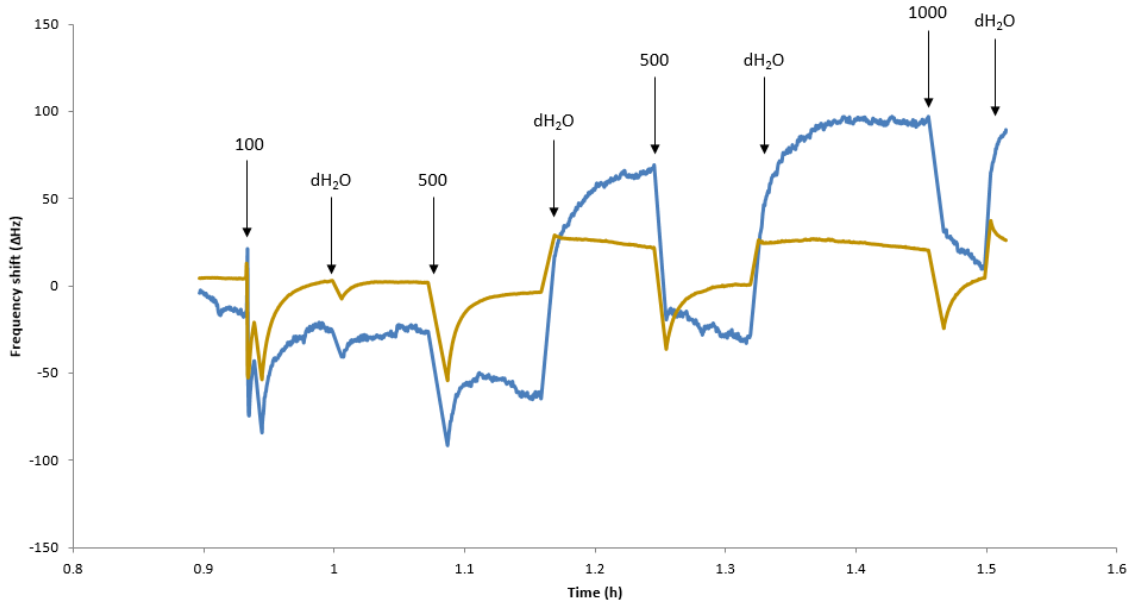

Figure 75: Zoom of low-concentration area of Figure 74.

It can be concluded that the alternative EGDMA-AA process gives rise to a stable, reusable sensor with significant discrimination between imprinted and uncoated channel for the detection of lysozyme up to 500 ppm. Especially at larger concentrations, it is a very powerful method for the detection of lysozyme. Therefore, it has potential to be implemented as a saliva sensor since lysozyme is overly present in this bodily liquid.

The outcome of a QCM where only a 10 µL mixture of acrylic acid and lysozyme is used as MIP side, is given in Figure 76. 10 µL of prepolymer is used to fabricate the NIP. This reference side gives an idea of unselective protein binding onto the polymer. Frequency alterations can be observed starting from 1000 ppm, namely -85 Hz on the MIP side compared to -40 Hz on the reference side. Higher amounts of protein lead to increased imprinting factors, namely further differentiate the effect between MIP and NIP. The IF increases from 2 towards 3 from 1000-5000 ppm. Finally, the sensor was exposed to a washing step using water. Also the drift in the signal has to be accounted for. Compared to the previous method, it can be said that the protein does not bind to the non-imprinted polymer as much as to the imprinted side. From this, one can state that imprinting is successful. Aside of that, the NIP surface gives rise to more fluctuating signals. This is most probably due to the rougher surface compared to blank gold electrodes.

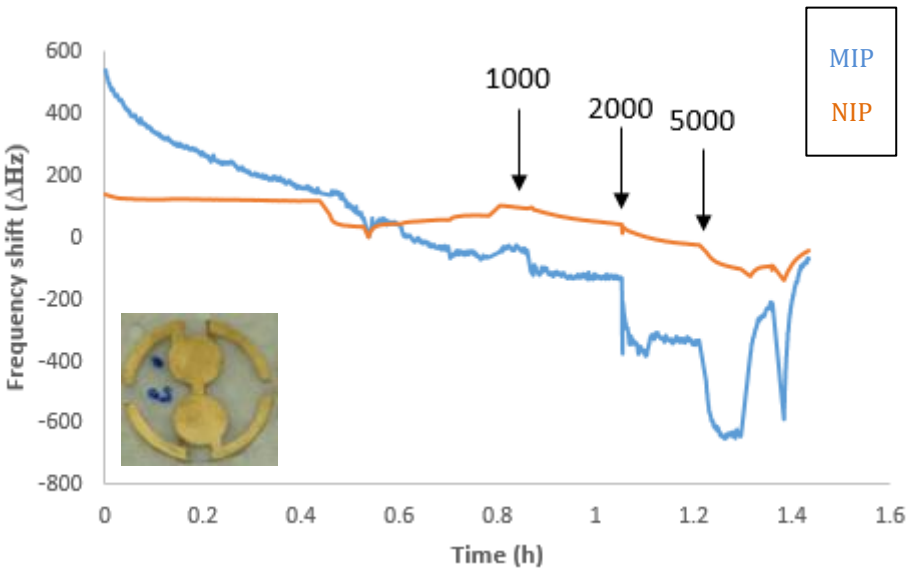

Figure 76: QCM result of a quartz where acrylic acid and lysozyme are used for the preparation of a MIP channel. The dot on the QCM marks the MIP side.

Previous observations make it questionable, if the polymer interacts with the protein at all. To test this, we coated one electrode of a QCM with a non-imprinted polymer and left the other electrode untreated. Figure 77 shows the outcome of that trial: differences between polymer-coated and blank electrodes are not significant. Moreover, both channels do not respond (proportionally) to increasing concentrations. Hence this trial proved only minor unselective binding of lysozyme towards the polymer.

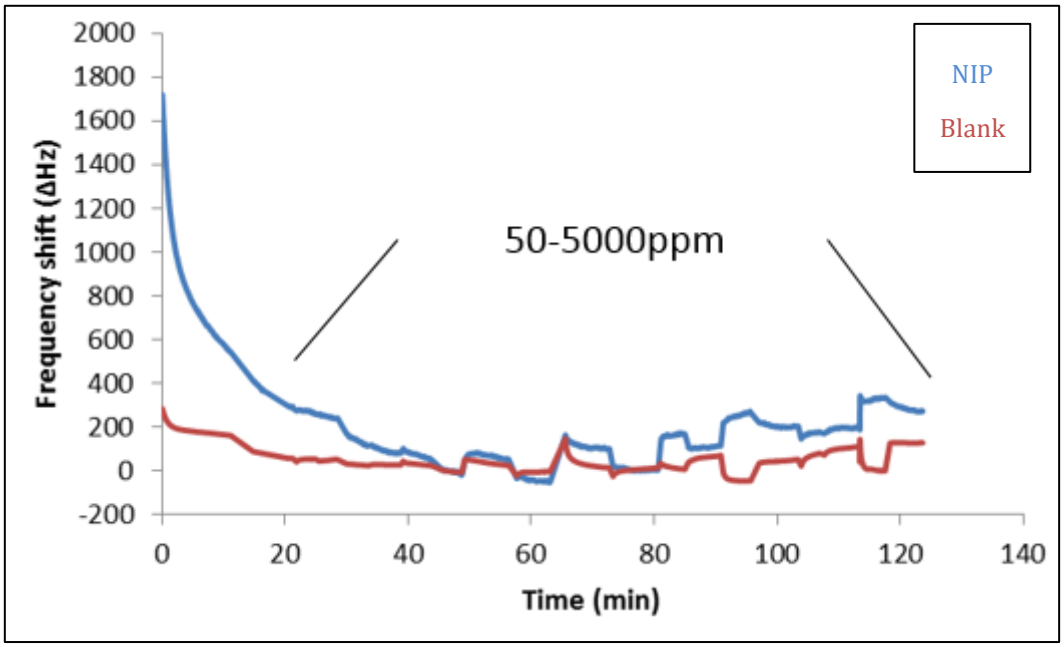

Figure 77: Sensor response towards lysozyme (50-5000 ppm) on: Blue line) NIP, Red line) blank electrode.

Additional methods benefiting the use of PDMS stamps did not lead to appreciable results since the damping values were extremely negative (being below -21dB) in that case. Also a so-called "sandwich MIP" did not result in successful sensors. Here, a lysozyme-acrylic acid solution was sandwiched between two layers of prepolymer. Also this gave rise to damping values below -15dB after coating. By the following washing step, almost the whole sandwich was washed away from the quartz surface. Other strategies tried with this polymer system did not lead to significant, concentration dependent results.

Polyurethane

In order to test the importance of the type of monomers used, we tested another polymer system: polyurethane. Its synthesis is explained in detail in 2.3.2. Stamp, bulk and sedimentation procedures for PU imprinting are discussed in this subchapter. All quartzes presented here are characterized by an imprinted channel as well as a non-imprinted reference channel.

Stamp

Two different stamp methods are shown (procedures 1&5). Both just differ in the fact that the prepolymer is diluted 10 times in the latter case before spincoating. This small detail has great consequences on the outcome of the coated electrodes. The undiluted prepolymer gives rise to poor damping values and the quartz is therefore unsuitable for further experiments.

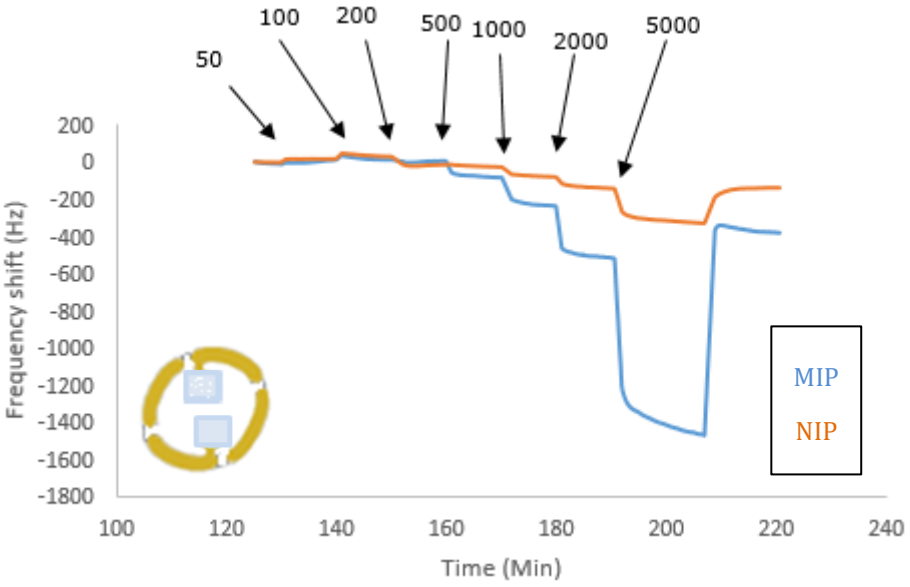

Figure 78: QCM response characteristic of stamp-imprinted lysozyme MIP.

Figure 78 depicts the outcome of the PU MIP prepared by stamp imprinting using diluted PU. Concentrations of lysozyme were increased stepwise without washing after each injection. The blue curve describes the response on the MIP channel whereas the orange line represents unselective binding on the NIP side.

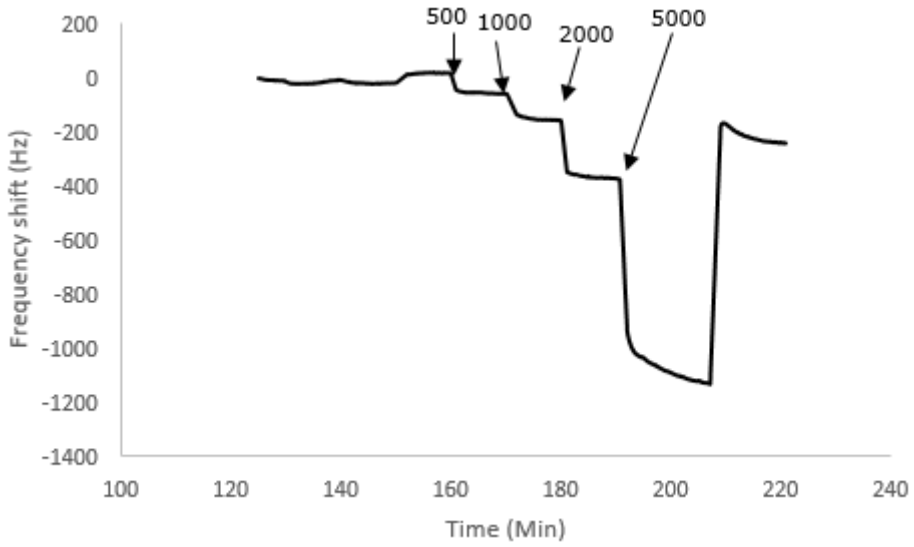

Figure 79: Signal of MIP-NIP from QCM synthesized by strategy number 5 of the PU approach. Gradual addition of higher concentrated lysozyme solutions results in larger effects.

Unfortunately, it was impossible to clearly differentiate between binding on imprinted and non-imprinted sites for concentrations of 200 ppm and below. At 500 ppm, nevertheless, a distinction of around 75 Hz can be made between both channels. It can be affirmed that the sensor response is significant. At the end of the measurement, the signal does not fully return to the baseline value. A reason for this might be insufficient washing because of the powerful binding between lysozyme and polymer.

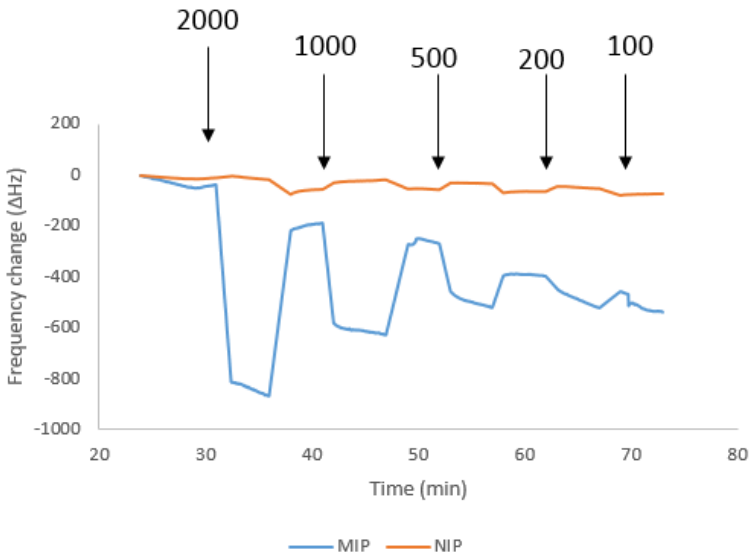

Figure 80: QCM calibration for a lysozyme imprinted PU sensor. Concentrations of lysozyme solution range from 2000 to 100 ppm.

Figure 80 shows another experiment where decreasingly concentrated lysozyme solutions are added into the measurement cell. The quartz used here is different compared to previous one. Its synthesis is the same however. When exposed to the protein, reactions on the MIP side are more pronounced compared to the NIP side: For a concentration of 2000 ppm, a decrease of around 800 Hz can be seen. Addition of 1000 ppm leads to a change of -400 Hz, whereas 500 and 200 ppm result in a shift of -270 and -120 Hz respectively. Unfortunately, washing steps are not completely successful and the MIP side represented by the blue line suffers from some drift.

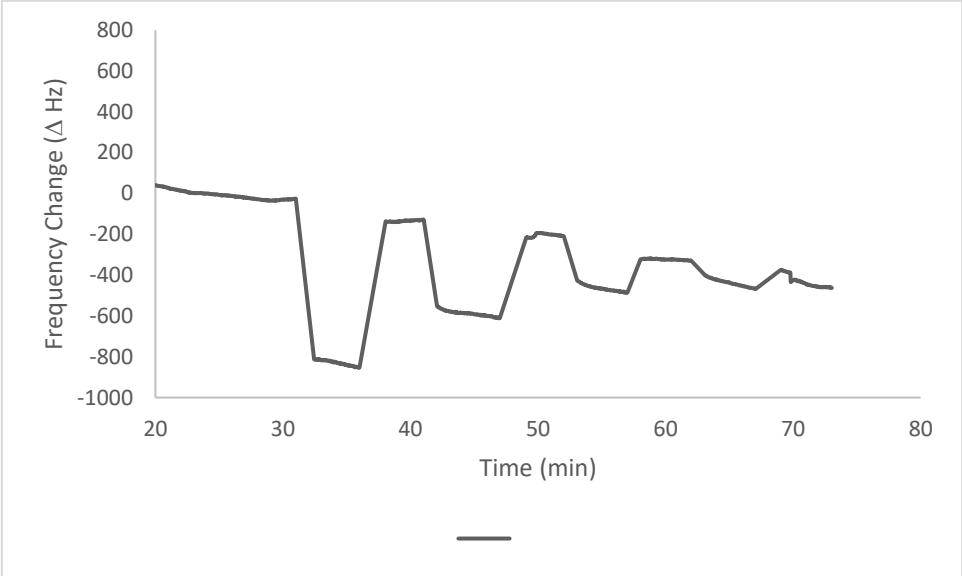

Figure 81: Difference signal of Figure 80.

Figure 81 displays the difference signal of MIP-NIP from Figure 80. Here, it can be seen that effects are more pronounced at elevated concentrations. Concentrations as low as 200 ppm still result in significant changes between both imprinted and non-imprinted channels.

Another general PU was prepared and pressed by the glass slide. The method of synthesis is the same as the previous discussed one. The result can be found in Figure 82 and Figure 83. Here, the stamp differs from previously discussed imprinting procedures. The protein is diluted up to 0.01 mg/L followed by application onto the glass slide. As shown in *Figure 67*, this results in flatter, more homogeneous layers. Exposing the sensor to a 1000 ppm lysozyme solution results in a significant frequency drop of -190 Hz on the imprinted channel. The NIP channel responds as well, however only by a limited amount of -90 Hz. The same step was repeated to examine the repeatability of the sensor. It can be stated that addition of the same (rather large) concentrated protein solution, evokes an equivalent change. Washing out the analyte by distilled water did not lead to any problems. Unfortunately, the MIP side of the sensor is suffering from some signal drift.

Because of this and the limited imprinting effect, no further experiments are performed. It seems that successful stamp imprinting procedures rely on high protein coverage of the stamp.

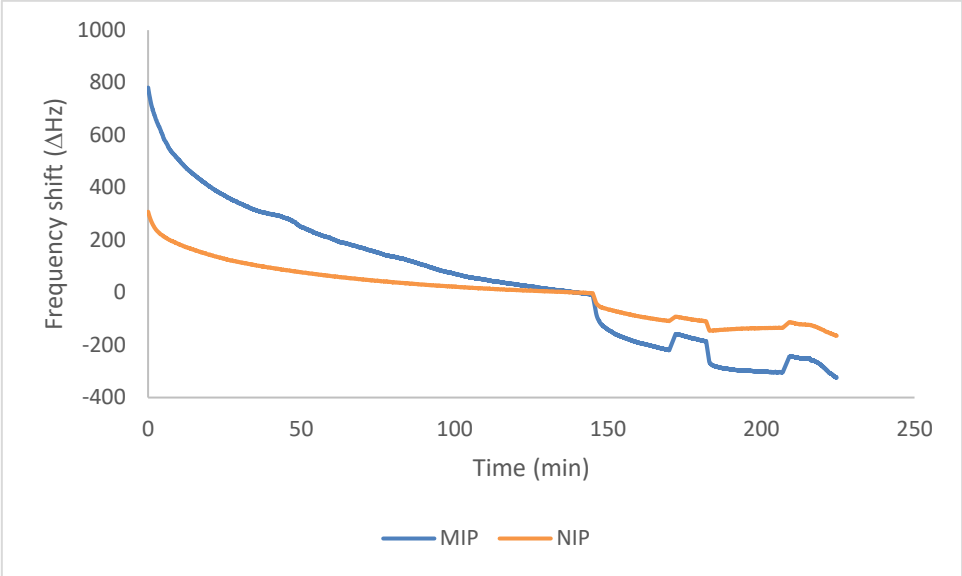

Figure 82: Sensor response after addition of 1000 mg/L lysozyme solution. The experiment was repeated a second time for confirmation.

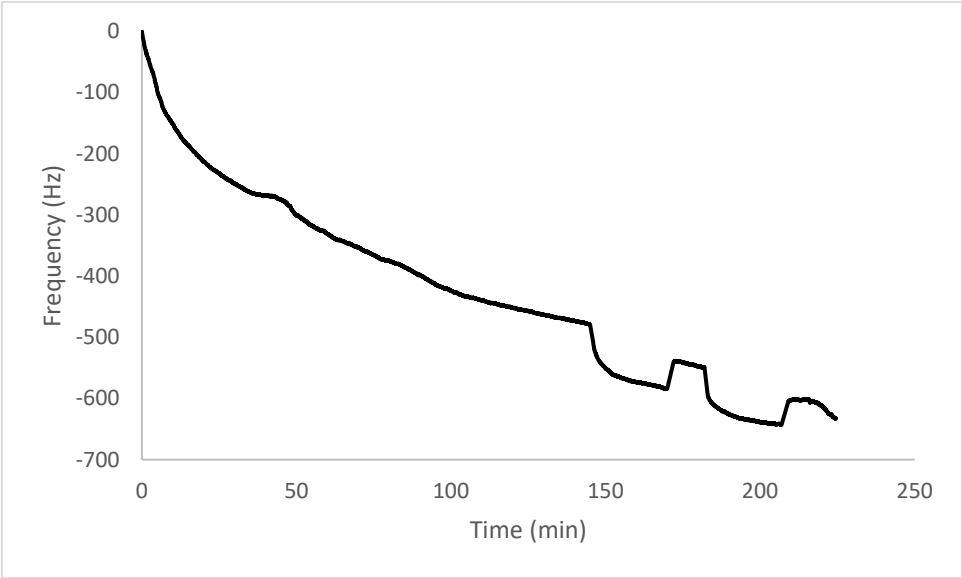

Figure 83: MIP-NIP signal of the Figure 82.

Bulk

Aside from stamp imprinting, we also perform bulk imprinting procedures. This enables to compare the imprinting strategies based on sensitivity, selectivity and stability. Fabrication of the sensor is described in 2.3.2 under the standard PU bulk imprinting approach.

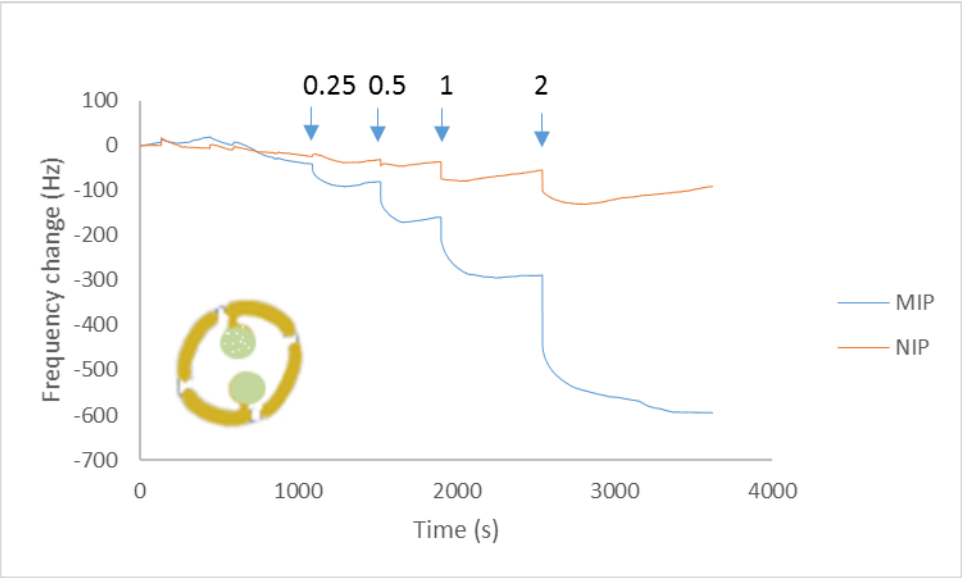

Figure 84: Increasingly concentrated lysozyme solutions giving rise to larger sensor responses for a lysozyme imprinted polyurethane sensor synthesized in a dilute manner.

Figure 84 shows the result of a concentration dependent frequency shift for a lysozyme imprinted polymer sensor. Characteristically for this sensor is the large amount of lysozyme present in the polymer-protein mixture. This allows more imprinted cavities to be present in the polymer matrix and thus increases the maximum lysozyme uptake. The outcome of the experiment also shows significant differences between MIP and NIP (IF>4 for 1000 and 2000 ppm) and moreover stable signals. Figure 85 also reveals linear sensor characteristic which is proven by the R^2 of 0.999. It has to be mentioned, however, that only four different points/concentrations are plotted. The MIP to NIP ratio is the most prominent at a concentration of 1 mg/mL but also exceeds a value of two at a concentration of 250 ppm. Exact numbers are given in Table 11.

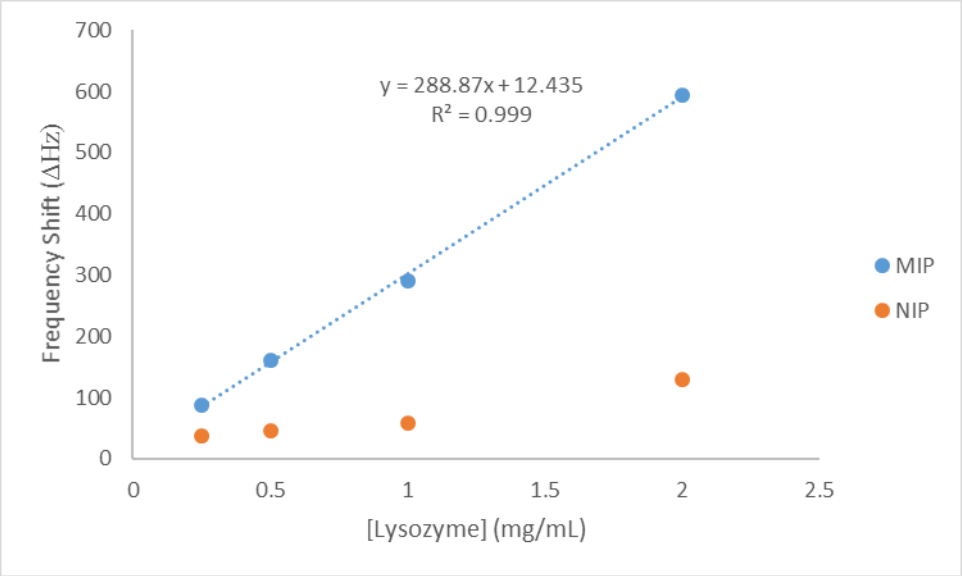

Figure 85: Calibration curve for the outcome of Figure 84.

Table 11: Sensor response of MIP and NIP channel for the respective lysozyme concentration.

[Lys] (mg/mL)	MIP (ΔHz)	NIP (ΔHz)	MIP/NIP Ratio
2	594	129	4.6
1	291	58	5.0
0.5	161	46	3.5
0.25	87	37	2.4

To test the repeatability of the sensor, the measurement is repeated once more. Aside of that, a washing step is implemented after each protein solution addition. From Figure 86, one can see the concentration dependency of the sensor again. Applying 2000 ppm (2mg/mL) leads to a frequency decrease of approximately 130 Hz, solutions below 500 ppm even to responses below 20 Hz. Also injection of the same concentration (2 mg/mL) during the same experiment resulted in two significantly distinct responses. Compared to the first trial, responses are significantly lower (-150 instead of -594 Hz for the MIP side of both trials respectively). The NIP channel does not respond much and washing using water is successful. To conclude, it can be said that the sensor shows concentration dependency over a range of 2000-200 ppm and significant differences between imprinted and non-imprinted channels are observed in this concentration area. However, the absolute response signals are significantly reduced for the second trial. This is possibly due to incomplete removal of lysozyme from the sensor surface after the first attempt. Investigation towards stronger solvents for breaking lysozyme-polymer bonds can provide a solution to this issue.

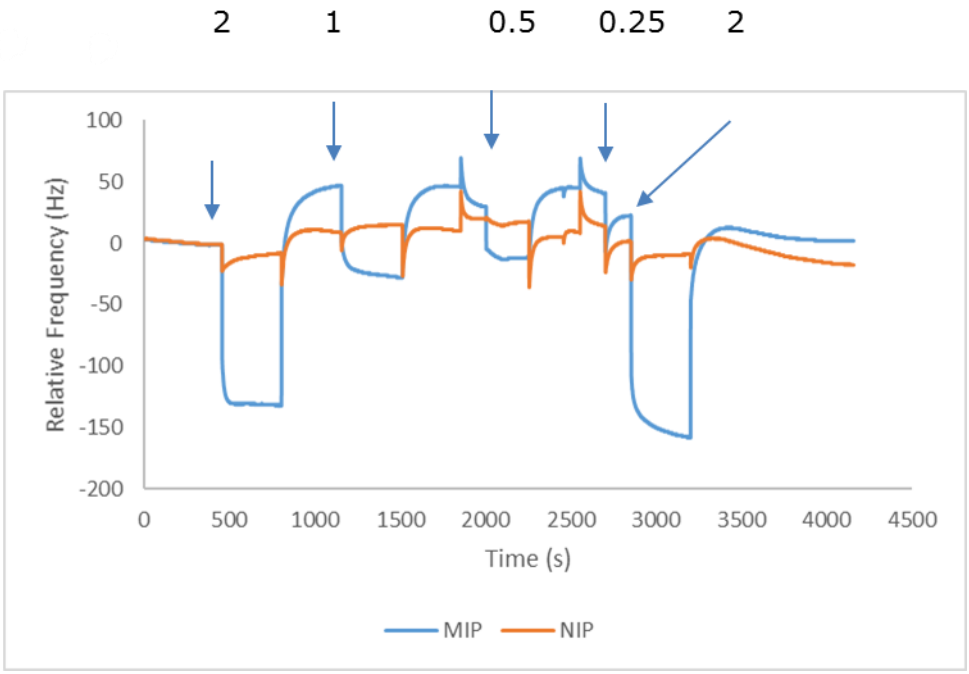

Figure 86: QCM measurement of the alternative bulk-imprinted PU lysozyme MIP. Concentration values are given in mg/ml.

In order to obtain more significant sensor responses, a modified recipe is proposed. Procedures 2&3 in section 2.3.2 describe these concrete synthesis approaches. These two strategies differ in the way how lysozyme is added onto the polymer. In the case of procedure 2, 1 mg of lysozyme powder is dissolved in prepolymer. In procedure 3, however, lysozyme is dissolved in distilled water prior to addition onto the prepolymer.

To evaluate the effect of the lysozyme concentration on the outcome of MIP fabrication, another approach is proposed. Figure 87 gives the outcome of a QCM experiment performed on a bulk-imprinted QCM towards lysozyme fabricated *via* procedure 2. Instead of a 20 mg/mL lysozyme solution, 10 mg/mL lysozyme solution is used for MIP synthesis.

From the sensor response, it can be seen that the lower concentrations have negligible influence. Both MIP and NIP side react in the same way to the protein in the solution. Increasing the amount of lysozyme present in the sample, however, leads to larger discrimination of both electrodes. Figure 88 visualizes the outcome of this experiment by plotting the difference of MIP-NIP over time. It has to be noted, however that each shift corresponding to a certain concentration has to be measured in response to the baseline signal. This is the signal before addition of the analyte. The signal related to it needs some time to stabilize and to reach equilibrium. Considering the drift in the signal, significant changes can be observed staring from 500 ppm. At this particular point, the NIP channel even responds by an increase in signal. This denotes the unselective behavior of the protein towards this reference channel.

Gradual addition of more and more increasingly concentrated lysozyme solutions leads to more pronounced shifts. At 2000 ppm, the sensor achieves an imprinting factor of circa 2. In the first experiment, a step-wise increase of lysozyme concentrated solutions is added onto the quartz. No washing steps are performed between two measurements. The second measurement displays the response of the same quartz where a washing step takes place between exposing the sensor to two different concentrations of lysozyme.

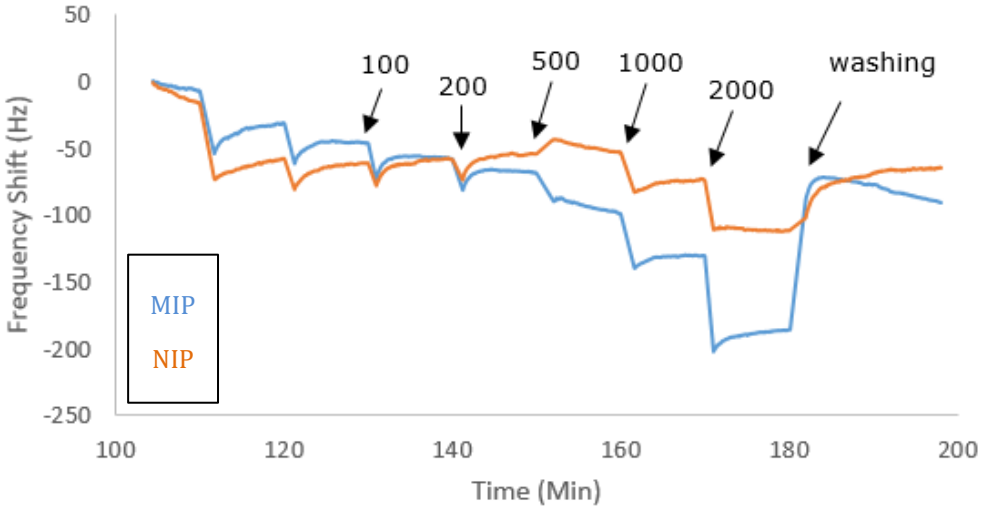

Figure 87: QCM measurement for a PU bulk-imprinted lysozyme sensor (blue line) versus the reference NIP channel (orange line) according to procedure strategy 2.

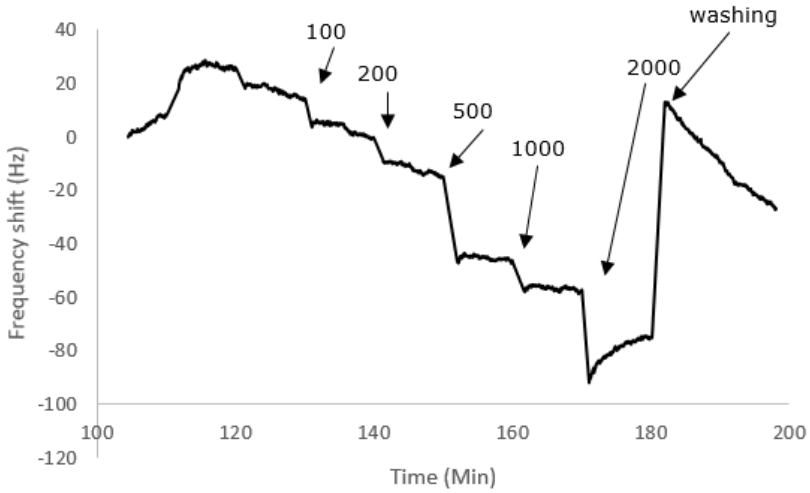

Figure 88: Difference MIP-NIP signal for increasingly concentrations of lysozyme onto the sensor synthesized by procedure 2 followed by an ultimate washing step.

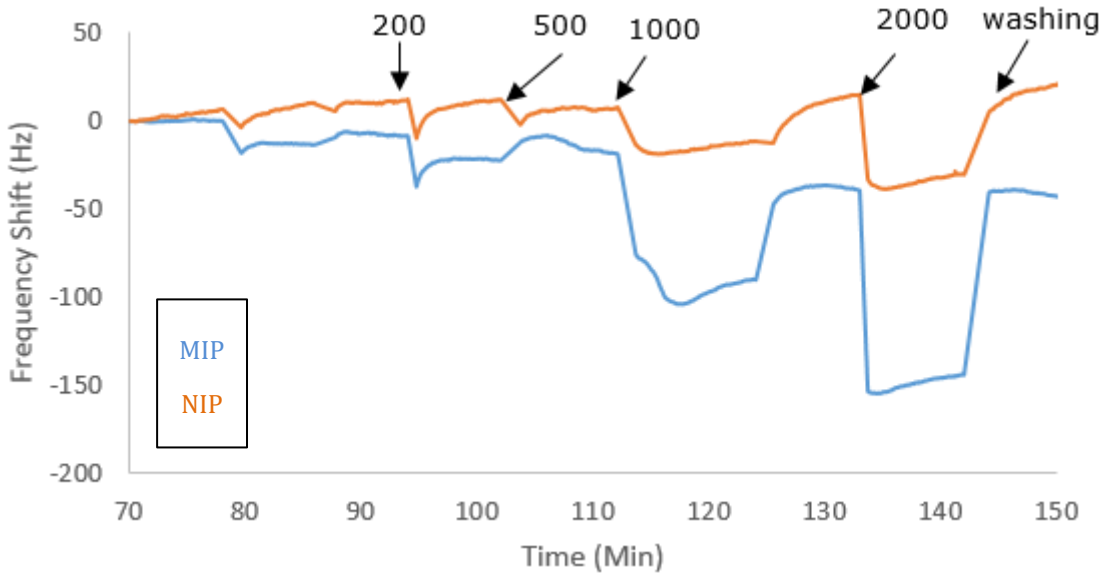

Figure 89: Repeated measurement for strategy number 2 for PU MIP synthesis.

Figure 89 displays a repetition of the measurement performed in Figure 87. The only change being that a washing step is executed after each protein solution administration. Washing is successful and the signal shows more stability. A significant difference of about 75 and 110 Hz can be observed at 1000 and 2000 ppm respectively. Compared to the previous measurement, differences at concentrations below 500 ppm are less pronounced.

Compared to the first trial of the first bulk-imprinting recipe, significantly lower responses are identified. From this experiment, it can be stated that large amounts of lysozyme present in the prepolymer mixture allow for significantly larger sensor responses (-600 versus -200 Hz at 2mg/mL). Moreover, larger imprinting factors are achieved by the first method. Finally, the first sensor suffers from less drift signal contributing to the stability of the device. However, when comparing the latter sensor with the second attempt of the first PU-bulk imprinted device, minor changes are observed. Adding the 2000 ppm lysozyme solution evokes -200 Hz change for this sensor whereas the previously presented sensor only gave a response of about -150 Hz.

Figure 90 describes the result of a QCM measurement synthesized *via* bulk imprinting (procedure 3). As a reminder: lysozyme is dissolved into water before mixing it with the prepolymer. Lysozyme solutions are added in a step-wise manner without intermediate washing steps. The concentration range lies between 100 and 5000 ppm. It can be said that the NIP channel suffers from instability displaying frequency increases (the so-called anti-Sauerbrey effect) at higher concentrations. This anomaly becomes particularly remarkable after addition of 500 ppm lysozyme. Paying attention to the MIP side, a concentration dependent fashion can be observed. Washing out the protein in the end is successful, proven by the reversible signal going up near the baseline level. It is impossible to discriminate between 500 and 1000 ppm since both are characterized by a frequency decrease of about -85 Hz. Although responses are slightly more pronounced for this sensor in comparison with the one prepared according to procedure 2 (Δf = 200 versus 150 Hz), the reference channel of this sensor is less stable.

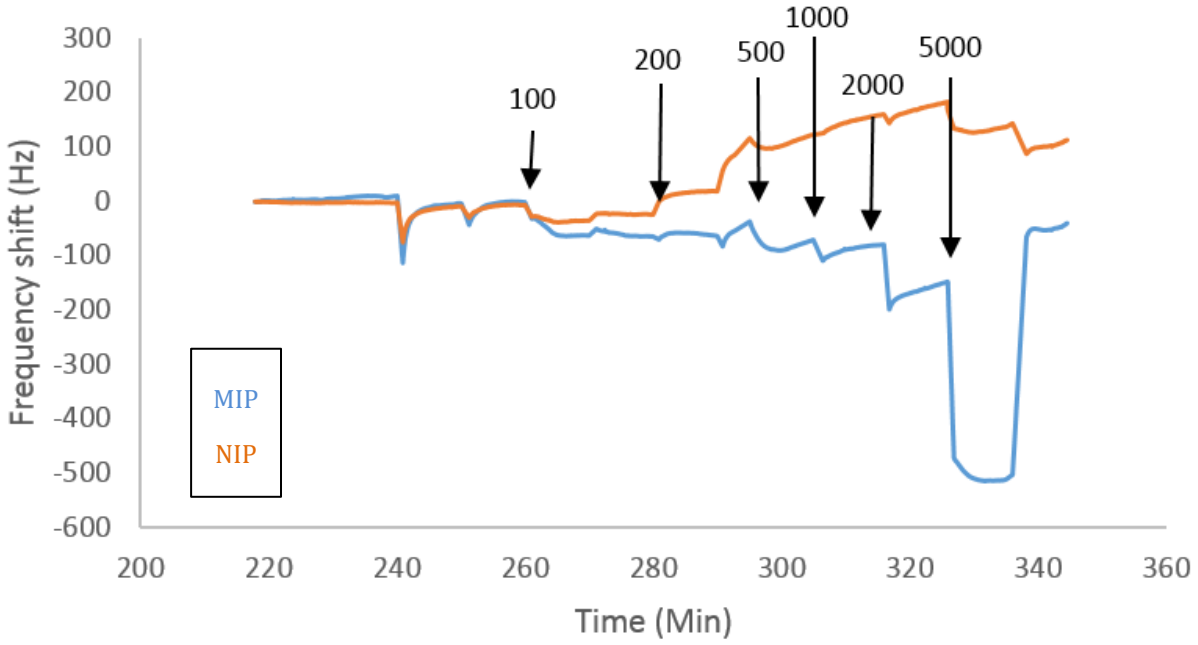

Figure 90: QCM outcome after lysozyme bulk imprinting using polyurethane. Synthesis is given in 2.3.2 under strategy 3.

Figure 91 summarizes the concentration dependent behavior of lysozyme on a sensor based on bulk imprinting. Here, the difference between MIP and NIP are visualized. Doing this, there is an even more pronounced distinction between imprinted and reference side. This way, one can already differentiate between MIP and NIP at a concentration of 100 ppm.

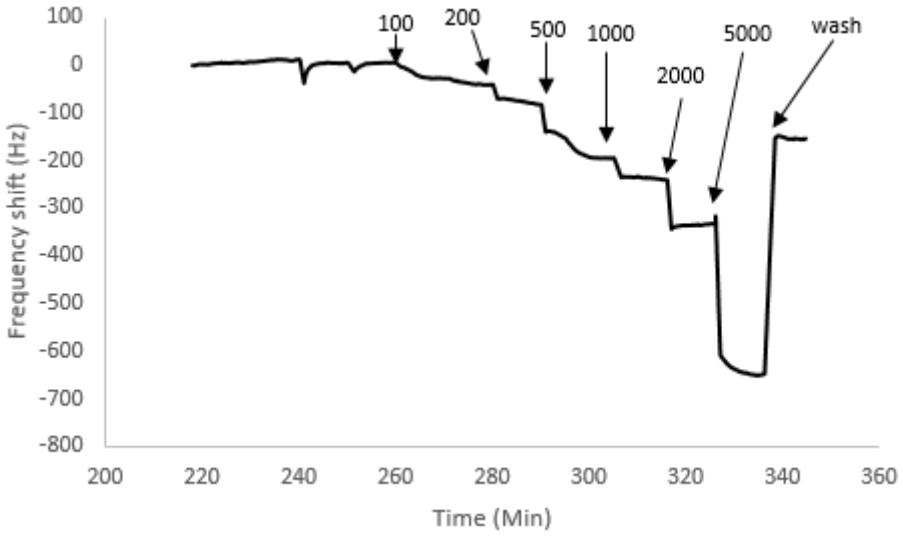

Figure 91: Signal of MIP-NIP for QCM coated with PU by bulk imprinting procedure 3.

Sedimentation

Apart from bulk and stamp imprinting methods for PU, also sedimentation imprinting is tested. A highly concentrated (10 mg/mL) lysozyme solution is applied onto a PU layer. Additionally, pressure is applied to become imprints on top of the polymer surface. The exact manufacturing is listed in 2.3.2 under polyurethane procedure 4. Figure 92 displays the outcome of this sedimentation imprinting procedure. The signal of the NIP channel is stable whereas the MIP side suffers from drift. After injection of 2000 ppm lysozyme, the response went down by approximately 250 Hz. The MIP signal, on the other side displays a very unstable behavior. Because these results, the sensor is not useful and no further trials with sedimentation-imprinted PU are completed.

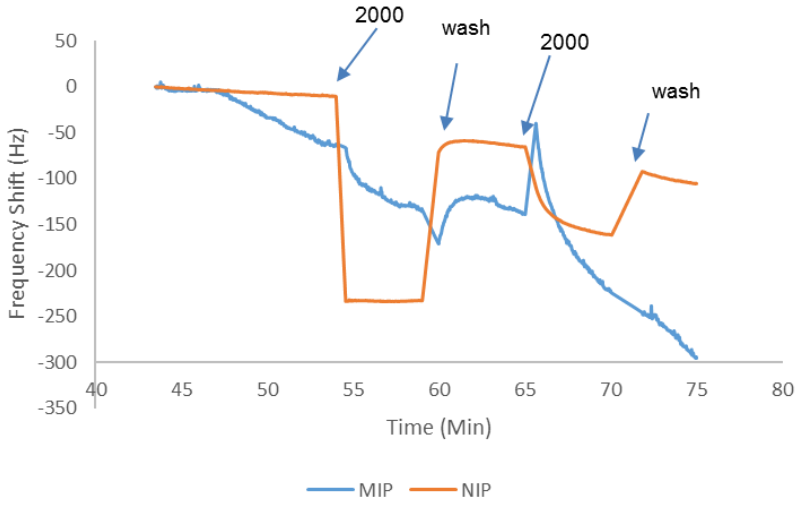

Figure 92: Sedimentation imprinted PU according to procedure 4.

3.2.3. Selectivity

Sensitivity is important, but to assess MIP quality, one needs to know selectivity. Figure 93 shows the result of a QCM designed for lysozyme. The sensor is coated with an EGDMA-AA polymer and imprinted for lysozyme. The sensitivity response of a sensor relying on this polymer is displayed in Figure 69. The exact synthesis approach is described in 2.3.2. This sensor gives the best outcome allowing detection of lysozyme at 50 ppm. In order to test its selectivity, the quartz was subjected to same (weight) concentrations of lysozyme as well as BSA.

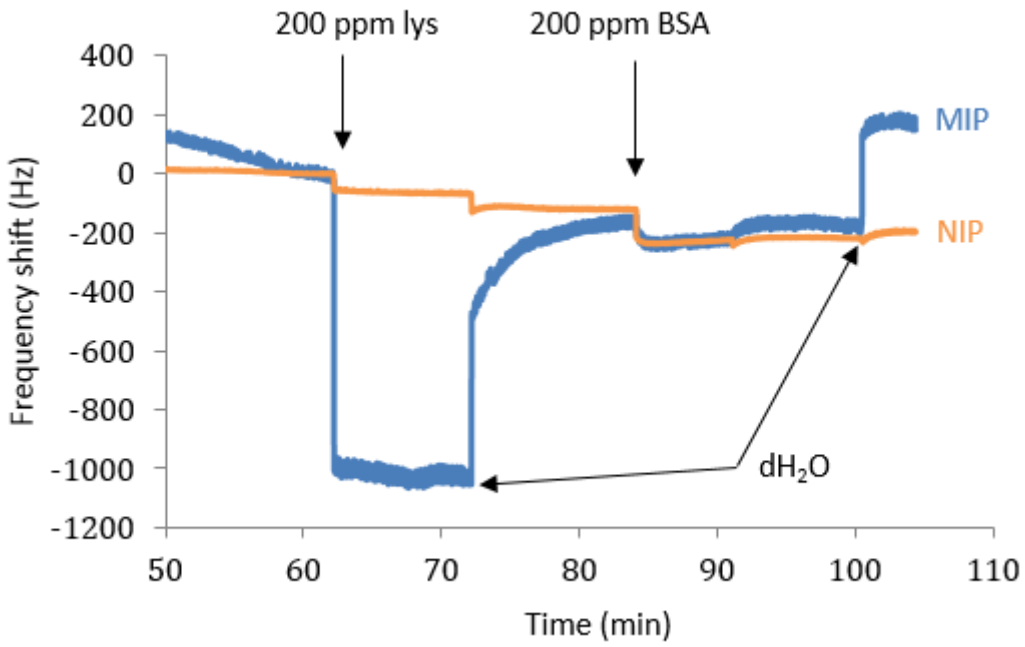

Figure 93: Selectivity pattern for a lysozyme-imprinted quartz generated by method 2.3.2.

It can be clearly seen that injection of a 200 ppm lysozyme solution resulted in a shift of 1000 Hz whereas the addition of BSA lead to almost no change. As already stated, the molar masses of lysozyme and BSA are 14.3 kDa and 66.5 kDa respectively, meaning that more lysozyme molecules are present in solution. However, if one albumin molecule binds the surface, it has a larger response compared to lysozyme. The time axis starts at 50 minutes because the sensor needed this time to become stable during the stabilization phase. The NIP channel showed less than -100 Hz response after the lysozyme solution was injected, an indication that only minor nonspecific binding occurs. This unselective signal was more provoked after BSA administration, however still marginal compared to the lysozyme response on the MIP side. Hence, one can conclude that the sensor exhibits notably sensitivity and selectivity towards the analyte for which it was imprinted. On the other hand, it does not respond to any kind of protein making the sensor selective as well.

The sensor prepared *via* the alternative EGDMA-AA approach which sensitivity profile is represented in Figure 74, was also tested for selectivity. For that purpose, it was exposed to the same weight concentration of lysozyme as well as to pepsin, a 35.5 kDa protein. The result is represented in Figure 94. Addition of 2 mg/mL of lysozyme leads to a frequency decrease of 150 Hz whereas addition of pepsin results in a 120 Hz frequency decrease. There is a difference between the two signals, however the pepsin also seems to react strongly to the EGDMA-AA polymer/imprints.

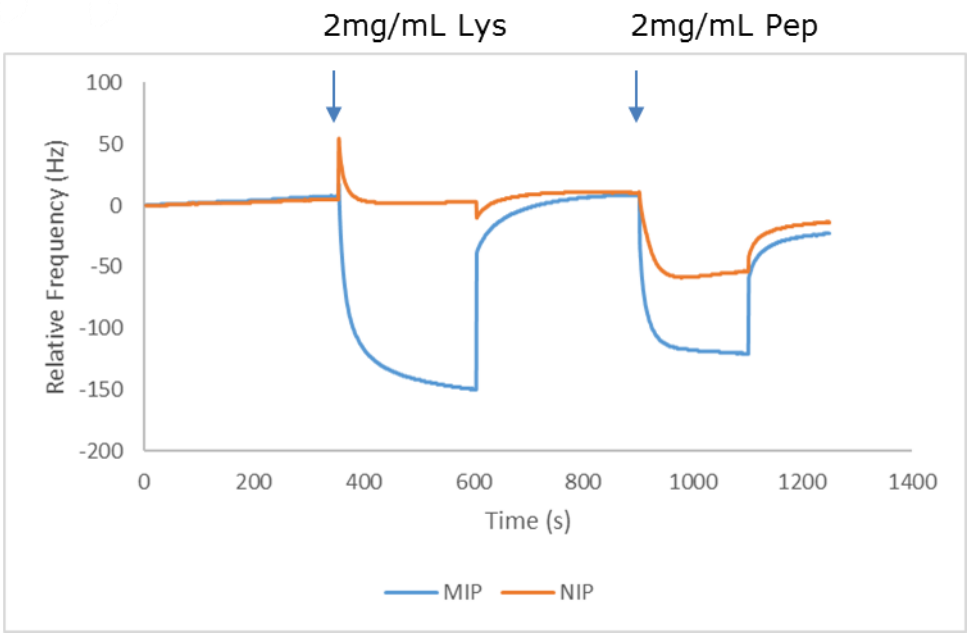

Figure 94: Selectivity measurement for a lysozyme imprinted sensor. The sensor was tested for lysozyme and pepsin at a concentration of 2 mg/mL.

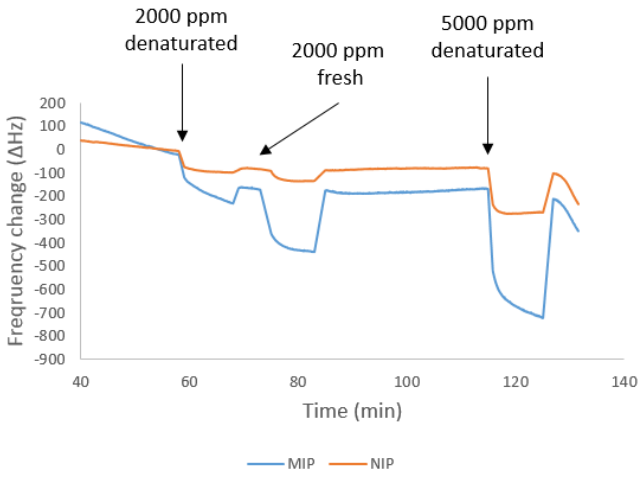

Figure 95: Selectivity measurement of a PU bulk MIP produced by strategy 2; Influence of denaturation on sensor response.

In order to test the importance of protein conformation for molecular recognition, we applied fresh as well as denatured lysozyme to the sensor. The sensor is a bulk-imprinted PU sensor towards lysozyme. Both electrodes were covered by 5 µL of diluted polymer. One day on beforehand, 3 µL of a (20 mg/mL in dH_2O) lysozyme solution was pipetted onto a clean glass slide and dried in the fridge overnight. This glass slide was placed onto the channel denoted MIP. The NIP side remained untreated and was covered by a blank glass slide. It can indeed be observed that addition of 2000 ppm of denatured lysozyme resulted in a frequency change half of the value when normal lysozyme is applied (-210 instead of -440 Hz). Therefore, it can be concluded that the native conformation allows for double as high binding effect. Increasing the concentration to 5000 ppm results in a significantly larger sensor response of -700 Hz. This signal is more than 3 times higher than the signal at 2000 ppm of denatured protein. Possibly, it this high concentration, unselective binding of lysozyme onto the surface becomes very strong. Another explanation is that the protein recoveres from denaturation. Remark that the signal recovered to baseline after the washing step. This is important for creating reusable sensors.

3.2.4. pH Dependency

The influence of pH on the sensor response is also assessed. Addition of 2 mg/mL lysozyme at three different pH values (3, 5 and 8) results in different responses. All solutions prepared are PBS buffers. This way, not only the acidity but also the salt concentration is different to our conventional measurements. If not stated so, measurements are always performed in distilled water. From Figure 96, it can be deduced that not only the concentration of the analyte affects the change in signal but also the acidity of the solution wherein it is applied. Lysozyme in a solution of pH 5 resulted in a large shift of between -7400 to -8400 Hz. Signals at pH 3 and 8 are significantly less intensive (-500 and -2000 Hz). Almost no response can be observed on the reference channel. All solutions are 10mM PBS buffer adjusted to the correct pH value meaning there is no significant difference in salt concentration. Any signal response differences are the effect of acidity. These effects might indicate that also electric/charging effects may affect the measurement because changing pH values lead to modified dipole-dipole interactions. Proteins become more or less charged depending on the acidity of the solution. According to Sigma-Aldrich, the protein is active from pH 6-9. Moreover, it reaches maximal activity over a wide range of ionic strengths at pH 6.2. In our test, the largest response is seen at pH 5. As already mentioned in 1.6.2, the isoelectric point of lysozyme is located at pH 11. Since all solutions applied are marked by a lower pH value, the protein appears in its positive form all the time. Aside of that, the binding response seems to be the biggest at pH 8.

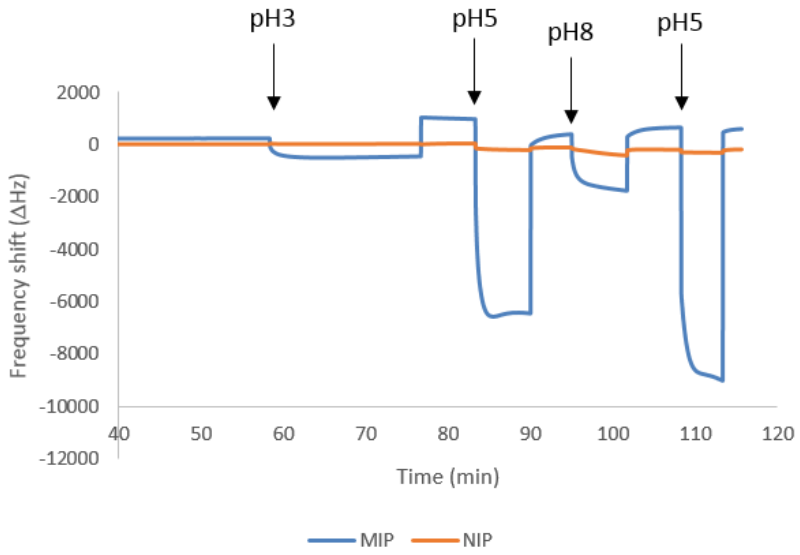

Figure 96: pH dependent measurement for a lysozyme-imprinted sensor. All lysozyme solutions have a concentration of 2000 ppm.

3.3. Synthesis of Core Shell Nanoparticles

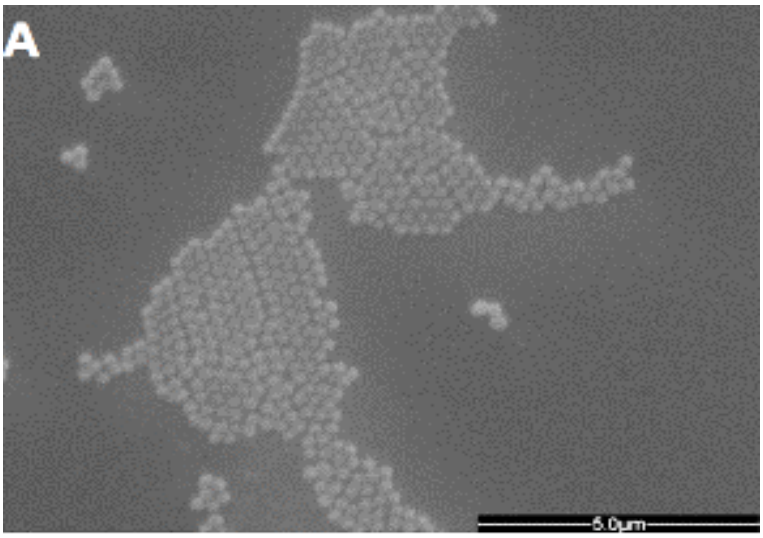

Figure 97: SEM picture displaying silica core nanoparticles.

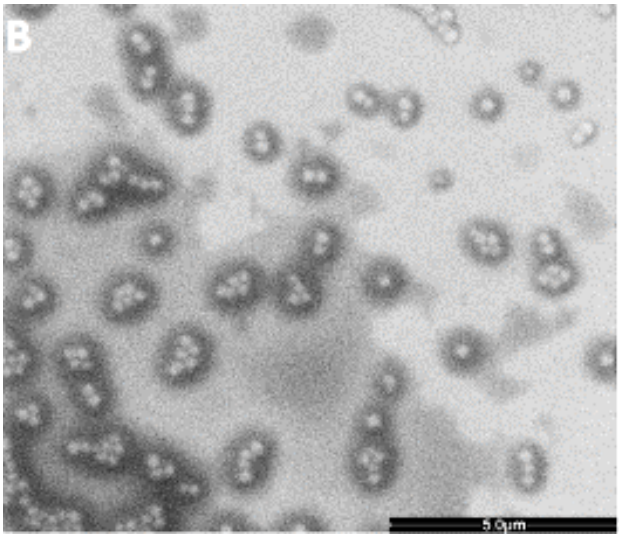

Figure 98: SEM image displaying silica core nanoparticles coated with 3-trimethoxysilyl-propyl methacrylate.

Goal of the project was to obtain better insights in the synthesis and characterization of core shell nanoparticles. NPs are characterized by their large surface to volume ratio enabling the detection of more analytes per surface area. As a result, a more sensitive sensor can be developed. Each target is characterized by specific dimensions and based on that, an appropriate shell thickness has to be chosen. At this stage, however, I did not fixate on one particular template but just wanted to get confident with their synthesis. After discussing what would be the best candidate to function as core, the choice fell on silicon.

The next step would be to functionalize these particles with methacrylate end groups. In the beginning, the focus was set on reproducing experiments established by current members of the group “Materials Solutions”.

A first batch of experiments was performed using tetraethylorthosilicate (TEOS) in combination with 3-trimethoxysilyl-propyl methacrylate dissolved in a mixture of distilled water and ammonium hydroxide. Six different mixtures were prepared where the latter three ingredients were present in varying concentrations. All samples were stirred for 2 hours at room temperature. Particles sizes were measured then with a Zetasizer Nano (Nano-S) particle-size analyser from Malvern Instruments to get an indication of their diameter size. All six samples were extremely different in visual appearance as well as in measured size. Thereby, the polydispersity index was fairly high, characteristic for non-uniform particles.

I achieved to obtain monodisperse particles. Here, we changed the setup by polymerizing phenyltrimethoxysilane dissolved in water and ammonium hydroxide at 60 °C in a reactor supplied with nitrogen gas. Experiments are performed at 60 °C and the reaction was stopped on ice. This process led to particles of around 360 nm in diameter. Next, the cores were coated with 3-trimethoxysilyl-propyl methacrylate and DLS was performed again. An increase of 50 nm was observed as compared to the DLS experiment before addition of the methacrylate. Then, TEOS was used instead of phenyltrimethoxysilane. After this procedure, scanning electron microscopy (SEM) experiments are performed.

Also a new procedure using TEOS dissolved in ethanol and ammonium hydroxide was established successfully. Very small (40 nm) uniform nanoparticles are formed by means of this straightforward overnight synthesis.

4. CONCLUSION & OUTLOOK

In this work, we present the development of various sensors for the detection of bovine serum albumin and lysozyme. For both analytes, multiple suitable polymer systems were tested and evaluated.

As a starting point, the work of a predecessor was continued to optimize the BSA imprinting procedure. DHEBA-MAA, DHEBA-AA-VP and HEMA-EbAM were used as polymers. The first one allows for clear differentiation between working and reference electrode at 100 ppm whereas the working electrode of the second system suffers from drift. Starting from 200 ppm, a significant distinction between the two electrodes can be observed. Changing the polymer to HEMA-EbAM leads to the best result. Addition of 200 ppm BSA evokes sensor responses around -1500 Hz. Moreover, the signal stays stable over the complete measurement. As a drawback, anti-Sauerbrey effect is noticed on the reference channel. Selectivity studies do not show good results since the sensor is also extremely responsive towards other proteins. SDS and water allow for full removal of the protein from the sensor. Addition of protein solutions using a peristaltic pump leads to larger sensor responses but also evokes more fluctuations in the signal. These conclusions gave me valuable insights in the molecular imprinting process in order to continue with my ultimate target of interest, namely lysozyme.

Concerning lysozyme, more attempts were performed to obtain a sensitive and selective sensor. Sedimentation, stamp and bulk imprinting procedures were tested. Sensors prepared using the sedimentation approach did not lead to satisfactory measurements.

Bulk imprinted EGDMA-AA polymers show concentration-dependent sensor responses (R^2 = 0.9852) with an LOD of around 50 ppm. Addition of 2000 ppm leads to a sensor response of approximately -400 Hz whereas the reference channel responds with about -200 Hz. The measurement can also be performed in TRIS buffer. As an alternative procedure, lysozyme was dissolved in acrylic acid rather than in TRIS buffer. Here, differences are observed starting at a concentration of 500 ppm.

Next, different PU synthesis approaches were evaluated. Stamp imprinting shows concentration dependent signals with a limit of detection between 200 and 500 ppm. Bulk imprinting of the protein results in similar outcome looking at the sensor responses (-600 Hz versus -800 Hz for 2000 ppm). However, it is feasible to discriminate at 250 ppm in case of bulk imprinting. Additionally, this procedure gives rise to imprinting factors of three and more. In a repeatability test, however, the signal responses are significantly reduced (-130 instead of -600 Hz). This may be due to the fact that not all protein has been successfully removed from the sensor. Further

experiments should be executed to test this phenomenon. The influence of the amount of protein present in the prepolymer mixture was tested as well. Decreasing the amount of lysozyme is not helpful to ameliorate the sensor. On the contrary, it leads to less stable and less prominent signals. Repeating the test gives rise to the same values. First dissolving lysozyme in water before addition is also shown to be beneficial for the sensor. Differences between MIP and NIP are observable at 100 ppm. Despite the NIP channel being unstable, the MIP side shows good concentration-dependent sensor characteristics.

Selectivity is tested for the standard EGDMA-AA lysozyme bulk-imprinted sensor. The sensor can discriminate easily between 200 ppm BSA and lysozyme. The alternative EGDMA-AA lysozyme bulk-imprinted sensor was also subjected to a selectivity test. Here, the signals response upon pepsin and lysozyme addition is less significant. Finally, the sensor was also tested on pH of protein solution as well as on conformation status of the protein. At 2000 ppm, the sensor gives a signal half of the original value (-210 instead of -440 Hz) when the protein is added in its denatured form. However, addition of 5000 ppm of denatured protein gives a high response of about -700Hz. Lysozyme (2000 ppm) added in a buffer of pH 5 gives a significantly larger response compared to application of the same protein concentration at pH 3 or 8.

AFM measurements allowed us to determine the topography of our stamps. More specific, the homogeneity of the glass slide could be determined. It can also be expanded to characterization of the polymer surface on the quartz. Xanthoprotein test can be used to evaluate the quality of the washing step by indicating its presence through a color reaction. FTIR is used to monitor the PU synthesis. This way, it is convienient to create more reproducible MIPs. We also managed to create silica nanoparticles coated with a polymer shell. In the future, these modified particles can be imprinted by target molecules.

Further research has to be done to improve the sensitivity and even more the selectivity of the sensors. It should also be checked whether it is feasible under normal conditions (i.e. directly in saliva, blood plasma,…).

5. Abstract

This work describes the fabrication of biomimetic sensors for the detection of bovine serum albumin as well as lysozyme. The measurement principle is based on combining molecular imprinted polymers with quartz crystal microbalance.

Various polymer systems including polyurethane, methacrylates, bisacrylamides and acrylic acids are tested for both analytes. By continuing the experiments of a predecessor, it was possible to detect BSA at a concentration of 100 ppm using a DHEBA-AA-VP polymer system. However, washing out the analyte was challenging. Changing the polymer system towards HEMA-EbAM, on the other hand, allowed for successful removal of the albumin from the cavities. The creation of an EGDMA-AA imprinted quartz gave good results for the detection of lysozyme. It was feasible to reach a detection limit below 50 mg/L. There was a significant discrimination between imprinted and reference (non-imprinted) channel. Furthermore, it possesses linear behavior in the concentration range from 50-2000 mg/L. A polyurethane bulk imprinting process also resulted in the fabrication of a sensor displaying concentration dependency in a range from 100-5000 mg/L.

Additionally, several washing procedures such as SDS, PBS and acetic acid are tested to demonstrate the reusability of the sensor. However, mostly it was possible to remove the analyte from the cavities by thoroughly washing with distilled water. Furthermore, pH dependency of the sensor towards lysozyme in solutions of various acidity is investigated. To test the selectivity of the lysozyme sensor, it is exposed towards equal concentrations of various analytes such as pepsin, BSA and HAS. The EGDMA-AA imprinted lysozyme sensor is able to discriminate upon addition of 200 ppm lysozyme and BSA by a factor of 10. Its sensor responses are -1000 Hz and -100 Hz respectively.

Atomic force microscopy (AFM) is used to indicate the presence of the respective proteins on the glass stamps. This technique can also be used in the future to characterize the formation of cavities in the polymer.

In short, we developed several sensors for the detection of BSA and lysozyme at a detection limit of approximately 100 mg/L. Polyurethane and EGDMA-AA possess the best results for sensitivity, stability and concentration dependency.

6. Zusammenfassung

Diese Arbeit beschreibt die Herstellung eines biomimetischen Sensors zur Detektion von Bovinem Serumalbumin und Lysozym. Das Messprinzip basiert auf einer Kombination aus molekular geprägten Polymeren und Quarzmikrowaagen.

Verschiedene Polymersysteme wie z.B. Polyurethan, Methacrylate, Acrylamide und Acrylsäure wurden für beide Analyte getestet. Durch die Fortsetzung/Weiterführung von Experimenten eines Vorgängers war es möglich, BSA bis zu einer Konzentration von 100 ppm mittels DHEBA-AA-VP Polymer zu detektieren. Allerdings stellte das Auswaschen des Analyten eine Herausforderung dar. Die Änderung vom Polymer zu HEMA EbAM ermöglichte eine erfolgreiche Entfernung des Albumins aus den Kavitäten. Die Herstellung von EGDMA-AA Polymeren ergab gute Ergebnisse für die Detektion von Lysozym. Es wurde eine Nachweisgrenze unterhalb von 50 mg/L erreicht. Bulk Imprinting in Polyurethan ergab Konzentrationsabhängigkeit in einem Bereich von 100-5000 mg/L.

Zusätzlich wurden verschiedene Waschprozeduren mit SDS, PBS und Essigsäure getestet worden, um die Wiederverwendbarkeit des Sensors zu demonstrieren. Dabei war es meistens möglich die Analyten aus den Hohlräumen zu entfernen. Außerdem wurde die pH-Abhängigkeit des Sensors für Lysozym in Lösungen bei verschiedenen Azidität untersucht. Um die Selektivität dieser Lysozymsensoren zu testen, wurden sie verschiedenen Analyten (BSA-Pepsin-HSA) bei gleichbleibender Konzentration ausgesetzt. Der Lysozym-geprägte EGDMA-AA Sensor zeigt ein zehnmal höheres Signal bei Zugabe von 200 ppm Lysozym verglichen zu BSA in gleicher Konzentration. Das Ansprechen beträgt -1000 Hz beziehungsweise -100 Hz.

Rasterkraftmikroskopie wurde benutzt um die Anwesenheit der entsprechenden Proteine auf Glasstempeln nachzuweisen. Diese Technik kann auch benutzt werden um Kavitäten nachzuweisen.

Zusammengefasst haben wir verschiedene Sensoren für BSA und Lysozym mit einer Nachweisgrenze von circa 100 mg/L entwickelt. Polyurethan und EGDMA-AA liefern die besten Ergebnisse für Sensitivität, Stabilität und Konzentrationsabhängigkeit.

7. Abbreviations

AA	Acrylic Acid
AB	Antibody
AFM	Atomic Force Microscopy
AFR	Acoustic Film Resonance
AG	Antigen
AIBN	2,2-azobis(2-methylpropionitrile)
APTES	(3-Aminopropyl) triethoxysilane
AR	Anomalous reflection
ATR	Attenuated Total Reflectance
ATRP	Atom Transfer Radical Polymerization
BAW	Bulk Acoustic Wave
BCA	Bicinchonic Acid
BCG	Bromocresol Green
BCP	Bromocresol Purple
BPA	Bisphenol A
BSA	Bovine Serum Albumin
BSE	Backscattered Electron
CAS	Chemical Abstracts Service
CRP	Controlled/Living Radical Polymerization
CTA	Chain Transfer Agent
DABCO	1,4-diazabicyclo[2.2.2]octane
DHEBA	N,N-(1,2-Dihydroxyethylene)bis-acrylamide
DLS	Dynamic Light Scattering
DMAEMA	2-(dimethylamino)ethyl Methacrylate
DMAPMA	Dimethylamino Propyl Methacrylamide
DPDI	4,4'-methylenediphenyl Diisocyanate
EbAM	N,N′-Ethylenebis(acrylamide)
EGDMA	Ethylene Glycol Dimethacrylate
ELISA	Enzyme Linked Immunosorbent Assay
ERMAP	Erythroid Membrane Associated Protein
FRP	Free Radical Polymerization
FTIR	Fourier Transform Infrared
Glu	Glutamine
HEMA	Hydroxyethylmethacrylate
HPLC	High-performance Liquid Chromatography
IAGT	Indirect Anti-globulin Test
IDT	Interdigital Transducer
IEF	Isoelectric Focusing
Ig	Immunoglobulin
LOD	Limit of Detection
LOQ	Limit of Quantification
LPS	Lipopolysaccharides
MAA	Methacrylic Acid
MHz	Megahertz
MIP	Molecularly Imprinted Polymer
MM	Molar mass
NAG	N-acetyl-D-glucosamine
NAM	N-acetylmuramic Acid
NIP	Non-imprinted Polymer
NMP	Nitroxide Mediated Polymerization
NP	Nanoparticle

P	Electrical Polarization
PBS	Phosphate Buffered Saline
PDI	Polydispersity Index
PDMS	Polydimethylsiloxane
PG	Phloroglucinol
Phe	Phenylalanine
ppm	Parts per Million
PS	Polystyrene
PU	Polyurethane
PVP	Polyvinylpyrrolidone
QCM	Quartz Crystal Microbalance
QCM-D	Quartz Crystal Microbalance with Dissipation Monitoring
RAFT	Reversible Addition Fragmentation Polymerization
RDRP	Reversible Deactivation Radical Polymerization
RT	Room Temperature
SA	Serum Albumin
SAW	Surface Acoustic Wave
SC	Scianna Blood Type
SE	Secondary Electron
SEM	Scanning Electron Microscopy
SPE	Serum Protein Electrophoresis
SPM	Scanning Probe Microscopy
SPR	Surface Plasmon Resonance
STM	Scanning Tunneling Microscopy
TEMPO	2,2,6,6-Tetramethylpiperidinyloxyl
TEOS	Tetraethyl Orthosilicate
THF	Tetrahydrofurane
TrenMe	Tris(2-dimethylaminoethyl)amine
Trp	Tryptophan
TRIS	Tromethamine
Tyr	Tyrosine
UV	Ultraviolet
VDW	Vanderwaals
VP	1-vinyl-2-pyrrolidinone
WHO	World Health Organisation

8. Symbols

A	Surface area
A	Ampere
c	Concentration
C_M	Monomer Concentration
C_L	Crosslinking Degree
°C	Degrees Celsius
d	Crystal Thickness
Da	Dalton
dB	Decibel
DNA	Deoxyribonucleic Acid
ϵ	Well Depth
f	Frequency
f_0	Resonant Frequency
Δf	Frequency Change
μ	Shear Modulus
N	Newton
$\tilde{\upsilon}$	Wavenumber
$\nu_{crystal}$	Speed of Sound in Quartz
η	Viscosity
$\phi(r)$	Lennard-Jones Potential
r	Interatomic Distance
rpm	Rounds per Minute
RT	Room Temperature
ρ	Density
$\rho_{crystal}$	Crystal Density
σ	Distance where Intermolecular Potential between Two Particles is Zero
T	Temperature
T_m	Melting Temperature

9. Appendix

Table 12: Sequence Human Serum Lysozyme (HAS)

1	MET	2	LYS	3	ALA	4	LEU	5	ILE
6	VAL	7	LEU	8	GLY	9	LEU	10	VAL
11	LEU	12	LEU	13	SER	14	VAL	15	THR
16	VAL	17	GLN	18	GLY	19	LYS	20	VAL
21	PHE	22	GLU	23	ARG	24	CYS	25	GLU
26	LEU	27	ALA	28	ARG	29	THR	30	LEU
31	LYS	32	ARG	33	LEU	34	GLY	35	MET
36	ASP	37	GLY	38	TYR	39	ARG	40	GLY
41	ILE	42	SER	43	LEU	44	ALA	45	ASN
46	TRP	47	MET	48	CYS	49	LEU	50	ALA
51	LYS	52	TRP	53	GLU	54	SER	55	GLY
56	TYR	57	ASN	58	THR	59	ARG	60	ALA
61	THR	62	ASN	63	TYR	64	ASN	65	ALA
66	GLY	67	ASP	68	ARG	69	SER	70	THR
71	ASP	72	TYR	73	GLY	74	ILE	75	PHE
76	GLN	77	ILE	78	ASN	79	SER	80	ARG
81	TYR	82	TRP	83	CYS	84	ASN	85	ASP
86	GLY	87	LYS	88	THR	89	PRO	90	GLY
91	ALA	92	VAL	93	ASN	94	ALA	95	CYS
96	HIS	97	LEU	98	SER	99	CYS	100	SER
101	ALA	102	LEU	103	LEU	104	GLN	105	ASP
106	ASN	107	ILE	108	ALA	109	ASP	110	ALA
111	VAL	112	ALA	113	CYS	114	ALA	115	LYS
116	ARG	117	VAL	118	VAL	119	ARG	120	ASP
121	PRO	122	GLN	123	GLY	124	ILE	125	ARG
126	ALA	127	TRP	128	VAL	129	ALA	130	TRP
131	ARG	132	ASN	133	ARG	134	CYS	135	GLN
136	ASN	137	ARG	138	ASP	139	VAL	140	ARG
141	GLN	142	TYR	143	VAL	144	GLN	145	GLY
146	CYS	147	GLY	148	VAL				

10. References

1. Brown A. J.D. Bernal: The Sage of Science2005.
2. Widłak W. Protein Structure and Function. Molecular Biology: Springer, Berlin, Heidelberg; 2013.
3. Buzanovskii VA. Determination of proteins in blood. Part 1: Determination of total protein and albumin. Review Journal of Chemistry. 2017;7(1):79-124.
4. Vickery HB. The origin of the word protein. The Yale journal of biology and medicine. 1950;22(5):387-93.
5. Bolognesi B, Lehner B. Reaching the limit. eLife. 2018;7:e39804.
6. Teoh G, Urashima M, Ogata A, Chauhan D, DeCaprio JA, Treon SP, et al. MDM2 protein overexpression promotes proliferation and survival of multiple myeloma cells. Blood. 1997;90(5):1982-92.
7. Hung C-M, Huang W-C, Pan H-L, Chien P-H, Lin C-W, Chen L-C, et al. Hepatitis B virus X upregulates HuR protein level to stabilize HER2 expression in hepatocellular carcinoma cells. BioMed research international. 2014;2014:827415-.
8. Ocak S, Friedman DB, Chen H, Ausborn JA, Hassanein M, Detry B, et al. Discovery of new membrane-associated proteins overexpressed in small-cell lung cancer. Journal of thoracic oncology : official publication of the International Association for the Study of Lung Cancer. 2014;9(3):324-36.
9. Alves FC, Sun J, Qureshi AR, Dai L, Snaedal S, Bárány P, et al. The higher mortality associated with low serum albumin is dependent on systemic inflammation in end-stage kidney disease. PloS one. 2018;13(1):e0190410-e.
10. Yin M, Si L, Qin W, Li C, Zhang J, Yang H, et al. Predictive Value of Serum Albumin Level for the Prognosis of Severe Sepsis Without Exogenous Human Albumin Administration: A Prospective Cohort Study. J Intensive Care Med. 2018;33(12):687-94.
11. Gutman AB, Moore DH, Gutman EB, McClellan V, Kabat EA. FRACTIONATION OF SERUM PROTEINS IN HYPERPROTEINEMIA, WITH SPECIAL REFERENCE TO MULTIPLE MYELOMA. The Journal of clinical investigation. 1941;20(6):765-83.
12. Casem ML. Chapter 3 - Proteins. In: Casem ML, editor. Case Studies in Cell Biology. Boston: Academic Press; 2016. p. 23-71.
13. Chaudhuri TK, Paul S. Protein-misfolding diseases and chaperone-based therapeutic approaches. Febs j. 2006;273(7):1331-49.
14. Sweeney P, Park H, Baumann M, Dunlop J, Frydman J, Kopito R, et al. Protein misfolding in neurodegenerative diseases: implications and strategies. Translational neurodegeneration. 2017;6:6-.
15. Swaminathan R, Ravi VK, Kumar S, Kumar MV, Chandra N. Lysozyme: a model protein for amyloid research. Adv Protein Chem Struct Biol. 2011;84:63-111.
16. Helmfors L. Understanding the dual nature of lysozyme: part villain – part hero : A Drosophila melanogaster model of lysozyme amyloidosis [Doctoral thesis, comprehensive summary]. Linköping: Linköping University Electronic Press; 2014.
17. Cegielska-Radziejewska R, Leśnierowski G, Kijowski J. Properties and application of egg white lysozyme and its modified preparations - a review2008. 5-10 p.
18. Doumas BT. Standards for total serum protein assays--a collaborative study. Clin Chem. 1975;21(8):1159-66.
19. Hemrika MH, Costongs GM, Engels LG, Bos LP, Janson PC, Flendrig JA. Clinical relevance of lysozyme in the faeces. Neth J Med. 1989;34(3-4):174-81.
20. Hankiewicz J, Swierczek E. Lysozyme in human body fluids. Clinica Chimica Acta. 1974;57(3):205-9.
21. Chien SC, Chen CY, Lin CF, Yeh HI. Critical appraisal of the role of serum albumin in cardiovascular disease. Biomark Res. 2017;5:31.
22. Syahir A, Usui K, Tomizaki K-Y, Kajikawa K, Mihara H. Label and Label-Free Detection Techniques for Protein Microarrays. Microarrays (Basel, Switzerland). 2015;4(2):228-44.
23. Westermeier R, Marouga R. Protein Detection Methods in Proteomics Research2005. 19-32 p.

24. Han X, Aslanian A, Yates JR, 3rd. Mass spectrometry for proteomics. Current opinion in chemical biology. 2008;12(5):483-90.
25. Ghosh R, Gilda JE, Gomes AV. The necessity of and strategies for improving confidence in the accuracy of western blots. Expert review of proteomics. 2014;11(5):549-60.
26. Floeter MK, Gerloff C, Kouri J, Hallett M. Cutaneous withdrawal reflexes of the upper extremity. Muscle Nerve. 1998;21(5):591-8.
27. Dewald JP, Beer RF, Given JD, McGuire JR, Rymer WZ. Reorganization of flexion reflexes in the upper extremity of hemiparetic subjects. Muscle Nerve. 1999;22(9):1209-21.
28. McGrath MJ, C.N. S. Sensing and Sensor Fundamentals. Sensor Technologies: Apress, Berkeley, CA; 2013. p. 15-55.
29. Mehrotra P. Biosensors and their applications - A review. Journal of oral biology and craniofacial research. 2016;6(2):153-9.
30. Ahmad R, Salama KN, editors. Physical Sensors for Biomedical Applications. 2018 IEEE SENSORS; 2018 28-31 Oct. 2018.
31. Vadgama P. Biomedical Sensors: Materials. In: Buschow KHJ, Cahn RW, Flemings MC, Ilschner B, Kramer EJ, Mahajan S, et al., editors. Encyclopedia of Materials: Science and Technology. Oxford: Elsevier; 2001. p. 592-5.
32. Kassal P, Steinberg MD, Steinberg IM. Wireless chemical sensors and biosensors: A review. Sensors and Actuators B: Chemical. 2018;266:228-45.
33. Bhalla N, Jolly P, Formisano N, Estrela P. Introduction to biosensors. Essays in biochemistry. 2016;60(1):1-8.
34. LaFleur L, Yager P. Chapter II.5.13 - Medical Biosensors. In: Ratner BD, Hoffman AS, Schoen FJ, Lemons JE, editors. Biomaterials Science (Third Edition): Academic Press; 2013. p. 996-1006.
35. Yoo E-H, Lee S-Y. Glucose biosensors: an overview of use in clinical practice. Sensors (Basel, Switzerland). 2010;10(5):4558-76.
36. Campbell AS, Kim J, Wang J. Wearable electrochemical alcohol biosensors. Current Opinion in Electrochemistry. 2018;10:126-35.
37. Balakrishnan SR, Hashim U, Gopinath SCB, Poopalan P, Ramayya HR, Iqbal Omar M, et al. A Point-of-Care Immunosensor for Human Chorionic Gonadotropin in Clinical Urine Samples Using a Cuneated Polysilicon Nanogap Lab-on-Chip. PloS one. 2015;10(9):e0137891-e.
38. Vidic J, Manzano M, Chang C-M, Jaffrezic-Renault N. Advanced biosensors for detection of pathogens related to livestock and poultry. Veterinary research. 2017;48(1):11-.
39. Parsajoo C, Kauffmann JM, Elkaoutit M. 9 - Biosensors for drug testing and discovery. In: Higson S, editor. Biosensors for Medical Applications: Woodhead Publishing; 2012. p. 233-62.
40. Lu L, Hu X, Zhu Z. Biomimetic sensors and biosensors for qualitative and quantitative analyses of five basic tastes. TrAC Trends in Analytical Chemistry. 2017;87:58-70.
41. Mosbach K, Ramström O. The Emerging Technique of Molecular Imprinting and Its Future Impact on Biotechnology. Bio/Technology. 1996;14(2):163-70.
42. Wulff G. Molecular Imprinting in Cross-Linked Materials with the Aid of Molecular Templates— A Way towards Artificial Antibodies1995. 1812-32 p.
43. Alexander C, Andersson HS, Andersson LI, Ansell RJ, Kirsch N, Nicholls IA, et al. Molecular imprinting science and technology: a survey of the literature for the years up to and including 2003. J Mol Recognit. 2006;19(2):106-80.
44. Vasapollo G, Sole RD, Mergola L, Lazzoi MR, Scardino A, Scorrano S, et al. Molecularly imprinted polymers: present and future prospective. Int J Mol Sci. 2011;12(9):5908-45.
45. Chen L, Xu S, Li J. Recent advances in molecular imprinting technology: current status, challenges and highlighted applications. Chemical Society Reviews. 2011;40(5):2922-42.
46. Cramer F. Biochemical correctness: Emil Fischer's lock and key hypothesis, a hundred years after — an essay. Pharmaceutica Acta Helvetiae. 1995;69(4):193-203.
47. Koshland DE. Application of a Theory of Enzyme Specificity to Protein Synthesis. Proc Natl Acad Sci U S A. 1958;44(2):98-104.
48. Huang YJ, Chang R, Zhu QJ. Synthesis and Characterization of a Molecularly Imprinted Polymer of Spermidine and the Exploration of Its Molecular Recognition Properties. Polymers (Basel). 2018;10(12).

49. Ertürk G, Mattiasson B. Molecular Imprinting Techniques Used for the Preparation of Biosensors. Sensors (Basel, Switzerland). 2017;17(2):288.
50. Whitcombe MJ, Chianella I, Larcombe L, Piletsky SA, Noble J, Porter R, et al. The rational development of molecularly imprinted polymer-based sensors for protein detection. Chem Soc Rev. 2011;40(3):1547-71.
51. Lieberzeit PA, Jungmann C, Schranzhofer L. Molecular Imprinting on the Nanoscale – Rapid Detection of Ag Nanoparticles by QCM Sensors. Procedia Engineering. 2014;87:236-9.
52. Zhang H. Water-compatible molecularly imprinted polymers: Promising synthetic substitutes for biological receptors. Polymer. 2014;55(3):699-714.
53. Schirhagl R, Qian J, Dickert FL. Immunosensing with artificial antibodies in organic solvents or complex matrices. Sensors and Actuators B: Chemical. 2012;173:585-90.
54. Svenson J, Nicholls IA. On the thermal and chemical stability of molecularly imprinted polymers. Analytica Chimica Acta. 2001;435(1):19-24.
55. Turner NW, Jeans CW, Brain KR, Allender CJ, Hlady V, Britt DW. From 3D to 2D: a review of the molecular imprinting of proteins. Biotechnol Prog. 2006;22(6):1474-89.
56. Su W-F. Radical Chain Polymerization. In: Su W-F, editor. Principles of Polymer Design and Synthesis. Berlin, Heidelberg: Springer Berlin Heidelberg; 2013. p. 137-83.
57. Perrier S. 50th Anniversary Perspective: RAFT Polymerization—A User Guide. Macromolecules. 2017;50(19):7433-47.
58. Greszta D, Mardare D, Matyjaszewski K. "Living" radical polymerization. 1. Possibilities and limitations. Macromolecules. 1994;27(3):638-44.
59. Hawker CJ, Piotti ME, Saldívar-Guerra E. Nitroxide-Mediated Free Radical Polymerization. Reference Module in Materials Science and Materials Engineering: Elsevier; 2016.
60. Matyjaszewski K. Atom Transfer Radical Polymerization: From Mechanisms to Applications. Israel Journal of Chemistry. 2012;52(3-4):206-20.
61. Rizzardo E, Chen M, Chong B, Moad G, Skidmore M, Thang S. RAFT Polymerization: Adding to the picture2007. 104-16 p.
62. Godwin A, Mahitha Shri K, Balaji M. NANOPARTICLES AND THEIR APPLICATIONS – A MINI REVIEW2015.
63. Stöber W, Fink A, Bohn E. Controlled growth of monodisperse silica spheres in the micron size range. Journal of Colloid and Interface Science. 1968;26(1):62-9.
64. Takeda Y, Komori Y, Yoshitake H. Direct stöber synthesis of monodisperse silica particles functionalized with mercapto-, vinyl- and aminopropylsilanes in alcohol–water mixed solvents. Colloids and Surfaces A: Physicochemical and Engineering Aspects. 2013;422:68-74.
65. Tichý J, Erhart J, Kittinger E, Přívratská J. Fundamentals of Piezoelectric Sensorics Mechanical, Dielectric, and Thermodynamical Properties of Piezoelectric Materials2010.
66. Vashist SK, Vashist P. Recent Advances in Quartz Crystal Microbalance-Based Sensors. 2011. p. 1-13.
67. J. C, P. C. Phénomènes électriques des cristaux hémièdres à faces inclinées. J. Phys. Theor. Appl.1882. p. 245-51.
68. Mould RF. Pierre curie, 1859-1906. Current oncology (Toronto, Ont). 2007;14(2):74-82.
69. Brown CS, Kell RC, Taylor R, Thomas LA. Piezoelectric Materials, A Review of Progress1963. 193-211 p.
70. Company H-P. Fundamentals of Quartz Oscillators. Electronic Counters Series [Internet]. 1997. Available from: http://leapsecond.com/hpan/an200-2.pdf.
71. Janshoff A, Galla HJ, Steinem C. Piezoelectric Mass-Sensing Devices as Biosensors-An Alternative to Optical Biosensors? Angew Chem Int Ed Engl. 2000;39(22):4004-32.
72. Sauerbrey GZ. Verwendung von Schwingquarzen zur Wägung dünner Schichten und zur Mikrowägung. Zeitschrift Für Physik1959. p. 206–22.
73. Sohna Sohna JE, Cooper MA. Does the Sauerbrey equation hold true for binding of peptides and globular proteins to a QCM?: A systematic study of mass dependence of peptide and protein binding with a piezoelectric sensor. Sensing and Bio-Sensing Research. 2016;11:71-7.
74. Rodziewicz P, Goclon J. Structural flexibility of 4,4'-methylene diphenyl diisocyanate (4,4'-MDI): evidence from first principles calculations. Journal of molecular modeling. 2014;20(2):2097-.

75. Lu C-S, Lewis O. Investigation of Film-thickness Determination by Oscillating Quartz Resonators with Large Mass Load1972. 4385-90 p.
76. Keiji Kanazawa K, Gordon JG. The oscillation frequency of a quartz resonator in contact with liquid. Analytica Chimica Acta. 1985;175:99-105.
77. Huang X, Bai Q, Hu J, Hou D. A Practical Model of Quartz Crystal Microbalance in Actual Applications. Sensors (Basel, Switzerland). 2017;17(8):1785.
78. Hashimoto K-y. Bulk Acoustic and Surface Acoustic Waves. In: Hashimoto K-y, editor. Surface Acoustic Wave Devices in Telecommunications: Modelling and Simulation. Berlin, Heidelberg: Springer Berlin Heidelberg; 2000. p. 1-23.
79. Fuchiwaki Y, Tanaka M, Makita Y, Ooie T. New approach to a practical quartz crystal microbalance sensor utilizing an inkjet printing system. Sensors (Basel, Switzerland). 2014;14(11):20468-79.
80. Mujahid A, Mustafa G, Dickert FL. Label-Free Bioanalyte Detection from Nanometer to Micrometer Dimensions-Molecular Imprinting and QCMs (†). Biosensors. 2018;8(2):52.
81. Sharma S, Gahan D, Scullin P, Doyle J, Lennon J, K Vijayaraghavan R, et al. Measurement of deposition rate and ion energy distribution in a pulsed dc magnetron sputtering system using a retarding field analyzer with embedded quartz crystal microbalance2016. 43511-31507 p.
82. Latif U, Can S, Hayden O, Grillberger P, Dickert FL. Sauerbrey and anti-Sauerbrey behavioral studies in QCM sensors—Detection of bioanalytes. Sensors and Actuators B: Chemical. 2013;176:825-30.
83. Reviakine I, Johannsmann D, Richter RP. Hearing What You Cannot See and Visualizing What You Hear: Interpreting Quartz Crystal Microbalance Data from Solvated Interfaces. Analytical Chemistry. 2011;83(23):8838-48.
84. Merlot AM, Kalinowski DS, Richardson DR. Unraveling the mysteries of serum albumin-more than just a serum protein. Frontiers in physiology. 2014;5:299-.
85. Brennan SO, Carrell RW. A circulating variant of human proalbumin. Nature. 1978;274(5674):908-9.
86. Schreiber G. The synthesis and secretion of plasma proteins in the liver. Pathology. 1978;10(4):394.
87. Moman R, Varacallo M. Physiology, Albumin2018.
88. Barber MD, Ross JA, Fearon KC. Changes in nutritional, functional, and inflammatory markers in advanced pancreatic cancer. Nutr Cancer. 1999;35(2):106-10.
89. Levitt DG, Levitt MD. Human serum albumin homeostasis: a new look at the roles of synthesis, catabolism, renal and gastrointestinal excretion, and the clinical value of serum albumin measurements. International journal of general medicine. 2016;9:229-55.
90. Arques S, Ambrosi P. Human serum albumin in the clinical syndrome of heart failure. J Card Fail. 2011;17(6):451-8.
91. Hirayama K, Akashi S, Furuya M, Fukuhara K-i. Rapid confirmation and revision of the primary structure of bovine serum albumin by ESIMS and frit-FAB LC/MS. Biochemical and Biophysical Research Communications. 1990;173(2):639-46.
92. Majorek KA, Porebski PJ, Dayal A, Zimmerman MD, Jablonska K, Stewart AJ, et al. Structural and immunologic characterization of bovine, horse, and rabbit serum albumins. Mol Immunol. 2012;52(3-4):174-82.
93. Khatun S, Riyazuddeen. Interaction of colchicine with BSA: spectroscopic, calorimetric and molecular modeling approaches. Journal of Biomolecular Structure and Dynamics. 2018;36(12):3122-9.
94. Joshi R, Jadhao M, Kumar H, Ghosh SK. Is the Sudlow site I of human serum albumin more generous to adopt prospective anti-cancer bioorganic compound than that of bovine: A combined spectroscopic and docking simulation approach. Bioorganic Chemistry. 2017;75:332-46.
95. Salameh S, Nouel D, Flores C, Hoops D. An optimized immunohistochemistry protocol for detecting the guidance cue Netrin-1 in neural tissue. MethodsX. 2017;5:1-7.
96. Xiao Y, Isaacs SN. Enzyme-linked immunosorbent assay (ELISA) and blocking with bovine serum albumin (BSA)--not all BSAs are alike. Journal of immunological methods. 2012;384(1-2):148-51.
97. Wenz B, Apuzzo J. Polyethylene glycol improves the indirect antiglobulin test. Transfusion. 1989;29(3):218-20.

98. Francis GL. Albumin and mammalian cell culture: implications for biotechnology applications. Cytotechnology. 2010;62(1):1-16.
99. Loughney JW, Lancaster C, Ha S, Rustandi RR. Residual bovine serum albumin (BSA) quantitation in vaccines using automated Capillary Western technology. Anal Biochem. 2014;461:49-56.
100. Chruszcz M, Mikolajczak K, Mank N, Majorek KA, Porebski PJ, Minor W. Serum albumins-unusual allergens. Biochimica et biophysica acta. 2013;1830(12):5375-81.
101. Fuentes Aparicio V, Sanchez Marcen I, Perez Montero A, Baeza ML, de Barrio Fernandez M. Allergy to mammal's meat in adult life: immunologic and follow-up study. J Investig Allergol Clin Immunol. 2005;15(3):228-31.
102. Raoufinia R, Mota A, Keyhanvar N, Safari F, Shamekhi S, Abdolalizadeh J. Overview of Albumin and Its Purification Methods. Advanced pharmaceutical bulletin. 2016;6(4):495-507.
103. Meloun B, Moravek L, Kostka V. Complete amino acid sequence of human serum albumin. FEBS Lett. 1975;58(1):134-7.
104. Bhattacharya AA, Curry S, Franks NP. Binding of the general anesthetics propofol and halothane to human serum albumin. High resolution crystal structures. J Biol Chem. 2000;275(49):38731-8.
105. Brackeen GL, Dover JS, Long CL. Serum albumin. Differences in assay specificity. Nutr Clin Pract. 1989;4(6):203-5.
106. Walayat S, Martin D, Patel J, Ahmed U, N Asghar M, Pai AU, et al. Role of albumin in cirrhosis: from a hospitalist's perspective. Journal of community hospital internal medicine perspectives. 2017;7(1):8-14.
107. Atmeh RF, Shabsoug B. Detection and semiquantitation of albumin forms in fresh human plasma separated on gradient polyacrylamide gel by means of electroblotting on agarose gel matrix. Electrophoresis. 1997;18(11):2055-8.
108. Choi S, Choi EY, Kim DJ, Kim JH, Kim TS, Oh SW. A rapid, simple measurement of human albumin in whole blood using a fluorescence immunoassay (I). Clinica Chimica Acta. 2004;339(1):147-56.
109. Ito S, Yamamoto D. Identification of two bromocresol purple binding sites on human serum albumin. Clin Chim Acta. 2010;411(19-20):1536-8.
110. Fleming A, Wright Almroth E. On a remarkable bacteriolytic element found in tissues and secretions. Proceedings of the Royal Society of London Series B, Containing Papers of a Biological Character. 1922;93(653):306-17.
111. Jesman C, Mludzik A, Cybulska M. [History of antibiotics and sulphonamides discoveries]. Pol Merkur Lekarski. 2011;30(179):320-2.
112. Blake CCF, Koenig DF, Mair GA, North ACT, Phillips DC, Sarma VR. Structure of Hen Egg-White Lysozyme: A Three-dimensional Fourier Synthesis at 2 Å Resolution. Nature. 1965;206(4986):757-61.
113. Canfield RE. THE AMINO ACID SEQUENCE OF EGG WHITE LYSOZYME. J Biol Chem. 1963;238:2698-707.
114. Weiss MS, Palm GJ, Hilgenfeld R. Crystallization, structure solution and refinement of hen egg-white lysozyme at pH 8.0 in the presence of MPD. Acta Crystallogr D Biol Crystallogr. 2000;56(Pt 8):952-8.
115. Parmar AS, Muschol M. Hydration and hydrodynamic interactions of lysozyme: effects of chaotropic versus kosmotropic ions. Biophysical journal. 2009;97(2):590-8.
116. Venkataramani S, Truntzer J, Coleman DR. Thermal stability of high concentration lysozyme across varying pH: A Fourier Transform Infrared study. J Pharm Bioallied Sci. 2013;5(2):148-53.
117. Chang JY, Li L. The unfolding mechanism and the disulfide structures of denatured lysozyme. FEBS Lett. 2002;511(1-3):73-8.
118. Mishra RK, Hayat A, Mishra GK, Catanante G, Sharma V, Marty JL. A novel colorimetric competitive aptamer assay for lysozyme detection based on superparamagnetic nanobeads. Talanta. 2017;165:436-41.
119. Aine E, Morsky P. Lysozyme concentration in tears--assessment of reference values in normal subjects. Acta Ophthalmol (Copenh). 1984;62(6):932-8.
120. Zhong Y, Patel S. Binding structures of tri-N-acetyl-β-glucosamine in hen egg white lysozyme using molecular dynamics with a polarizable force field. Journal of computational chemistry. 2013;34(3):163-74.

121. Silvetti T, Morandi S, Hintersteiner M, Brasca M. Use of Hen Egg White Lysozyme in the Food Industry. 2017. p. 233-42.
122. Cappannella E, Benucci I, Lombardelli C, Liburdi K, Bavaro T, Esti M. Immobilized lysozyme for the continuous lysis of lactic bacteria in wine: Bench-scale fluidized-bed reactor study. Food Chem. 2016;210:49-55.
123. Silvetti T, Brasca M, Lodi R, Vanoni L, Chiolerio F, de Groot M, et al. Effects of Lysozyme on the Microbiological Stability and Organoleptic Properties of Unpasteurized Beer. Journal of the Institute of Brewing. 2010;116(1):33-40.
124. Thompson A, Bhandari V. Pulmonary Biomarkers of Bronchopulmonary Dysplasia. Biomarker insights.3:361-73.
125. Revenis ME, Kaliner MA. Lactoferrin and lysozyme deficiency in airway secretions: association with the development of bronchopulmonary dysplasia. J Pediatr. 1992;121(2):262-70.
126. Sen DK, Sarin GS. Immunoassay of tear lysozyme in conjunctival diseases. The British journal of ophthalmology. 1982;66(11):732-5.
127. E. Perillie P, Khan K, Finch S. Serum lysozyme in pulmonary tuberculosis1973. 297-302 p.
128. Moscinski LC, Kasnic G, Jr., Saker A, Jr. The significance of an elevated serum lysozyme value in acute myelogenous leukemia with eosinophilia. Am J Clin Pathol. 1992;97(2):195-201.
129. Niscola P, Neri B, Morino L, de Fabritiis P. Monoclonal Gammopathy Responsive to Decitabine Given for Acute Myeloid Leukemia in a Frail Patient. Acta Haematologica. 2018;139(1):58-9.
130. Serra C, Vizoso F, Alonso L, Rodríguez JC, González LO, Fernández M, et al. Expression and prognostic significance of lysozyme in male breast cancer. Breast cancer research : BCR. 2002;4(6):R16-R.
131. Smirnow J, Wislowska M. Lysozyme and its biological value in rheumatoid arthritis (RA). Arthritis Research. 2001;3(Suppl A):P014-P.
132. Sandin L, Nath S, Armstrong A, Janefjord C, McCann H, Halliday G, et al. The role of lysozyme in Alzheimer's disease2015. P477-P8 p.
133. Salton MRJ. Cell Wall of Micrococcus Lysodeikticus as the Substrate of Lysozyme. Nature. 1952;170(4331):746-7.
134. Liao YH, Brown MB, Martin GP. Turbidimetric and HPLC assays for the determination of formulated lysozyme activity. J Pharm Pharmacol. 2001;53(4):549-54.
135. Poms R, Klein C, Anklam E. Methods for allergen analysis in food: A review2004. 1-31 p.
136. Yang C, Ji X-F, Cao W-Q, Wang J, Zhang Q, Zhong T-L, et al. Molecularly imprinted polymer based sensor directly responsive to attomole bovine serum albumin. Talanta. 2019;196:402-7.
137. Tan CJ, Chua HG, Ker KH, Tong YW. Preparation of Bovine Serum Albumin Surface-Imprinted Submicrometer Particles with Magnetic Susceptibility through Core–Shell Miniemulsion Polymerization. Analytical Chemistry. 2008;80(3):683-92.
138. Makki F. Thermal inactivation kinetics of lysozyme and preservative effect beer [Text]1996.
139. Sassi P, Giugliarelli A, Paolantoni M, Morresi A, Onori G. Unfolding and aggregation of lysozyme: a thermodynamic and kinetic study by FTIR spectroscopy. Biophys Chem. 2011;158(1):46-53.
140. Martinez LM, Videa M, Mederos-Henry F, De Moral Y. Preservation Effect of Vitreous non Reducing Carbohydrates on the Enzymatic Activity, Denaturation Temperature and Retention of Native Structure of Lysozyme2011. 185 p.
141. What is the hydrodynamic radius.doc.

11. Publications & Conferences

11.1. Publications

2019

- Mass-Sensitive Sensing of Melamine in Dairy Products with Molecularly Imprinted Polymers: Matrix Challenges

*Zeilinger, M., Sussitz, H., **Cuypers, W**., Jungmann, C. & Lieberzeit, P., 2 Mai 2019, in : Sensors. 19, 10, 10 S., 2366.*

2018

- Combining Two Selection Principles: Sensor Arrays Based on Both Biomimetic Recognition and Chemometrics

***Cuypers, W**. & Lieberzeit, P. A., 2 Aug 2018, in : Frontiers in Chemistry. 6, 10 S., 268.*

- A novel molecular imprinting approach for lysozyme detection

***Cuypers, W**. & Lieberzeit, P., 7 Feb 2018, PACCON 2018 Proceedings.*

2016

- Defining the synergetic pattern of composites for sensing volatile organic compounds

***Cuypers, W**., Jarujamrus, P. & Lieberzeit, P., 10 Jun 2016, Book of Abstracts.*

- MIP-nanoparticle Composites and Core-shell Nanoparticles leading to Materials with Strongly Enhanced Sensitivity

*Lieberzeit, P., Mustafa, G., **Cuypers, W**., Zeilinger, M., Navakul, K. & Sangma, C., 5 Jun 2016, Proceedings. Trans Tech Publications Inc.*

2014

- Real-time monitoring of aptamer functionalization and detection of Ara h1 by electrochemical impedance spectroscopy and dissipation-mode quartz crystal microbalance

*Jimenez-Monroy, K. L.; Libert, C.; Eurlings, Y.; **Cuypers, Wim**; Wackers, Gideon; Duchateau, Stijn; Robaeys, Pieter; Nesladek, Milos; van Grinsven, Bart; Perez-Ruiz, Elena; Lammertyn, Jeroen; Losada-Perez, Patricia; Wagner, Patrick, 21 Jul 2014, Journal of Biosensors and Bioelectronics.*

- Boron-Doped Diamond Functionalization by an Electrografting/Alkyne–Azide Click Chemistry Sequence

*Weng Siang Yeap, Dr. Mohammed Sharif Murib, **Wim Cuypers**, Dr. Xianjie Liu, Dr. Bart van Grinsven, Prof. Dr. Marcel Ameloot, Prof. Dr. Mats Fahlman, Prof. Dr. Patrick Wagner, Prof. Dr. Wouter Maes, Prof. Dr. Ken Haenen, 24 Jun 2014, CHEMELECTROCHEM.*

11.2. Conferences

2019

Detecting Lysozyme via Molecular Locks: The Key to Success?

ENFI 2019, Leuven, Belgium; Presentation and Poster

2018

A novel molecular imprinting approach for lysozyme detection

PACCON 2018, Hat Yai, Thailand

2016

Defining the synergetic pattern of composites for sensing volatile organic compounds

Jung Analytiker Forum, Graz, Austria